An Analysis of the High Temperature Plastic Flow of Copper

AN ANALYSIS OF THE HIGH TEMPERATURE PLASTIC FLOW OF POLYCRYSTALLINE COPPER

by

Kenneth C. CADIEN

A thesis submitted to the Faculty of Graduate Studies and Research
in partial fulfilment of the requirements for the degree of
Master of Engineering

Department of Mining and Metallurgical Engineering
McGill University
Montreal, Canada

November 1976

To my wife, Betty Ann,
whose constant encouragement
was a source of great inspiration.

ABSTRACT

Compression tests were performed on polycrystalline samples of OFHC copper between 500 and 800°C at constant true strain rates from 5.2×10^{-5} to $5.2\times10^{-2}\,s^{-1}$. The stress at which macroscopic yielding begins was measured from the flow curves. These data were reduced by a method of activation analysis for elastic obstacles in terms of the modulus-reduced stress. The analytical scheme leads to activation volumes in the range 600 to 2800 b^3, which decrease with increasing stress. The zero stress value of the activation free energy was found to be 0.66 μb^3/atom which is much greater than the values reported for self-diffusion. It is concluded, from these results, that the thermally assisted unpinning of attractive junctions controls the rate of dislocation glide at high temperatures in copper. In addition, it is observed that the pre-exponential factor in the rate equation is independent of stress and temperature. The latter observation is rationalized by means of a dislocation model based on the distribution of segment lengths within the material.

RESUME

Des essais de compression ont été effectués sur les echantillons polycristallins dans le domaine de la vitesse de déformation réelle compris entre 5.2x10^{-5} et 5.2x10^{-2}s^{-1} et températures de 500 à 800^{o}C. Les tensions pour lesquelles la limite élastique macroscopique est depassée a été mesureé et utilisant des courbes d'elasticité. On a obtenu les donneés par une méthode d'analyse de l'activation pour les obstacles élastiques en fonction du rapport tension-module d'élasticité. Le schema analytique conduit à des valeurs de 600 à 2800 b^{3} pour les volumes d'activation, valeurs décroissantes par rapport à l'augmentation des tensions. On a détérminé une valeur de 0.66 μb^{3}/atom pour l'énérgie libre d'activation pour la tension nulle, valeur dépassant largement les valeurs rapportées pour l'autodiffusion. On peut conclure de ces résultats que la vitesse de glissement des dislocations aux temperatures élevées est détérminée par le désancrage des junctions favorisées du point de vue thermique. En plus, on a aussi observé que le facteur pré-exponentiel dont l'équation de la vitesse est indépendante de la tension et de la température. On a déduit la dernière observation au moyen d'un modèle basé sur la distribution de longueur des segments dans le matériau.

ACKNOWLEDGEMENTS

The author would like to express his gratitude to Dr. M.J. Luton, director of this research, for his guidance and many suggestions that helped to make this research fruitful. The author also wishes to thank Dr. J.J. Jonas for many stimulating discussions.

The author is indebted to the Chairman of the Department of Mining and Metallurgical Engineering, Dr. W.M. Williams, for the facilities provided for the experimental studies and for his thoughtful encouragement during the course of this work. Thanks are also due to Mr. M. Knoepfel for his assistance in the preparation of samples, and to my fellow graduate students for their interest and support during various stages of this work.

Finally, the author wishes to thank Noranda Metal Industries for supplying the material used in this investigation, and the National Research Council of Canada and the J.W. McConnell Foundation for the award of postgraduate fellowships.

TABLE OF CONTENTS

LIST OF FIGURES

LIST OF TABLES

LIST OF APPENDICES

LIST OF SYMBOLS

Prefixes

d	total differential
∂	partial derivative

Roman Letters

A	area swept by a dislocation
A_e	area of a thermodynamic system
A^*	activation area
A_i	instantaneous cross-sectional area of a sample during deformation
a	f.c.c. lattice parameter
B	numerical constant
b	Burgers vector
C	numerical constant
$\dot{C}$	dislocation climb rate
C_o	equilibrium vacancy concentration for a dislocation-free crystal
C_e	local vacancy concentration near a vacancy emitting jog
C_a	local vacancy concentration near a vacancy absorbing jog
C_{ij}	elastic stiffness coefficients
D	numerical constant
D_s	self-diffusion coefficient
D_V	diffusion coefficient for vacancies
d	distance between jogs
d_m	machine distortion

d_i	instantaneous crosshead displacement
E	numerical constant
F	Helmholtz free energy
F_o	instantaneous load
ΔF_o	total reversible work required to overcome an obstacle without the aid of external stress
ΔF_i	same as ΔF_o except there is an external stress
f_e	chemical force for a vacancy emitting jog
f_a	chemical force for a vacancy absorbing jog
G	Gibbs free energy
ΔG_o	same as ΔF_o
ΔG_i	intersection energy
ΔG_c	construction energy
ΔG_r	recombination energy
ΔG_j	free energy due to the jog left behind after intersection
ΔG_T	total free energy for the unpinning of an attractive junction
g	distance between adjacent dislocation pile-ups
H	enthalpy
H_a	heat
ΔH_{SD}	activation enthalpy for self-diffusion
ΔH_C	activation enthalpy for creep
ΔH_{HW}	activation enthalpy for hot working
ΔH^o	activation enthalpy in the absence of an applied stress
h_o	initial sample height
h_i	instantaneous sample height
h	work hardening coefficient

k	Boltzmann's constant
L	length of a dislocation pile-up
M	Taylor factor
$\overline{M}$	average Taylor factor
N	density of activatable sites
N_s	number of dislocation sources
n	stress coefficient
P	probability of an activated jump in the forward direction
P'	probability of a subsequent activated jump in the reverse direction
$\overline{P}$	net probability of a successful thermal fluctuation in the forward direction
P_T	probability of a thermal fluctuation of energy greater than ΔG
p	pressure
Q	activation energy
r	stacking fault width
$\dot{r}$	recovery rate
S	entropy
ΔS	activation entropy
S_{ij}	elastic compliances
T	temperature
t	time
U	internal energy
V	average dislocation velocity
V_e	average velocity of a vacancy emitting jog
V_a	average velocity of a vacancy absorbing jog
V_o	volume

V^*	activation volume
W	work
X	independent variable
x	slip distance
Y	Young's modulus

Greek Letters

$\alpha_{1,2,\ldots 6}$	numerical constants
β	numerical constant
γ	shear strain
$\dot{\gamma}$	shear strain rate
γ_s	surface energy
ε	normal strain
$\dot{\varepsilon}$	normal strain rate
$\dot{\varepsilon}_s$	steady state normal strain rate
$\dot{\varepsilon}_o$	pre-exponential factor
ε_p	strain to the peak stress
ε_c	critical strain for the initiation of dynamic recrystallization
ε_r	strain for completion of recrystallization
Λ	stacking fault energy
μ	shear modulus
μ_H	Hill Average
μ_R	Reuss Average
μ_V	Voigt Average
ν	dislocation attempt frequency
ν_D	Debye frequency

ξ	number of link lengths per unit volume and per unit interval of segment length
$\overline{\xi}$	average distribution factor
ρ_T	total dislocation density
ρ_m	mobile dislocation density
σ	applied normal stress
τ	applied shear stress
τ_b	back stress
τ^*	effective stress
τ_i	internal stress
τ_{BOW}	bow-out stress
ω	atomic frequency

Miscellaneous Symbols

ℓ	dislocation segment length
ℓ_{max}	maximum segment length that is thermally activatable
ℓ_{min}	minimum segment length that is thermally activatable
ℓ^*	average segment length of those segments with lengths between ℓ_{max} and ℓ_{min}
$\Delta\ell^*$	$\ell_{max} - \ell_{min}$
ℓ_{av}	average segment length in the entire network

CHAPTER 1

INTRODUCTION

The aim of this study was to throw some light on the processes that control the rate of deformation in metals at high temperatures. At present there exists a dichotomy regarding the mechanism controlling high temperature deformation. On the one hand, there is a school that argues that the deformation is diffusion controlled and that the activation enthalpy for creep and hot working should be that of self-diffusion. On the other hand, an alternative view is that dislocation glide is controlled by the thermally activated unpinning of nodes in the pre-existing dislocation network. In order to assess which of these hypotheses are valid a study of the mechanical behaviour of copper was undertaken.

It was decided that by gathering enough data on the temperature and strain rate dependence of the yield stress, it would be possible to clearly distinguish between the two approaches. By a consistent analytical scheme based on the properties of linear elastic obstacles and reaction rate theory, the activation parameters which describe the properties of the rate controlling process can be determined. In this way, it is possible to determine the rate controlling mechanism.

Before proceeding with a description of the method, equipment and results of this work, a review of the literature relevant to this investigation is presented.

CHAPTER 2

A REVIEW OF THE LITERATURE PERTINENT TO THE HIGH TEMPERATURE DEFORMATION OF F.C.C. METALS

This chapter is a review of some of the literature that is relevant to an understanding of the present work. The first section deals briefly with the phenomenology of high temperature flow, and the generally accepted theories that have been proposed to explain such phenomena. The next topic considered is the thermodynamic approach to high temperature flow. The final section concerns the shear modulus of polycrystalline cubic metals.

2.1 HIGH TEMPERATURE DEFORMATION

During the past decade several excellent reviews of high temperature deformation have been published (1-6). Therefore, the present review surveys only briefly the main features of high temperature flow. The various types of flow curves are dealt with first, followed by a discussion of the empirical flow relations. In the final section a description of some models for high temperature deformation is presented.

2.1.1 Phenomenology of High Temperature Deformation

High temperature deformation is defined as flow that occurs at sufficiently high temperatures so that the major restoration processes act concurrently with straining. There is a temperature limit below which these processes occur too slowly to significantly influence the rate of deformation. It has been estimated that this limit is approximately one-half of the absolute melting temperature (7).

The studies of high temperature flow can be divided into two groups, those carried out at constant stress and those at constant strain rate. During constant stress tests either the load or the stress is kept constant and the strain produced is measured as a function of time. The minimum developed strain rate usually does not exceed $10^{-4}s^{-1}$. This type of test is called a creep test. For tests at constant strain rate the dependent variable is the developed stress. The applied rate of deformation is usually in the range 10^{-6} to $10^{3}s^{-1}$. There are four modes of deformation that use constant strain rates. These are torsion, tension, and plane strain and axi-symmetric compression. Since only the latter mode was used in this investigation we will limit our discussion to results obtained in this way.

During axi-symmetric compression at constant true strain rates, two types of flow curves may be obtained. These are illustrated in Figure 2.1. The metals that exhibit the first type of behaviour (Figure 2.1a) include zirconium (4-8), α-iron (9-12), ferritic alloys (9,11,13-20), aluminium (9,21-24) and its alloys (25,26) and zinc (27). For these metals the flow stress increases monotonically with strain up to some limiting value, the steady state stress. This type of curve has been shown to be produced when dynamic recovery is the only operative restoration process during flow (11). The second type of behaviour is exemplified by Figure 2.1b and is typical of metals such as nickel (23,29,30) and nickel-based alloys (29-31), copper (23,29,99), γ-iron (36) and austenitic alloys (14-18). Here the stress peaks prior to the onset of steady state flow. At higher temperatures and lower strain rates there may be several damped oscillations of the stress

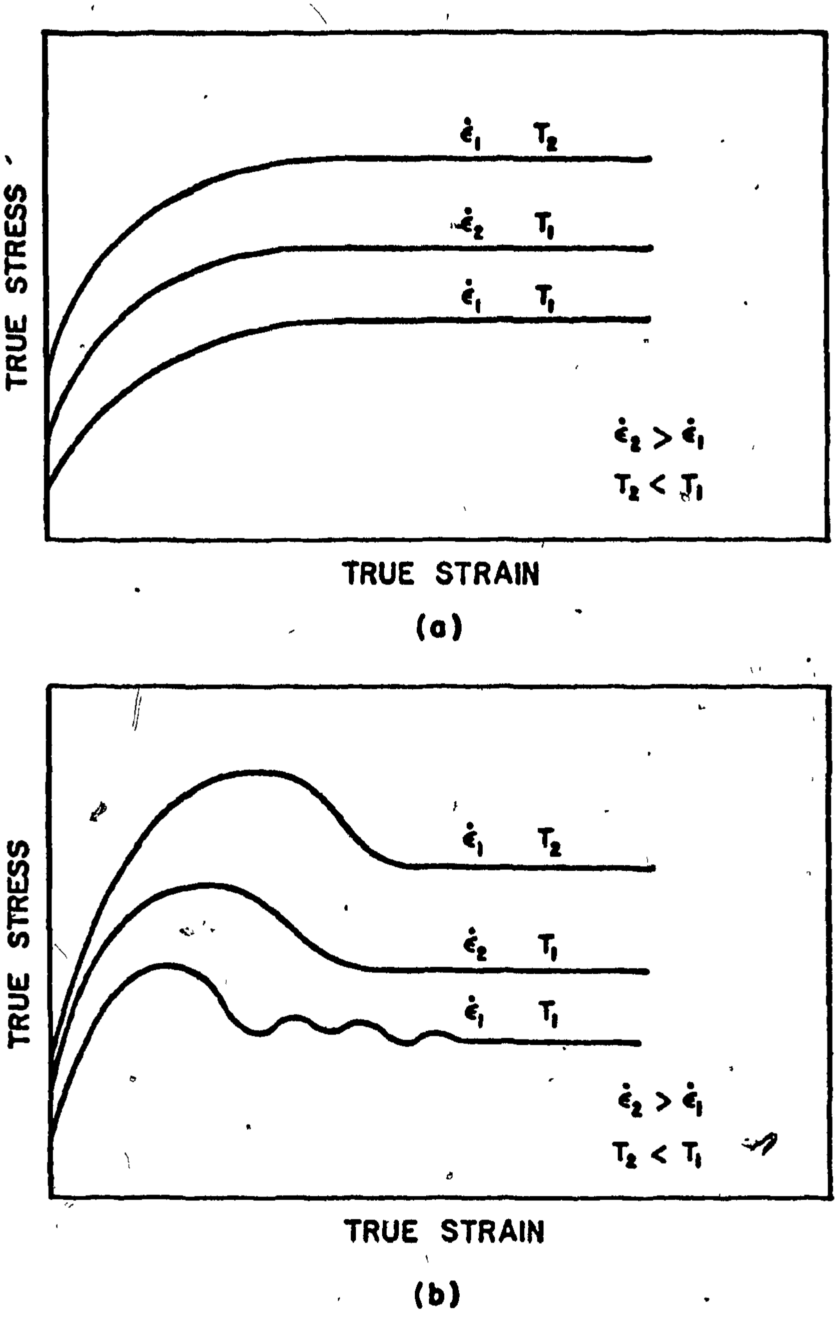

FIGURE 2.1 Constant strain rate flow curves:

a) Curves typical of materials that recover dynamically

b) Curves typical of materials that recrystallize dynamically before steady state flow is established (29). The strain to the peak is dependent upon temperature and strain rate; and, in addition, the peak height and its width are more pronounced at low temperatures and high strain rates (1,23). This type of flow behaviour has been shown to occur when dynamic recrystallization is the dominant softening process at strains superior to the peak value (1,29). Prior to the peak strain, dynamic recovery is the only restoration process.

Most of the previous experimental work has been carried out by means of creep testing, and hence the majority of the theories of high temperature flow were formulated to explain creep data. This means that in all of the equations that follow the stress rather than the strain rate will appear to be the independent variable. However, it should be kept in mind that in constant strain rate testing the stress is actually the dependent variable.

2.1.2 Empirical Flow Stress Relationships

Stress, temperature and strain rate are the three main parameters that influence high temperature deformation. In creep testing, stress and temperature have a major influence on the creep rate. Of course, the materials parameters will also affect the strain rate, but their precise influence is difficult to define. The stacking fault energy will add one component, the grain size another, but the largest contributions arise from the dislocation and the sub-boundary density. However, during steady-state creep it is usually assumed that the structure factor is constant.

Most metals exhibit similar temperature, as well as stress, dependencies that are described by empirically determined equations.

These relationships will now be presented.

2.1.2.1 Stress dependence of the strain rate

If the stress dependence of the steady-state creep rate is considered over a wide range of stresses, it is found that there are three types of stress dependencies (1,2).

At very low stresses, it has been observed that the steady-state creep rate, $\dot{\varepsilon}_s$, varies linearly with stress:

$$\dot{\varepsilon}_s = \alpha_1\sigma \tag{2.1}$$

At intermediate stresses the following relation is found to apply:

$$\dot{\varepsilon}_s = \alpha_2\sigma^n \tag{2.2}$$

At even higher stresses, the relation:

$$\dot{\varepsilon}_s = \alpha_3\exp(\alpha_4\sigma) \tag{2.3}$$

seems to best fit the data. In addition, it has been proposed that the two latter relations can be expressed by the equation:

$$\dot{\varepsilon}_s = \alpha_5\{\sinh(\alpha_6\sigma)\}^n \tag{2.4}$$

In these equations, the α's and n are stress-independent coefficients.

The intermediate stress region is usually the one of greatest interest. We will restrict our considerations to the simple power law that describes flow in this region (Equation 2.2). The stress exponent, n, usually has a value between 4 and 5 for pure metals and solid solutions. For precipitation hardened alloys the exponent is in the range 5-10. In dispersion hardened materials values up to 40 have been observed.

2.1.2.2 Temperature dependence of the strain rate

At elevated temperatures, deformation is a thermally activated process that can be represented by an equation of the type:

$$\dot{\varepsilon} = B \exp(-\frac{Q}{kT}) \qquad 2.5$$

where B is a function of σ and Q is the activation energy.

At high temperatures the activation energy does not vary with temperature or stress, and in creep it closely approaches the activation energy for self-diffusion. Under constant strain rate testing at high temperatures, however, Q seems to be stress dependent, indicating that the self-diffusion activation energy is probably a limiting case.

2.1.3 Models for High Temperature Deformation

Dislocation models of elevated temperature flow can be conveniently classified by whether recovery events or glide processes control dislocation motion. In glide controlled motion it is imagined that the dislocations move in a steady state manner, dragging pinning points along with them by diffusive processes. On the other hand, in recovery controlled processes, dislocation motion is considered to occur easily between barriers and pinning points, and then a separate recovery event is required for a dislocation to proceed and produce further strain. Without the recovery event, dislocations would glide to a barrier and stop. In the following section the dislocation glide theories are described.

2.1.3.1 Dislocation glide theories

The major glide theory is the jogged screw dislocation theory. The situation considered in this model is that of two dislocations of mixed or screw orientation that intersect to form a jog. Jogs on screw dislocations are always edge in character. If the screw dislocation moves, the jog cannot maintain its position in the dislocation by glide on its own slip plane. Therefore, in order for jogs to keep up with the dislocations they must move in a non-conservative manner by absorbing or emitting vacancies. This gives rise to a chemical force due to the deviation of the vacancy concentration from equilibrium. The chemical forces per unit length, f, on a vacancy emitting (e) and a vacancy absorbing (a) jog are given by

$$f_e = \frac{kT}{b^2} \ln \frac{C_e}{C_o} \qquad 2.6a$$

and

$$f_a = \frac{kT}{b^2} \ln \frac{C_o}{C_a} \qquad 2.6b$$

where C_o is the equilibrium vacancy concentration in a dislocation-free crystal, and C_a and C_e are the local concentrations near the jog. The steady-state velocities of the jogs, V, can be calculated from the concentration differences by using the equations,

$$V_e = 4\pi D_V b^2 (C_e - C_o) \tag{2.7a}$$

and

$$V_a = 4\pi D_V b^2 (C_a - C_o) \tag{2.7b}$$

where D_V is the diffusion coefficient for vacancies. By considering that the chemical force is balanced by a force, σbd, due to the applied stress, the jog velocities can now be expressed as

$$V_e = 4\pi b^2 C_o D_V \{\exp(\frac{\pi b^2 d}{kT}) - 1\} \tag{2.8a}$$

$$V_a = 4\pi b^2 C_o D_V \{1 - \exp(-\frac{\pi b^2 d}{kT})\} \tag{2.8b}$$

where d is the distance between jogs.

Barrett and Nix (37) related the jog velocities to the strain rate through the Orowan equation, and by assuming that the numbers of both types of jogs are equal they obtained the relation

$$\dot{\varepsilon} = BD_s \rho_m \sinh(\frac{\sigma b^2 d}{kT}) \tag{2.9}$$

where ρ_m is the mobile dislocation density and B is a constant.

The magnitude and stress dependence of ρ_m and d are not known. If it is assumed that they are not stress dependent then Equation 2.9 fits the empirical data reasonably well. For this type of model the activation enthalpy is of the order of the self-diffusion energy.

In a more recent treatment of this model, Nix (28) found that the strain rate was related to a hyperbolic tangent stress function similar to that shown in Equation 2.9, with the sinh replaced by a tanh function. However, the tanh law is not in agreement with experimental observations at high stresses.

2.1.3.2 Recovery-creep theories

The recovery-creep theories are based upon the knowledge that materials harden with strain and soften with time. According to this approach, under steady state,

$$\dot{\varepsilon}_s = (-\frac{\partial\sigma}{\partial t})/(\frac{\partial\sigma}{\partial\varepsilon}) = \dot{r}/h \qquad 2.10$$

where $\dot{r}$ is the recovery rate $(-\frac{\partial\sigma}{\partial t})$ and h is the strain hardening coefficient.

During the first stage of creep the dislocation density increases with strain, as does the rate of recovery, until a balance is reached between the recovery rate and work hardening. This process has been formulated by McLean (38) by means of the Arrhenius expression

$$\dot{\varepsilon} = \dot{\varepsilon}_0 \exp\{-\frac{bA(h\varepsilon - \dot{r}t)}{kT}\} \qquad 2.11$$

where $\dot{\varepsilon}_0$ is a pre-exponential factor similar to that in the rate equation for thermally activated flow.

Lagneborg (6) pointed out that this model is oversimplified because it treats h and $\dot{r}$ as constants. He proposed a model (39) that takes into account the increase in $\dot{r}$ and the decrease in h with strain. Furthermore, this model, in accord with direct observations, also considered the variation of $\dot{r}$ and h with the geometry of the three dimensional dislocation network. This network consists of a distribution of dislocation segment lengths that varies during creep as a result of three processes. First of all, dislocation links are released by the thermally activated unpinning of nodes in the network. This gives rise to a strain increment. The second event is work-hardening that occurs because new dislocation segments are created when the released links expand until they are arrested by the network. The last process is recovery, which Lagneborg postulated to occur by the growth of the large meshes in the network at the expense of the small ones. The shrinkage of the small meshes is expected to be climb-controlled. This model has been shown to be capable of describing the dislocation density-time and the strain-time behaviour of some stainless steels (39).

Weertman (32,33) has proposed a recovery model based upon the climb of dislocations. The situation that he considered is that of dislocations, generated at a source, which are subjected to strong interactions from pile-ups produced by neighbouring dislocation sources on parallel slip planes. This leads to the formation of pile-up groups on the adjacent planes, so that dislocation glide becomes inhibited. The stress acting on the leading dislocation in the pile-ups causes these dislocations to climb towards one another and become annihilated. Upon annihilation, the corresponding sources emit new dislocations and the old configuration is restored after an increment of strain. For such a process, the strain rate, $\dot{\varepsilon}$, can be expressed as

$$\dot{\varepsilon} = bAN_s\frac{\dot{C}}{g} \qquad 2.12$$

where $\dot{C}$ is the climb rate, g the distance between adjacent pile-up groups, N_s the number of dislocation sources, A the area swept out on the slip plane by the leading dislocation and b the Burgers vector. The dislocations climb at a rate controlled by the rate at which vacancies are supplied or removed, under the action of the applied stress and temperature, so that (32,33)

$$\dot{C} = \frac{2D_s\sigma^2Lb^4}{\mu kT} \qquad 2.13$$

where L is the length of the pile-up, D_s the self-diffusion coefficient, σ the stress, μ the shear modulus, k the Boltzman constant and T the temperature.

In order to determine the strain rate, it is necessary to estimate the climb distance, h. This can be obtained from the expression, $\sigma = \mu b/4\pi h$, where σ is the stress required to force two parallel dislocations past each other. In addition, the length of the pile-up groups, L, is required. It can be shown that L^2 is proportional to σ. With these estimates the relationship between strain rate, stress and temperature under steady-state conditions is:

$$\dot{\varepsilon} = \frac{BD_s\sigma^{4.5}}{b^{1/2}N_s^{1/2}\mu^{3.5}kT} \qquad 2.14$$

where B is a numerical constant ≈ 0.2.

The stress exponent in Equation 2.14 is in close agreement with experimental observations in pure metals and some solid solutions (6). However, many of the assumptions tend to make this equation less than attractive. First of all, in order to obtain a stress exponent of 4.5 the stress dependence of N_s was neglected. In fact, it seems likely that N_s would increase with stress. Furthermore, the stress dependence assigned to L can also be questioned. Also, the dislocation pile-ups, which are the basis of this theory, have never been observed in crept metals. On the other hand, the activation enthalpy predicted by this model is that of self-diffusion. This agrees well with enthalpies determined from creep data for cubic metals, but the agreement is poor in the case of hexagonal close packed metals.

2.2 THE THERMODYNAMIC APPROACH TO THE ANALYSIS OF HIGH TEMPERATURE DEFORMATION

The empirical flow stress relationships are of little use in throwing some light on the rate controlling mechanisms of plastic flow. The dislocation models described earlier are too mechanistic.

That is, a specific mechanism is assumed to be operative, and then various calculations are made to determine whether or not the assumptions give rise to the observed stress and temperature dependence of the strain rate. The thermodynamic approach, however, uses an analytical scheme that is based on a simple form of the rate equation and a simple model where the dislocations overcome unspecified local obstacles. The aim of the analysis is to yield various activation parameters which will aid the researcher in identifying the rate controlling obstacles to dislocation motion.

In the following section thermally activated dislocation glide and the appropriate form of the rate equation will be discussed. This will be followed by a review of the various analytical schemes and a brief discussion of the internal stress at elevated temperatures.

2.2.1 Thermally Activated Flow and Rate Theory

Some aspects of the observed behaviour of metals at high temperatures can be explained in terms of the thermally assisted motion of dislocations over localized obstacles.

Becker (50), as early as 1925, made the suggestion that plastic deformation could be a thermally activated process. Eyring (51) was the first to apply absolute rate theory to plastic deformation. However, these early theories were based on bulk-behaviour considerations. It was not until the advent of the theory of crystal dislocations that Kauzmann (52) and Seitz and Read (53) were able to formulate a general rate theory of plasticity based upon a "unit of flow", the motion a dislocation segment over a localized barrier. It is now generally accepted that the plastic deformation of crystalline solids can be a thermally activated process (43,45,46,54-65).

The obstacles to dislocation motion are due to the interaction of the stress fields of gliding dislocations with the stress fields of forest dislocations, parallel dislocations, the lattice, point defects, etc.. These interactions may be classified according to whether the range of the interaction is short or long. Short range interactions act over distances of a few Burgers vectors, while long range interactions may have an influence up to several hundred Burgers vectors. Some examples of various interactions that influence dislocation motion are shown in Table 2.1. Long range obstacles, in general, can be by-passed by gliding dislocations under the action of the applied stress alone. Temperature fluctuations play no role in this process and consequently long range obstacles have an athermal character.

Consider a material at a macroscopically measureable constant temperature. On the atomic scale there will always be thermal fluctuations. If these fluctuations are coherent they can assist the applied stress in moving dislocations past barriers (40). However, the probability of a coherent fluctuation varies as some inverse function of the distance over which the coherency exists. Consequently, these fluctuations can only assist dislocations in overcoming only relatively short range interactions. Furthermore, the energy available in a thermal fluctuation is relatively small and will only significantly reduce the energy that has to be supplied mechanically for low energy obstacles. The term "low energy obstacle" refers to those whose total strength is less than about 50 kT (35). Thus, the stress to bypass long range obstacles usually depends on temperature only through the

TABLE 2.1

Interactions Which Influence Dislocation Motion (after Altstetter (74))

Interaction of the gliding dislocation with:	range of interaction
1. the lattice	
a) Peierls-Nabarro forces	short
b) other	short
2. parallel dislocations	
a) isolated	long
b) pile-ups	long
c) dipoles	short
d) small angle boundaries	short or long
e) Cottrell-Lomer barriers	long
3. intersecting dislocations (forest)	
a) jog formation alone	short
b) non-conservative jog motion alone	short
c) reactions alone	short
d) stress fields alone	long
e) constriction of extended dislocations	short
4. point defects	
a) vacancies or interstitials (climb)	short or long
b) clusters of vacancies	long
c) dislocation loops and tetrahedra	short
d) solute atoms	short or long
e) ions	long
5. surface defects	
a) free surface	long
b) grain boundaries	short
c) small angle boundaries	short or long
d) twin boundaries	short or long
e) stacking faults	short
6. volume defects	
a) coherent second phases	long or short
b) non-coherent phases	long or short
c) short range order	short
d) long range order	short
e) G.-P. zones	long or short
f) atmospheres	long

shear modulus, while the stress to surmount short range barriers is strongly temperature dependent (41,43).

The rate at which a dislocation segment overcomes short range obstacles can be derived from rate theory in an intuitive manner (43). Cottrell (44) has suggested that the shear strain rate, $\dot{\gamma}$, produced by the glide of mobile dislocations of average velocity V is given by

$$\dot{\gamma} = \rho_m bV \qquad 2.15$$

The glide velocity is, in turn, determined by the rate at which thermal activation allows dislocation segments to overcome local barriers (45). For simplicity it is assumed that all of these local barriers have the same strength.. It then follows that V is given by

$$V = \nu\overline{P}(A/\ell) \qquad 2.16$$

Here ν is the frequency at which the segment attempts to overcome the obstacle, $\overline{P}$ the net probability of a successful thermal fluctuation in the forward direction of a dislocation segment of average length ℓ, and A is the average area swept out by a thermally activated segment (46). The net probability, $\overline{P}$, is the difference between the probability, P, of an activated jump in the forward direction and the probability, P', that it would subsequently make a jump in the opposite direction. Hence:

$$\overline{P} = P - P' \qquad 2.17$$

where P' is, in general, much less than P (43) and therefore $\overline{P} = P$.

Various authors (47-49) have shown that the probability, P_T, of a thermal fluctuation having an energy greater than a given value ΔG, at a temperature T, is given by the Boltzmann function of this energy; that is:

$$P_T = \exp(-\frac{\Delta G}{kT}) \qquad 2.18$$

If ΔG is the energy required to overcome the rate controlling obstacles, then $P_T = \overline{P}$. Combining Equations 2.15 and 2.16, we obtain

$$\dot{\gamma} = (\rho_m bA/\ell)\nu\overline{P} \qquad 2.19$$

Combining Equations 2.18 and 2.19 the rate equation is then obtained:

$$\dot{\gamma} = (\rho_m bA\nu/\ell)\exp(-\frac{\Delta G}{kT}) \qquad 2.20$$

In this investigation the mode of deformation is axi-symmetric compression and hence the measured strain rate is the normal strain rate, $\dot{\varepsilon}$, where $\dot{\varepsilon} = \dot{\gamma}/M$ (164). For polycrystals, M is the Taylor factor (105). Therefore, we may write Equation 2.20 as follows:

$$\dot{\varepsilon} = (\rho_m bA\nu/M\ell)\exp(-\frac{\Delta G}{kT}) \qquad 2.21$$

The factor $(\rho_m bA\nu/M\ell)$ is called the pre-exponential factor and will be denoted by the symbol $\dot{\varepsilon}_o$.

2.2.2 The Analytical Schemes

There are at present two schools of thought concerning the analysis of thermally activated glide. Gibbs (43,56-58) and Schoeck (55) have developed an analytical scheme in which the independent variables are temperature, T, and the applied shear stress, τ. Here, the thermodynamic system under consideration is the entire crystal (59). In an earlier approach, proposed by Basinski (54,66), and subsequently by Conrad and Wiedersich (67), and extended by Li (60,61,68) and Christian and Masters (69), the effective stress, τ^*, and T, were used as the independent variables. Here, $\tau^* = (\tau - \tau_i)$ is the local difference between the applied stress and the internal (athermal) stress, τ_i. In this analysis the system is not the entire crystal, but is, instead, a model sub-system which is the localized region about a dislocation reaction site (59). However, Hirth and Nix (62), Gibbs (59) and more recently Surek et al (63) have reviewed the two schemes and have demonstrated that they are self-consistent and mutually compatable as long as the thermodynamic parameters are consistently defined in terms of τ or τ^*. The compatability conditions between the two approaches have been derived by these authors.

In Equation 2.21, the symbol used to denote the energy required to overcome the rate controlling obstacle was ΔG, which is the Gibbs free energy change during activation. Originally, it was thought that the activation entropy, ΔS, was negligible, and consequently activation enthalpy, ΔH, was used in place of ΔG in the rate equation (6). However, various authors, Gibbs (43), Evans and Rawlings (70), Schoek (55), and Hirth and Nix (62) have shown that for a rigorous analysis, ΔS cannot be neglected. Luton and Jonas and co-workers (71-73) have demonstrated the importance of ΔS in rationalizing experimental results. In addition, Surek et al (63) have shown that there are some important inconsistancies in the Schoeck analysis (55), and have developed a systematic analytical scheme for analysing experimental data in terms of the effective stress. This scheme has been used successfully to analyze deformation on Armco iron and silicon steel (5,75), polycrystalline zirconium (64,76), polycrystalline ice (76) and magnesium single crystals (76). Therefore, this analysis was chosen as the most suitable to interpret the data in the present work and will be reviewed here. Before describing the analytical scheme its thermodynamic basis will be presented.

2.2.2.1 The thermodynamic basis

The basis of the thermodynamic analysis of high temperature flow rests on the thermodynamic description of the obstacle-dislocation interaction.

The first law of thermodynamics states that

$$U = H_a - W \qquad 2.22$$

and

$$H = U + pV_o \qquad 2.23$$

where U is the internal energy of the system, H_a the heat absorbed by the system, W the work done by the system, H the enthalpy and p and V_o are the pressure and volume, respectively. Furthermore, the Gibbs free energy, G, and the Helmholtz free energy, F, of the system, are defined in the usual way, as follows:

$$G = H - TS \tag{2.24}$$

$$F = U - TS \tag{2.25}$$

where S is the entropy. The Gibbs function is particularly well suited to the study of isothermal, isobaric systems, and can, therefore, be applied to plastic deformation (77). In plastic flow the free energy of the crystalline system is given as (78,79):

$$G = U - TS \quad pV_o - \sigma\varepsilon - \gamma_s A_e - \ldots \tag{2.26}$$

where γ_s, A_e, σ and ε are respectively the surface energy, area, applied stress and strain of the system.

It is possible to ascribe a free energy change to the system when the dislocation segment is activated over a localized obstacle to glide. The Gibbs free energy change, ΔG, can be associated with this obstacle. The back stress, τ_b, exerted by the obstacle on a dislocation segment of length ℓ is related to the Helmholtz free energy of the interaction, F, at zero effective stress by the relation

$$\tau_b = \frac{1}{b}\left(\frac{\partial F}{\partial A}\right)_\ell \tag{2.27}$$

Here, $A = \ell x$ is the area swept out by a dislocation when it moves a distance x along the slip plane. This is shown schematically in Figure 2.2. When an effective stress is applied to the system, the dislocation segment moves until τ^* is balanced by the back stress, that is, it moves from its zero stress equilibrium position, A_1, to the new stable position A_1^*; here it is assumed that the effective stress is acting from left to right. The position A_2^* is unstable, so that once the segment moves from A_1^* to A_2^* by means of a sufficiently large thermal fluctuation it will continue to move until it is once more opposed by an equal back stress. Due to the localized nature of thermally activatable obstacles under consideration, when the dislocation reaches another barrier it is no longer influenced by the back stress of the previous barrier; that is, the obstacles are considered to be widely separated. The free energy profile corresponding to the interaction when the dislocation is at the position A_1^*, is represented by the curve G_a in Figure 2.2. The Helmholtz free energy change associated with the reversible motion of a dislocation from A_1^* to A_2^*, given by

$$\Delta F_i = b\int_{A_1^*(T,\tau^*)}^{A_2^*(T,\tau^*)} \tau_b(A,T)dA \qquad 2.28$$

The work done by the effective stress during this event is represented by the cross-hatched area, ΔW, and is given by

$$\Delta W = b\tau^*A^*(T,\tau^*) \qquad 2.29$$

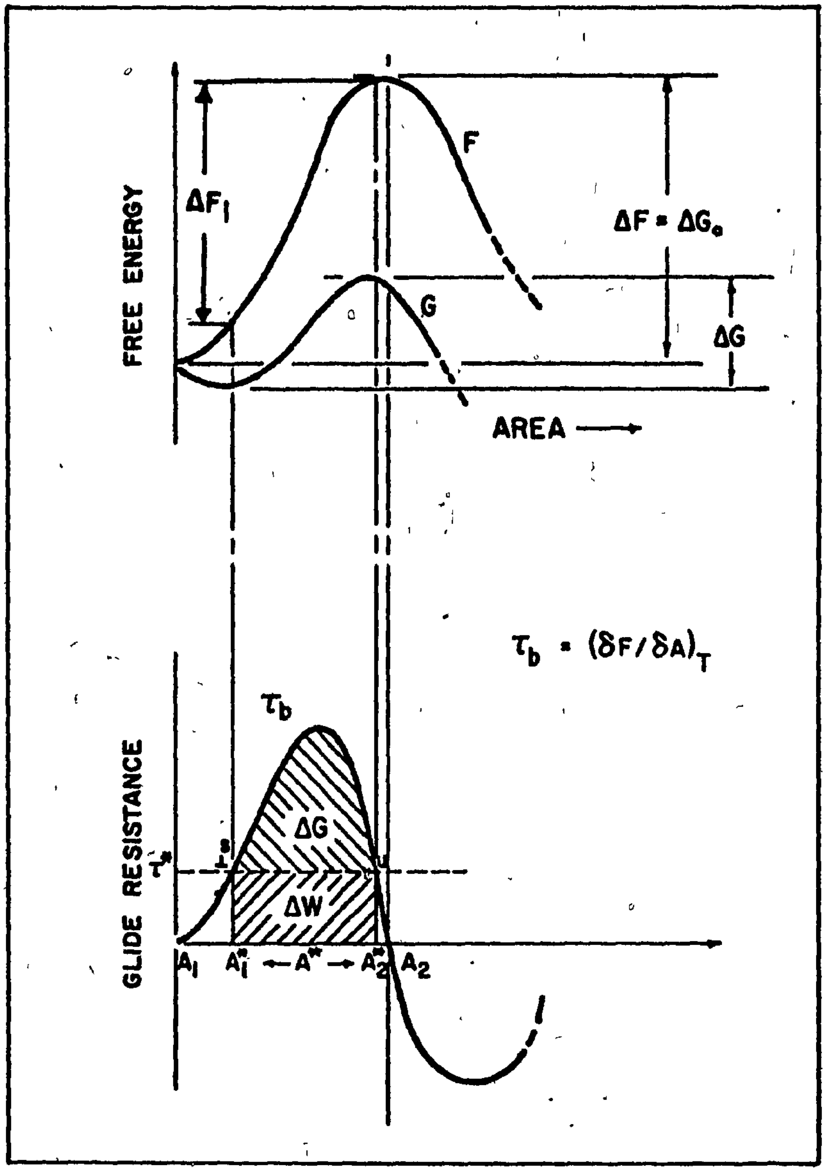

FIGURE 2.2 Schematic representation of the dislocation-obstacle interaction:

a) The Helmholtz free energy (F) and the Gibbs free energy (G) as a function of the area swept by the dislocation

b) The back stress profile felt by the dislocation in the vicinity of the obstacle as a function of slipped area.

The Gibbs free energy change during activation is $\Delta G = \Delta F_i - \Delta W$, and is therefore

$$\Delta G = b\int_{A_1^*(T,\tau^*)}^{A_2^*(T,\tau^*)} \tau_b(A,T)dA - b\tau^*A^*(T,\tau^*) \qquad 2.30$$

or

$$\Delta G = \Delta F_i(T,\tau^*) - b\tau^*A^*(T,\tau^*) \qquad 2.31$$

$A^*(T,\tau^*) = A_2^* - A_1^*$ is defined as the activation area and $V^*(T,\tau^*) = bA^*$ is the so-called activation volume.

In the case of "linear elastic" obstacles[†] it is assumed that the temperature dependence of the obstacle back stress is similar to that of the shear modulus, μ, that is, (63)

$$\tau_b(T) = g(A) \cdot \mu(T) \qquad 2.32$$

where g(A) is a shape factor determined by the shape of the free energy barrier, F. Consequently, the first term on the right-hand side of Equation 2.30 includes the linear elastic contributions which can arise from partition function terms in the equilibrium and activated states. In addition, the non-linear elastic contribu-

---

[†] Linear elastic obstacles are "rigid" ($\tau_b \neq \tau_b(\tau^*)$) and τ_b has a temperature dependence similar to the shear modulus (Equation 2.32).

tions have been neglected (63).

The temperature and stress dependence of ΔF_i and A* makes an estimation of ΔG very difficult. However, if we follow Surek et al (63) in using the formulism of Li (61) we can write

$$\Delta G = \Delta F_o(T) - b\bar{A}\tau^* \qquad 2.33$$

where

$$\bar{A}(T,\tau^*) = \frac{1}{\tau^*}\int_o^{\tau^*} A^*(T,\tau^*)d\tau^* \qquad 2.34$$

and

$$\Delta F_o(T) = b\int_{A_1(T)}^{A_2(T)} \tau_b(A,T)dA \qquad 2.35$$

ΔF_o is the total reversible work required to overcome an obstacle without the aid of external stress. This is an intrinsic property that is characteristic of the barrier-dislocation interaction, and is, therefore, the quantity that must be derived in order to determine the nature of the obstacles that control dislocation glide. The notation of Surek et al (63) will be used, so that ΔF_o, the total free energy of activation, is called ΔG_o. It is implicit in the basic assumptions of these authors that the obstacles are rigid. For "non-rigid" barriers, Equations 2.34 and 2.35 would have to be derived for some $\tau_b'(A,T,\tau^*)$ replacing $\tau_b(A,T)$.

If the obstacles are linear elastic (that is, rigid) then (63)

$$\Delta F_0(T) = \Delta G_0(T) = \text{constant} \cdot \mu(T) \qquad 2.36$$

which arises from the assumption expressed in Equation 2.32. Having completely described the obstacle-dislocation interaction in this way, it is possible to determine the relationships between the activation parameters.

2.2.2.2 The activation parameters in terms of the effective stress

The activation enthalpy and entropy are given by the following thermodynamic relationships (63,77)

$$\Delta H_{\tau^*} = \left\{\frac{\partial(\Delta G/T)}{\partial(1/T)}\right\}_{\tau^*} \qquad 2.37$$

$$\Delta S_{\tau^*} = -\left(\frac{\partial \Delta G}{\partial T}\right)_{\tau^*} \qquad 2.38$$

The activation area and volume are defined as follows (63):

$$V^*_{\tau^*} = bA^*_{\tau^*} = -\left(\frac{\partial \Delta G}{\partial \tau^*}\right)_T \qquad 2.39$$

Surek et al (63) have derived an equation for ΔG using Equations 2.31, 2.32, 2.36 and 2.38 and the standard thermodynamic relationship $\Delta G = \Delta H^* - T\Delta S^*$. They found ΔG to be

$$\Delta G = \frac{\Delta H_{\tau^*} + bA^*\tau^* \frac{T}{\mu}\frac{d\mu}{dT}}{1 - \frac{T}{\mu}\frac{d\mu}{dT}} \qquad 2.40$$

in agreement with Schoeck's (55) equation 12b. It should be noted that Equation 2.40 is an intrinsic property of linear elastic interactions.

In order to determine the activation parameters in terms of experimental quantities, the rate equation must be used. Rearranging Equation 2.21, the Gibbs free energy of activation can be expressed as

$$\Delta G(T,\tau^*) = - kT\ln(\dot{\varepsilon}(T,\tau^*)/\dot{\varepsilon}_0(T,\tau^*)) \qquad 2.41$$

where the dependencies of the variables are included. Combining Equation 2.41 with Equations 2.37 to 2.39 we obtain the following definitions for the parameters:

$$\Delta H_{\tau^*} = - k\left(\frac{\partial \ln\dot{\varepsilon}}{\partial 1/T}\right)_{\tau^*} + k\left(\frac{\partial \ln\dot{\varepsilon}_0}{\partial 1/T}\right)_{\tau^*} \qquad 2.42$$

$$\Delta S_{\tau^*} = k\ln(\dot{\varepsilon}/\dot{\varepsilon}_0) + kT\left(\frac{\partial \ln\dot{\varepsilon}}{\partial T}\right)_{\tau^*} - kT\left(\frac{\partial \ln\dot{\varepsilon}_0}{\partial T}\right)_{\tau^*} \qquad 2.43$$

and

$$V^*_{\tau^*} = - kT\left(\frac{\partial \ln\dot{\varepsilon}}{\partial \tau^*}\right)_T - kT\left(\frac{\partial \ln\dot{\varepsilon}_0}{\partial \tau^*}\right)_T \qquad 2.44$$

Since the activation entropy is not negligible (43,55,62,70-73) it must be included in the calculation of ΔG. The Gibbs free energy of activation is related to the entropy by the equation

$$\Delta G = \Delta H_{\tau^*} - T\Delta S_{\tau^*} \qquad 2.45$$

The problem with determining the activation parameters from experimental data lies in the fact that it is not possible to separate the dependence of the pre-exponential and the Gibbs free energy on temperature and the effective stress. Therefore, it is not possible to determine $\dot{\varepsilon}_o$ directly from experimental data (80). However, there are several approaches that have been developed to try and circumvent this problem.

i) Assume that the pre-exponential is constant, that is, independent of T and τ^*. Hence, Equations 2,42 and 2.44 reduce to give

$$\Delta H_{\tau^*} = -k\left(\frac{\partial \ln\dot{\varepsilon}}{\partial 1/T}\right)_{\tau^*} \qquad 2.46$$

and

$$V^*_{\tau^*} = kT\left(\frac{\partial \ln\dot{\varepsilon}}{\partial \tau^*}\right)_T \qquad 2.47$$

Therefore, ΔG can be determined in a straightforward manner from Equation 2.40. However, Immarigeon (5) has pointed out that many physical models imply a temperature and stress dependent pre-exponential, and therefore this assumption is not realistic.

ii) The pre-exponential can be estimated from a specific dislocation model (1,57,64) as in Equation 2.21. A problem arises, however, due to the uncertainty concerning the stress and temperature dependence of the mobile dislocation density, the segment length, the attempt frequency and the area swept out by the segment following a successful activation.

iii) Probably the most general and useful approach is to assume that $\dot{\varepsilon}_o$ is some function of τ^*/μ, the modulus-reduced effective stress. ΔG can then be calculated directly from Equation 2.40 once ΔH and A^* have been determined from Equations 2.42 and 2.44. By substituting these values of ΔG into the rate equation, it is then possible to obtain a matrix of $\dot{\varepsilon}_o$ values. These can then be tested for the validity of the original assumption. If the assumption is correct then the true activation parameters can be calculated directly since the stress and temperature dependence of $\dot{\varepsilon}_o$ is known. On the other hand, if $\dot{\varepsilon}_o$ is not a function of τ^*/μ only, then the iterative procedure proposed by Surek et al (64,76) can be tried.

2.2.2.3 Activation analysis in terms of the modulus-reduced effective stress

As has been shown in the previous section, a thermodynamic analysis in terms of the effective stress allows the rigorous determination of the activation parameters for the case of linear elastic obstacles. There is, however, a more direct route to these parameters.

Surek et al (76) have proposed a thermodynamic scheme of analysis in terms of the modulus-reduced effective stress, τ^*/μ. These authors have derived the compatability conditions which relate the respective parameters in the τ^* and τ^*/μ notations. This analysis will be presented here.

The first step in deriving the compatability conditions is to relate the functional dependencies of a common variable as is shown below. Rearranging Equation 2.21, we get

$$\ln(\dot{\varepsilon}/\dot{\varepsilon}_o) = -\Delta G/kT$$

In the τ^* notation $\ln(\dot{\varepsilon}/\dot{\varepsilon}_o) = f(T,\tau^*)$, while in the τ^*/μ notation $\ln(\dot{\varepsilon}/\dot{\varepsilon}_o) = g(T,\tau^*/\mu)$. In addition, $\tau^*/\mu = h(T,\tau^*)$. Taking the total differential of these functions, the following relations are obtained:

$$d(\ln(\dot{\varepsilon}/\dot{\varepsilon}_o)) = \left(\frac{\partial \ln(\dot{\varepsilon}/\dot{\varepsilon}_o)}{\partial T}\right)_{\tau^*/\mu} dT + \left(\frac{\partial \ln(\dot{\varepsilon}/\dot{\varepsilon}_o)}{\tau^*/\mu}\right)_T d(\tau^*/\mu) \quad .....2.48$$

$$d(\ln(\dot{\varepsilon}/\dot{\varepsilon}_o)) = \left(\frac{\partial \ln(\dot{\varepsilon}/\dot{\varepsilon}_o)}{\partial T}\right)_{\tau^*} dT + \left(\frac{\partial \ln(\dot{\varepsilon}/\dot{\varepsilon}_o)}{\partial \tau^*}\right)_T d\tau^* \quad .....2.49$$

and

$$d(\tau^*/\mu) = \left(\frac{\partial \tau^*/\mu}{\partial T}\right)_{\tau^*} dT + \left(\frac{\partial \tau^*/\mu}{\partial \tau^*}\right)_T d\tau^* \quad 2.50$$

These equations can be rearranged by equating Equations 2.48 and 2.49, and substituting Equation 2.50 for $d(\tau^*/\mu)$ in Equation 2.48, viz.,

$$\left(\frac{\partial \ln(\dot{\varepsilon}/\dot{\varepsilon}_o)}{\partial T}\right)_{\tau^*} dT + \left(\frac{\partial \ln(\dot{\varepsilon}/\dot{\varepsilon}_o)}{\partial \tau^*}\right)_T d\tau^*$$

$$= \left(\frac{\partial \ln(\dot{\varepsilon}/\dot{\varepsilon}_o)}{\partial T}\right)_{\tau^*/\mu} dT + \left(\frac{\partial \ln(\dot{\varepsilon}/\dot{\varepsilon}_o)}{\partial \tau^*/\mu}\right)_T \left\{\left(\frac{\partial \tau^*/\mu}{\partial T}\right)_{\tau^*} dT + \left(\frac{\partial \tau^*/\mu}{\partial \tau^*}\right)_T d\tau^*\right\} \quad .....2.51$$

This reduces simply to give

$$\left(\frac{\partial \ln(\dot{\varepsilon}/\dot{\varepsilon}_o)}{\partial T}\right)_{\tau^*} = \left(\frac{\partial \ln(\dot{\varepsilon}/\dot{\varepsilon}_o)}{\partial T}\right)_{\tau^*/\mu} + \left(\frac{\partial \ln(\dot{\varepsilon}/\dot{\varepsilon}_o)}{\partial \tau^*/\mu}\right)\left(\frac{\partial \tau^*/\mu}{\partial T}\right)_{\tau^*} \quad .....2.52$$

By differentiating Equation 2.50 with respect to τ^*, at constant τ^*/μ, it can be seen that

$$\left(\frac{\partial \tau^*/\mu}{\partial \tau^*}\right)_T \left(\frac{\partial T}{\partial \tau^*/\mu}\right)_{\tau^*} \left(\frac{\partial \tau^*}{\partial T}\right)_{\tau^*/\mu} = -1 \quad 2.53$$

Substituting Equation 2.53 in 2.52, it can be seen that

$$\left(\frac{\partial \ln(\dot{\varepsilon}/\dot{\varepsilon}_o)}{\partial T}\right)_{\tau^*/\mu} = \left(\frac{\partial \ln(\dot{\varepsilon}/\dot{\varepsilon}_o)}{\partial T}\right)_{\tau^*} + \left(\frac{\partial \ln(\dot{\varepsilon}/\dot{\varepsilon}_o)}{\partial \tau^*}\right)\left(\frac{\partial \tau^*}{\partial T}\right)_{\tau^*/\mu} \quad .....2.54$$

Equations 2.53 and 2.54 are the compatability conditions.

Since

$$\Delta H_{\tau^*/\mu} \equiv kT^2\left(\frac{\partial \ln(\dot{\varepsilon}/\dot{\varepsilon}_o)}{\partial T}\right)_{\tau^*/\mu} \quad 2.55$$

it can readily be shown that

$$\Delta H_{\tau^*/\mu} = \Delta H_{\tau^*} + V^*\tau^*\left(\frac{T}{\mu}\right)\left(\frac{d\mu}{dT}\right) \quad 2.56$$

Substituting this equation into Equation 2.40, an equation for ΔG is obtained:

$$\Delta G = \Delta H_{\tau^*/\mu}/\{1 - (\frac{T}{\mu})(\frac{d\mu}{dT})\} \qquad 2.57$$

An activation volume

$$V^*_{\tau/\mu} = -\frac{1}{\mu}(\frac{\partial \Delta G}{\partial \tau^*/\mu})_T = V^* \qquad 2.58$$

and activation entropy

$$\Delta S_{\tau/\mu} = -\frac{1}{\mu}(\frac{d\mu}{dT})\Delta G \qquad 2.59$$

can also be defined.

In order to analyse experimental data, an assumption has to be made regarding the stress and temperature dependence of the pre-exponential factor. Following the example of Surek et al (64,76), it is assumed that $\dot{\varepsilon}_o$ is some function of τ^*/μ only. In this instance, the activation parameters reduce to simple equations from which they can be deduced directly from data. For example, the equation for $\Delta H_{\tau^*/\mu}$ is

$$\Delta H_{\tau^*/\mu} = kT^2(\frac{\partial \ln \dot{\varepsilon}}{\partial T})_{\tau^*/\mu} \qquad 2.60$$

Similarly, ΔG, $\Delta S_{\tau^*/\mu}$ and V^* can be obtained from Equations 2.57 to 2.59. To check the assumption that $\dot{\varepsilon}_o = f(\tau^*/\mu)$, the back-substitution method described earlier is used.

It can be seen that in this scheme of analysis the activation enthalpy and free energy are obtained more readily than in the τ^* case.

In order to obtain the ΔH_{τ^*} value the correction term $V^*\tau^*(T/\mu)(d\mu/dT)$ must be subtracted as is shown in Equation 2.56.

The method described above will be used in the present work, the results of which will be presented below. Before an analysis can be carried out, however, it is necessary to separate the effective stress from the applied stress. In order to do this, some knowledge of the internal stress, τ_i, is required. This subject will be dealt with briefly in the following section.

2.2.2.4 The internal stress at elevated temperatures

The internal stress is that component of the flow stress that is athermal, that is, it is due to long range dislocation/dislocation interactions. It is now generally accepted that during constant strain rate testing at high temperatures, the strain hardening portion of the flow curve is partly caused by the build-up of a dislocation substructure that acts as an obstacle to dislocation motion (5,81). The internal stress is associated with either isolated dislocations of the network within the subgrains or with the cell boundaries themselves. Hence, as deformation proceeds the internal stress increases until it reaches its final value which is independent of strain. This occurs when a dynamic balance between the work hardening and the recovery rate is established. The analytical and experimental treatments of the internal stress are complicated, and there is still much confusion as to the actual magnitude of the stress. In the following section only a brief review of the subject, that pertains specifically to the present work, will be presented. For a more comprehensive review the reader is referred to Luton (4) and Immarigeon (5).

In the present work, yield stress data was used in the thermodynamic analysis. Luton (4) has shown qualitatively that it is reasonable to assume that the effective stress is much greater than the internal stress at the onset of macroscopic yielding. He argues that for zirconium and zirconium-tin alloys the yield stress, that is, the flow stress at 0.1% plastic strain, is approximately 70% of the steady state flow stress. If one assumes that the yield stress at high temperatures is negligible, and that the flow stress at all strains is equal to the internal stress introduced by the deformation, then this 70% of the steady state flow stress has to be developed in a plastic strain of 0.001. Since the flow stress is approximately proportional to the square root of the dislocation density, 50% of the steady state density must be introduced in this plastic strain interval. A 100 to 10,000-fold increase in dislocation density occurs from the initiation of plastic flow to the steady state. Thus a similar increase in density in the first 0.001 of plastic strain is required to explain the magnitude of the yield stress. Whereas, only a further two-fold increase in density is required to explain the additional increase in flow stress during the next 0.1 to 0.3 of strain. Thus, Luton concludes, this explanation of the flow curve is unlikely to be valid.

Luton goes on to argue that it is physically more realistic to consider the yield stress as being equal to the effective stress, since at the onset of macroscopic yielding the structure is much closer to that of the annealed material than to the steady state structure (88). In the present work it will therefore be assumed that the effective stress is equal to the macroscopic yield stress as defined by the stress at 0.1% plastic strain.

2.3 THE SHEAR MODULUS OF POLYCRYSTALLINE F.C.C. METALS

It has been shown in the preceding sections that in order to accurately evaluate the activation parameters from experimental data, it is necessary to have a knowledge of the appropriate shear modulus, μ, as well as its temperature dependence.

The shear modulus is defined as the constant of proportionality between the shear stress, τ, and the elastic shear strain, γ, viz.,

$$\tau = \mu\gamma \qquad 2.61$$

The modulii for metals are calculated from the elastic compliances and the elastic stiffness coefficients. These coefficients are the constants of proportionality in the generalized form of Hooke's Law. In order to show how these elastic constants arise mathematically, a brief review of the theory of the elasticity of crystals will be presented.

Essentially, no additions have been made to the mathematical theory of elasticity of isotropic crystals since the publication of Voigt's (82) treatise in 1928. He considered a small cube of material in a state of stress, and resolved this stress into its nine components so that the tractions, which act across all planes passing through a given point in the solid, could be completely specified. These components, shown in Figure 2.3, are

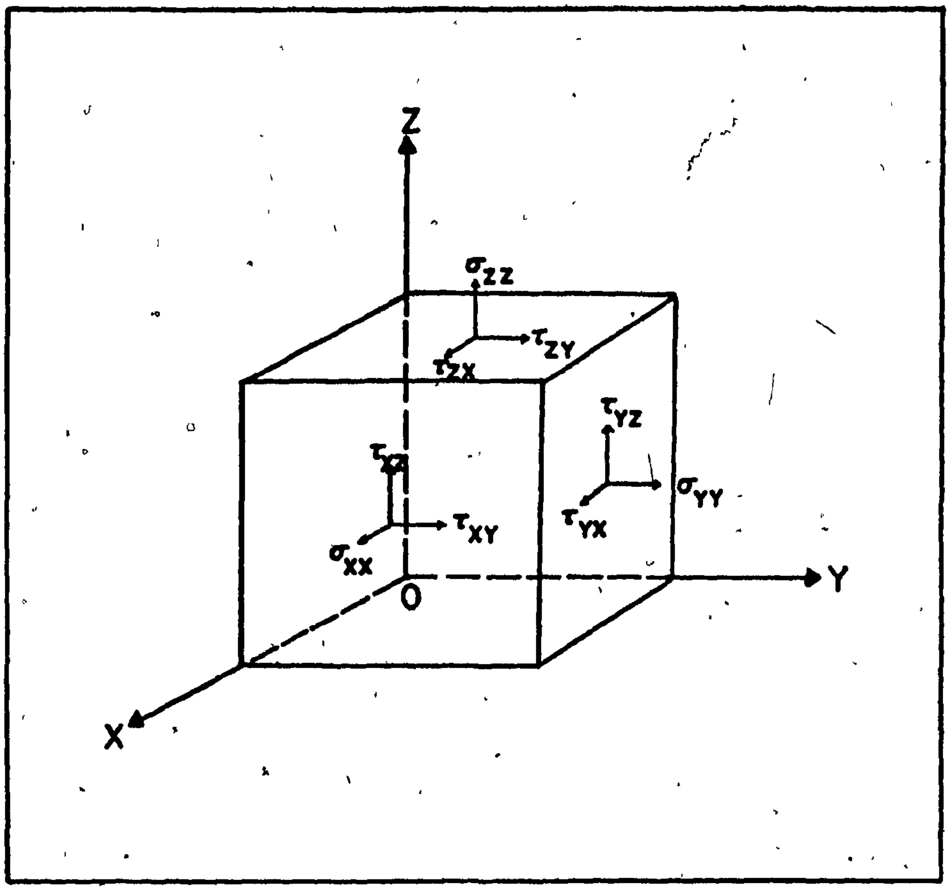

FIGURE 2.3 Stress components describing the general state of stress at a point, O.

$$\sigma_{xx} , \sigma_{yy} , \sigma_{zz}$$

$$\tau_{xy} , \tau_{yz} , \tau_{zx}$$

$$\tau_{yx} , \tau_{zy} , \tau_{xz}$$

According to this nomenclature, the first letter of the suffic denotes the plane of the stress and the second letter the direction in which it is acting. The tensile components, σ_{ij}, are all independent, while the six shear components, τ_{ij}, have only three independent components. This is because the shearing forces must balance so that no torque is applied to the element, that is, $\tau_{xy} = \tau_{yx}$, $\tau_{xz} = \tau_{zx}$ and $\tau_{yz} = \tau_{zy}$. Thus, there are a total of six independent stress components.

The concept of strain components was introduced to uniquely specify small deformations of the cube. The components of strain act in the direction of the stresses. There are six independent strain components:

$$\varepsilon_{xx} , \varepsilon_{yy} , \varepsilon_{zz}$$

$$\gamma_{xy} , \gamma_{yz} , \gamma_{zx}$$

The nomenclature of the suffixes is the same as that of the stress components.

The generalized form of Hooke's Law states that the stress components are linear functions of the strain components, viz.,

$$\begin{bmatrix} \sigma_{xx} \\ \sigma_{yy} \\ \sigma_{zz} \\ \tau_{xy} \\ \tau_{yz} \\ \tau_{zx} \end{bmatrix} = \begin{bmatrix} C_{11} & C_{12} & C_{13} & C_{14} & C_{15} & C_{16} \\ C_{21} & \cdot & \cdot & \cdot & \cdot & \cdot \\ C_{31} & \cdot & \cdot & \cdot & \cdot & \cdot \\ C_{41} & \cdot & C_{ij} & \cdot & \cdot & \cdot \\ C_{51} & \cdot & \cdot & \cdot & \cdot & \cdot \\ C_{61} & \cdot & \cdot & \cdot & \cdot & \cdot \end{bmatrix} \cdot \begin{bmatrix} \varepsilon_{xx} \\ \varepsilon_{yy} \\ \varepsilon_{zz} \\ \gamma_{yz} \\ \gamma_{zx} \\ \gamma_{xy} \end{bmatrix} \quad .....2.62$$

The constants, C_{ij}, are called the elastic stiffness constants. Conversely, the strain components are linear functions of the stress components:

$$\begin{bmatrix} \varepsilon_{xx} \\ \varepsilon_{yy} \\ \varepsilon_{zz} \\ \gamma_{xy} \\ \gamma_{yz} \\ \gamma_{zx} \end{bmatrix} = \begin{bmatrix} S_{11} & S_{12} & S_{13} & S_{14} & S_{15} & S_{16} \\ S_{21} & \cdot & \cdot & \cdot & \cdot & \cdot \\ S_{31} & \cdot & \cdot & \cdot & \cdot & \cdot \\ S_{41} & \cdot & S_{ij} & \cdot & \cdot & \cdot \\ S_{51} & \cdot & \cdot & \cdot & \cdot & \cdot \\ S_{61} & \cdot & \cdot & \cdot & \cdot & \cdot \end{bmatrix} \cdot \begin{bmatrix} \sigma_{xx} \\ \sigma_{yy} \\ \sigma_{zz} \\ \tau_{yz} \\ \tau_{zx} \\ \tau_{xy} \end{bmatrix} \quad .....2.63$$

The constants, S_{ij}, are the elastic compliances.

The matrix of the elastic compliances, (S), and the matrix of the elastic coefficients, (C), are the reciprocal of each other (83). In addition, symmetry conditions greatly reduce the number of necessary constants. In general (83),

$$C_{ij} = C_{ji} \qquad 2.64$$

and

$$S_{ij} = S_{ji} \qquad 2.65$$

Furthermore, the symmetry of the crystal under consideration reduces many of the constants to zero. Thus, for crystals of cubic symmetry each of the principal axes has a four-fold symmetry, and hence the following matrix of elastic coefficients is obtained (84,85):

$$\begin{bmatrix} C_{11} & C_{12} & C_{12} & 0 & 0 & 0 \\ C_{12} & C_{11} & C_{12} & 0 & 0 & 0 \\ C_{12} & C_{12} & C_{11} & 0 & 0 & 0 \\ 0 & 0 & 0 & C_{44} & 0 & 0 \\ 0 & 0 & 0 & 0 & C_{44} & 0 \\ 0 & 0 & 0 & 0 & 0 & C_{44} \end{bmatrix} \qquad 2.66$$

A similar matrix is obtained for the elastic compliances.

The elastic constants refer to single crystals. In polycrystalline materials there are many crystals all with different orientations with respect to each other. There are experimental and theoretical problems associated with the prediction of the elastic constants of a polycrystalline material on the basis of single crystal data. Experimentally, it is difficult to obtain truly isotropic samples as methods of preparation tend to give a texture to the specimen. The most isotropic samples are those with the smallest grain size. However, since the constants are measured by an ultrasonic technique, the smaller the grain size the greater the contributions due to the grain boundary relaxation effect and hence the greater the error in determining the constants. To try and circumvent these problems, compacted powders and sintered materials have been used which are truly isotropic. However, the densities of these materials are, in general, lower than ideal and this influences the elastic constants.

Theoretically, the problem arises in making the correct compromise between the assumption of uniform local stress (86) and uniform local strain (87). For f.c.c. polycrystalline metals the assumption of uniform local stress gives the Reuss Average, μ_R, for the shear modulus,

$$\mu_R = 5/(4S_{11} - 4S_{12} + 3S_{44}) \qquad 2.67$$

and, the assumption of uniform local strain gives the Voigt Average, μ_V,

$$\mu_V = (C_{11} - C_{12} + 3C_{44})/5 \qquad 2.68$$

However, it has been found empirically that the actual shear modulus of a randomly oriented polycrystal tends to cluster near the arithmetic mean of the Reuss and Voigt averages (84). This average is referred to as the Hill Average, μ_H, (89):

$$\mu_H = (\mu_V + \mu_R)/2 \qquad 2.69$$

The polycrystalline averages of Reuss and Voigt are the lower and upper bounds to the polycrystalline modulus. In the present work the Hill Average will be used as the polycrystalline shear modulus.

CHAPTER 3

EQUIPMENT AND EXPERIMENTAL PROCEDURE

3.1 MATERIAL PREPARATION

3.1.1 Material and Heat Treatment

The material used in this investigation was OFHC (oxygen-free high-conductivity) copper supplied by Noranda Metal Industries of Montreal, Quebec. The composition of the OFHC copper is given in Table 3.1. The as-received copper had been fully annealed and then cold drawn from 25.4 to 9.5 mm diameter rod in a single pass.

The plastic response of polycrystalline metals to deformation at high temperature is, in general, influenced by the initial grain size (13,90,91,96). It is, therefore, of the utmost importance to insure that all of the samples have the same grain size prior to being tested. Of particular importance at high temperatures is the effect of grain boundary sliding (92-95). Grain boundary sliding contributes to the overall specimen strain. Consequently, as the amount of sliding increases the bulk strain rate decreases and the flow stress is reduced. This, in turn, would influence the activation parameters derived from the data. The magnitude of the grain boundary contribution to the total strain depends upon the amount of grain boundary that is present in the specimen. The smaller the grain size the greater the grain boundary sliding contribution. Thus, in order to reduce the influence of sliding it is necessary to have a relatively coarse grain size. However, since this work pertains to the study of polycrystalline copper, the grain size must be small enough for there

TABLE 3.1

The Chemical Composition of the OFHC Copper used in this Investigation

Element	ppm
Pb	130.0
Ag	15.0
As	13.5
Ca	2.2
Fe	300.0
Mg	2.5
Mn	< 10.0
N	0.1
Ni	25.0
O	4.4
P	199.0
S	60.0
Zn	5.0
Si	< 10.0
Cu	Balance (≃ 99.922 wt%)

to be sufficient grains to ensure that the samples are truly polycrystalline. It has been found that if there are at least twenty grains per cross section (97), this condition would be satisfied.

Another factor to be taken into account is that the experiments were to be carried out at different temperatures. And further, that the samples were to be placed in the test machine and held for thirty minutes to allow the temperature to equilibriate before deformation. The initial grain size referred to in the previous paragraph pertains to the grain size at the start of deformation. Hence, the annealed grain size was required to be stable for at least thirty minutes at all the testing temperatures.

In order to determine the annealing conditions that would produce a grain size that meets these conditions, a set of annealing experiments were carried out.

To ensure that no contamination of the samples took place during annealing, a high vacuum annealing facility was constructed. The main features of the system are shown in Figure 3.1. The vacuum system consists of a fused silica tube (O.D. = 60 mm, I.D. = 51 mm) which was closed at one end. At the open end a fifteen centimetre length of clear crystalline quartz was attached and ground round in order to facilitate a good fit to the vacuum manifold. This fit was accomplished by means of a double 'O'-ring seal in a water cooled jacket. The jacket was attached to the manifold by means of a flange and an 'O'-ring seal. In addition, the manifold had four ports, one for a gas inlet, another for a high vacuum gage, a third for the vacuum pumps and finally the backplate, which could be removed to allow the samples to be inserted into or removed from the system.

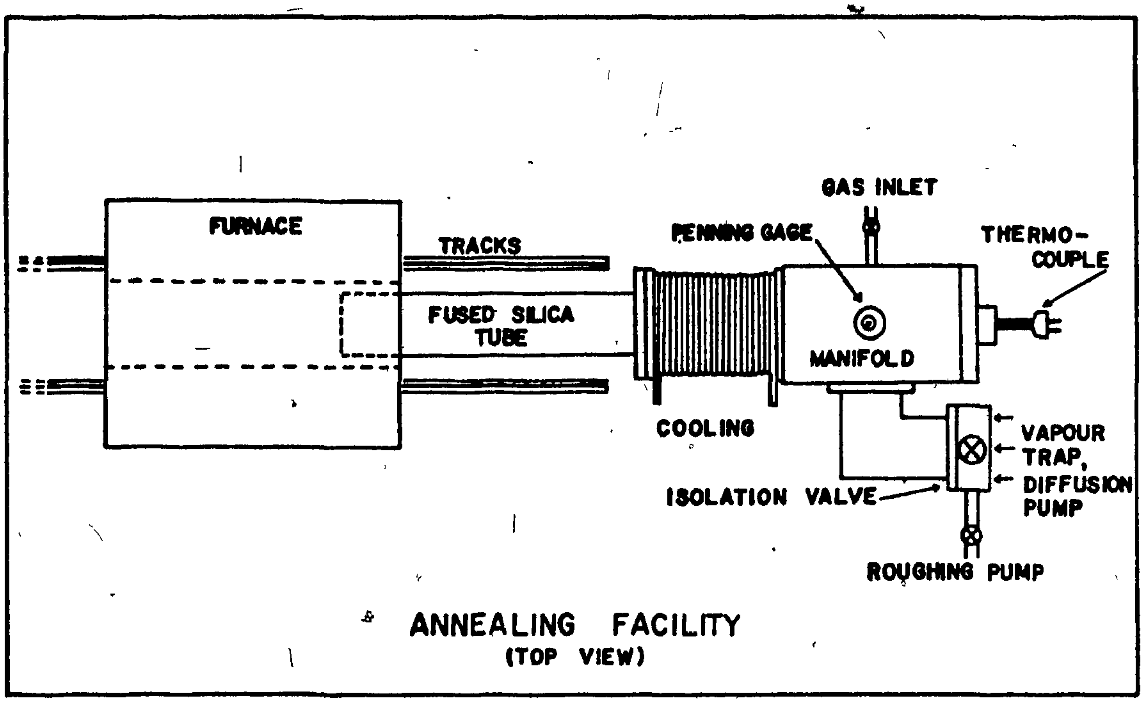

FIGURE 3.1 Schematic diagram of the annealing facility

Furthermore, the thermocouple seal was located in the backplate. The high vacuum was measured by means of a Penning gage (Model 6)[†]. The 50 mm diameter pumping port was connected to baffle isolation valve that isolated the diffusion system from the roughing pump[†] (Model CD-100). The roughing and backing vacuums were measured with a Pirani gage[†] (Model M7B). The diffusion system consisted of a liquid nitrogen vapour trap and a 25 mm oil diffusion pump[†] that used silicone oil*. The chromel-alumel thermocouple was enclosed in a 6 mm diameter closed end Inconel sheath and was long enough to reach the centre of the annealing tube. The sheath served not only to provide the thermocouple with mechanical strength, but also to make a good seal with the backplate. The high vacuum thermocouple seal allowed rotational and longitudinal motion of the thermocouple. This system was capable of maintaining a vacuum of 3×10^{-7} torr at room temperature.

The heating was achieved by means of a split Lindberg Hevi-Duty 3.4 KW furnace (Model 54352A) capable of continuous operation up to 1050°C. Temperature control was maintained by a Lindberg Model 59544 controller. The furnace was mounted on a trolley which ran on miniature railway tracks that allowed easy movement of the furnace onto and off of the annealing tube. When the furnace was rolled over the tube and up to the water cooled jacket, the centre of the furnace, that is, the constant temperature zone, was at the centre of the tube. During annealing tests, the system was flushed

---

[†] Supplied by Edwards High Vacuum Co.

* Type 704, supplied by Dow Corning Silicones Inter-America Ltd.

with argon and pumped down before the pre-heated furnace was rolled into position.

Using this equipment, a set of annealing experiments was carried out at 800°C. This temperature was selected as it was the maximum planned deformation temperature. It was assumed, therefore, that a grain structure that is stable at this temperature would be stable at lower temperatures. The as-received copper rods (9.5 mm diameter) were sectioned into samples approximately 20 mm long. Two samples were each annealed for one and two hours at 800°C. After annealing, the samples were sectioned in a plane transverse to the axis along which the cold drawing had taken place. The sections were then mounted in bakelite, ground and subsequently polished with alumina powder down to 0.3 microns. They were then etched* to reveal the grain boundaries.

The grain size of the samples was measured using the linear intercept method (98). Approximately three hundred grains were intersected per specimen. The mean intercept length was found to be 0.24 mm and 0.25 mm for the one and two hour anneals, respectively. This indicated that a one hour anneal produces a stable grain size. Furthermore, a grain size of 0.24 mm is coarse enough to make grain boundary sliding negligible, and is small enough so that the samples would behave as a polycrystal. For this grain size there are approximately forty grains across the cross section. Therefore, all the specimens that were prepared for mechanical testing were given an hour anneal

---

* Etching solution: 800 ml H_2O, 65 ml conc. H_2SO_4, 16 gms $K_2Cr_2O_7$ and 3 gms NaCl.

at 800°C in vacuum.

3.1.2 Specimen Geometry and Groove Design

The samples were machined from the available rods into right cylinders 13.1 mm high and 9.5 mm in diameter as shown in Figure 3.2. The diameter was chosen as large as possible so that the highest possible load would be developed during compression.

The end faces of the specimens were grooved in order to retain the glass lubricant used in high temperature axi-symmetric compression. The glasses and the temperature ranges of their applicability have been well documented by previous workers (4,5,8, 11,99) and will not be mentioned here. The groove geometry was based on the work of Luton (4), who found that flat bottomed grooves retained the lubricant the best. These grooves were machined by using a two teeth/mm thread chaser that had the top 16 μm ground off of the teeth, thereby producing grooves that are wider than the ridge between them.

3.2 TEST EQUIPMENT

The test equipment used in the present investigation is essentially the same as that described by Heritier (8), Immarigeon (5) and Petkovic-Luton (99). The only innovations made were in modifications to the data acquisition and control computer programs written by Luton, and a new data handling program. Consequently, only a brief description of the test hardware will be given, while the innovations will be described in detail.

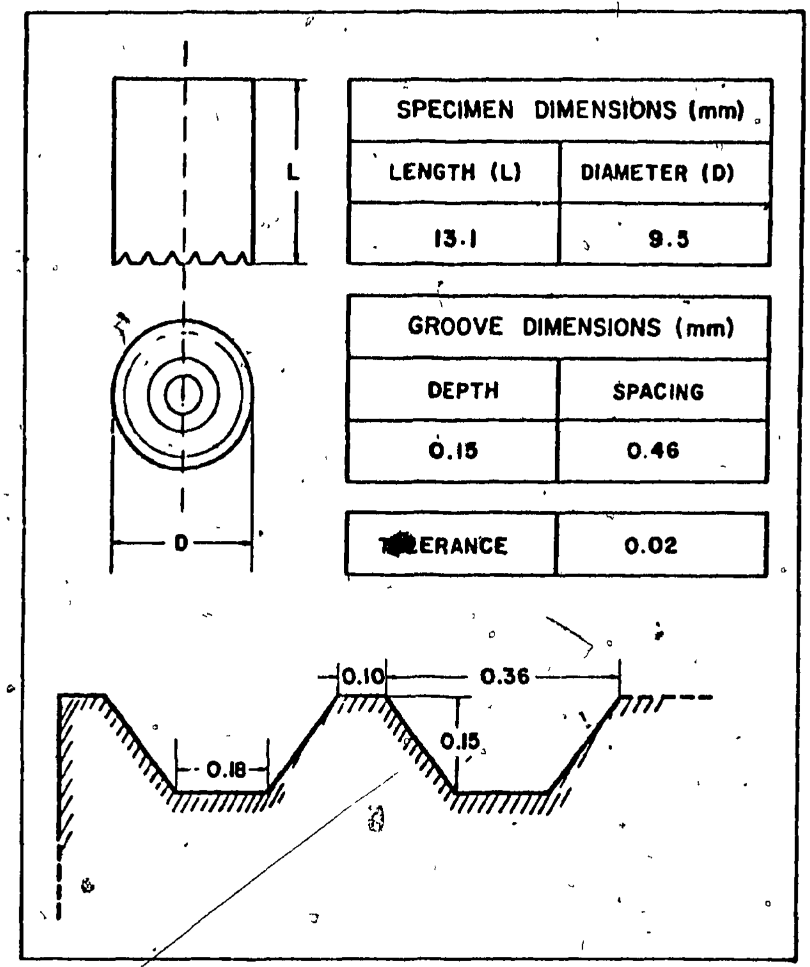

SPECIMEN DIMENSIONS (mm)	
LENGTH (L)	DIAMETER (D)
13.1	9.5

GROOVE DIMENSIONS (mm)	
DEPTH	SPACING
0.15	0.46

TOLERANCE	0.02

FIGURE 3.2 Specimen geometry and groove design

3.2.1 Testing Assembly

The basic machine in the testing assembly is a standard 10,000 Kg Instron testing frame (Model TT-D) that had been modified for high temperature, constant true strain rate axi-symmetric compression. The Instron was equipped with an extra decade speed reducer that produced a crosshead speed range of 50 cm/min to 0.005 cm/min.

A cross-section of the compression train within the furnace is given in Figure 3.3. The train consists of two loading members, the upper and the lower anvil and support. The water-cooled ram is connected to the crosshead, while the lower anvil rests on a water-cooled stainless steel base supported by a 2,000 Kg Lebow load cell (Model 3116). Incorporated into the design of the lower anvil is a quenching device which allows the test piece to be quenched within one or two seconds after the completion of the test.

The loading members are enclosed in an Inconel chamber which is sealed to the ram at the upper end and to the base support at the lower end. Both ends of the muffle are water cooled to allow the use of 'O'-ring assemblies. The upper seal is constructed so that the ram can [illegible]e independently of the muffle. The purpose of this retort is to permit the testing to be carried out in a controlled atmosphere over a wide range of temperatures. The muffle is surrounded by a Satec three-zone platinum-wound split furnace.

The two independent variables in uniaxial compression testing are temperature and strain rate. Furthermore, the testing environment also plays an important role in high temperature deformation (8). The control of these three parameters will be described briefly below.

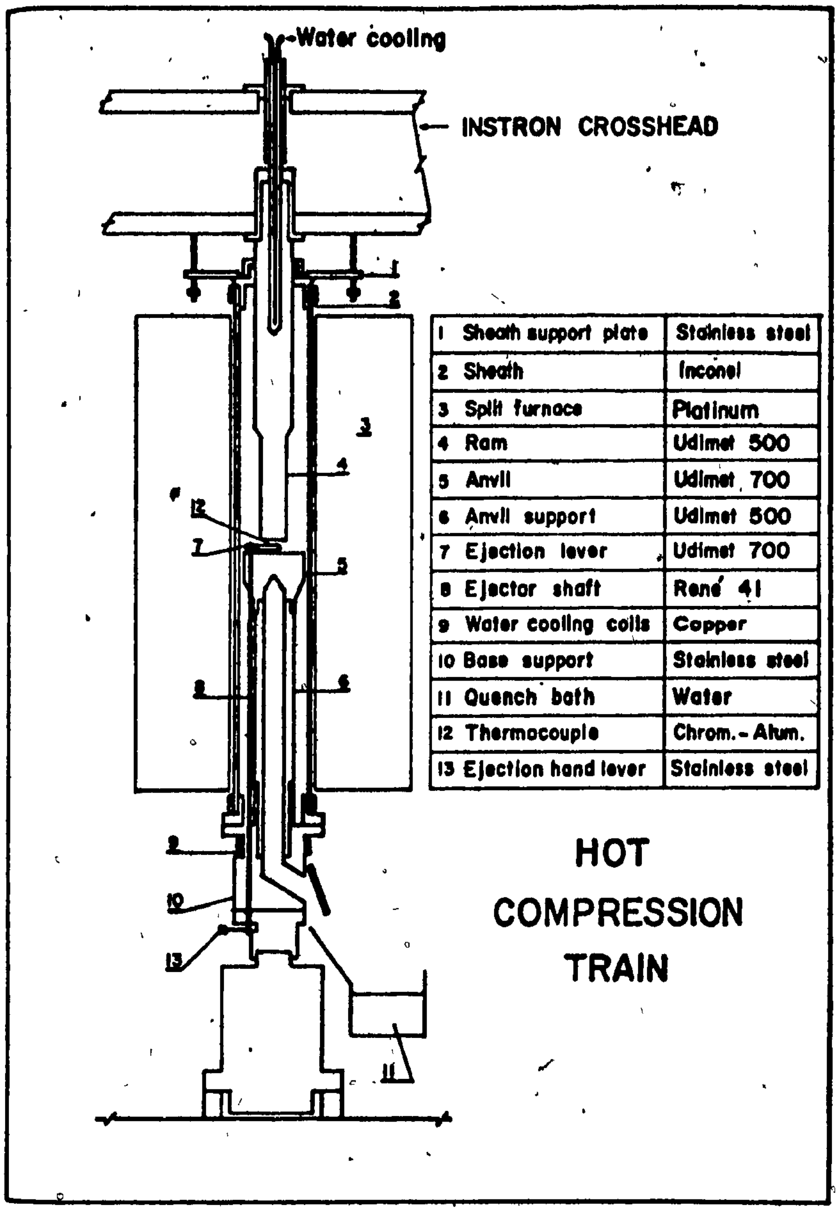

1 Sheath support plate	Stainless steel
2 Sheath	Inconel
3 Split furnace	Platinum
4 Ram	Udimet 500
5 Anvil	Udimet 700
6 Anvil support	Udimet 500
7 Ejection lever	Udimet 700
8 Ejector shaft	René 41
9 Water cooling coils	Copper
10 Base support	Stainless steel
11 Quench bath	Water
12 Thermocouple	Chrom.- Alum.
13 Ejection hand lever	Stainless steel

FIGURE 3.3 Schematic diagram of the hot compression train

3.2.2 Testing Environment

In order to prevent oxidation of the samples it was necessary to carry out the tests in an inert atmosphere. Although it is possible to operate the system under a vacuum, this was not done for several reasons. Firstly, atmospheric pressure acting on the rams would tend to produce a tensile force at the load cell. Secondly, it would be necessary to apply pressure to the 'O'-ring seal, thereby increasing friction and causing a compressive load at the load cell during loading. By using a small positive pressure of argon in the muffle there was no tensile load and no friction since the seal was not clamped.

To ensure that the inert shroud was established rapidly after the insertion of the specimen, the testing chamber was evacuated. A Precision Scientific (Model 75) two-stage rotary vacuum pump (75 l/min capacity) was used for this purpose. A vacuum of 5×10^{-2} torr could be reached within forty seconds, after which, high purity argon* was bled into the system. This procedure was repeated three times and then a positive pressure was maintained in the muffle by bubbling the gas through an oil trap.

---

* Supplied by Welding Products Ltd. Maximum impurities in ppm: O_2 = 0.1; N_2 = 23.0; H_2 = 2.0; CO_2 = 0.5; H_2O = 5.0; total hydrocarbon = 0.5. This was further purified by passing the gas through a catalytic and two drying towers (5,8,99).

3.2.3 Temperature Control

As mentioned earlier, the constant temperatures used in this work were obtained by the use of a three zone furnace. The temperature was controlled by a current proportioning Leeds and Northrup Electromax II controller, which drove three Magnetics Inc. SCR controllers in a master-slave configuration. The control thermocouples (Pt/Pt-13% Rh) were located in each of the three furnace zones. Since, during a test the sample is located near the middle of the furnace, only the central zone was controlled. Each zone was adjusted to give a uniform (± 2°C) temperature zone between the anvil ends.

The specimen temperature was measured by means of a chromel-alumel thermocouple that was attached to the lower anvil, on the same plane as the sample and about two centimetres away. The thermocouple was supplied in a superalloy sheath by Omega Ltd. The output from the thermocouple was measured by means of a John Fluke Co. digital multimeter (Model 8600A) with a resolution of 0.01 millivolts, which is equivalent to about 1/4°C.

3.2.4 Strain Rate Control

In a standard Instron the crosshead moves at a constant speed. But, in compression at a constant deformation rate, the strain rate would increase by a factor of 2.3 in a true strain interval of one (5). Since the flow stress of metals is highly strain rate dependent at elevated temperatures (101), uniaxial compression requires that the true strain rate be constant during a test. The present equipment was equipped with a device (100) that is used in conjunction with an Instron variable speed unit to produce a constant true strain rate. The design and use of this equipment is well documented (5,100) and will not be dealt with here. However, the performance of the apparatus will be discussed in as much as it influences the precision of the mechanical data.

Luton et al (100) have shown that with the constant true strain rate apparatus there can be a difference of 40% between the specimen strain rate and the nominal strain rate under initial loading conditions, for the fastest crosshead speed. However, for the slowest speed the strain rate difference is only of the order of 5%. Under steady state flow conditions the difference is generally less than 2%. These differences are due to the fact that the probe that indicates the change in gage length of the sample is attached to the moving crosshead. This was done because it is not possible to set up a reliable mechanical linkage from within the furnace and the environmental chamber. This means that because of the elastic deformation of the loading frame and the compression tools, the specimen strain rate is always lower than the nominal strain rate. At the onset of macroscopic yielding, that is, at 0.1% plastic strain, the error in strain rate is generally five times less than the error during the initial loading. In order to determine the influence of this strain rate error on the flow stress, the error is multiplied by the rate sensitivity of the material under test. Since the sensitivity at high temperatures is generally between 0.1 and 0.2, the flow stress error at 0.1% plastic strain due to this effect, is usually less than 1%.

3.3 TEST CONTROL AND DATA ACQUISITION

The test control and the data acquisition are divided into two segments: hardware and computer software. The hardware resides in two locations: the experimental equipment and the process control computer. This is illustrated schematically in Figure 3.4.

3.3.1 Hardware

Experimental equipment

The Instron controller is interfaced to a General Electric GE/PAC 4020 process control computer. The interface was designed to incorporate the normal modes of operation of the Instron, namely down, stop, return and normal, into the interface. The normal mode resets the machine for manual use so that the operator can carry out the initial setting up of the test manually. The interface consists of six relays which can be activated by the remote switches of the real time computer. In addition to this interface, the computer is also linked to the outputs of the load and displacement measuring devices.

As mentioned previously, the load is measured on a 2,000 Kg load cell while displacement is measured by a Hewlett-Packard (Model 7DCDT-500) displacement transducer with a range of ±1 cm, as primary elements. The core of the DCDT is attached to the crosshead and the coil to the Instron frame. These are located so that when the anvils are in contact, the core would be at its lowest position in the coil (-1 cm). Hence the maximum sample height that can be used with this set-up is approximately two centimeters. The load cell and the DCDT are excited by two Hewlett-Packard series 62000 dc power supplies. The low level output of the load cell, 15 mV/1000 Kg, is amplified

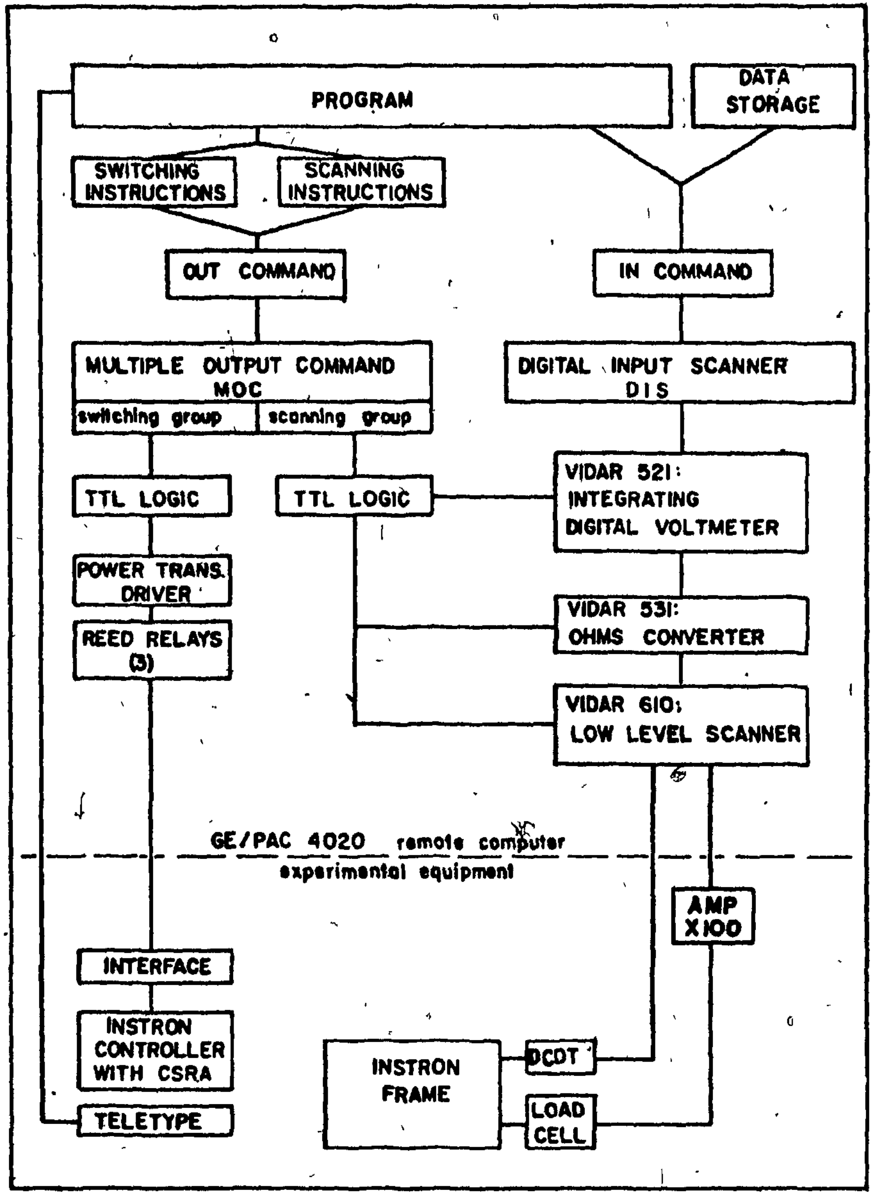

FIGURE 3.4 Block diagram illustrating the procedures for data acquisition and computer control

by a factor of one hundred using an Analog Devices 605 integrated amplifier. However, since the output of the DCDT is high level, 2.7 V/cm, it is connected directly to the computer. The two signals are transmitted to the computer via a 150 m length of communication cable[†] specially designed to minimize noise pickup.

Process control equipment

The hardware in the process control computer is shown schematically in Figure 3.4. The control interface on the Instron is linked to the switching group of the Multiple Output Controller (MOC) on the computer. An OUT* command at the MOC activates the TTL (transistor-to-transistor logic) logic which fires a power transistor that drives the reed relays. To switch the mode of operation a new OUT command is required. The decision when to switch the mode, is determined by the logic in the control software.

The analog outputs from the DCDT and the load cell amplifier are measured by the computer via an interface consisting of a multiplexed analog-to-digital converting system. The outputs are attached to a Vidar 610 low level scanner which is capable of sampling up to 1000 channels. The scanner is connected to a Vidar 531 ohms-converter or directly to a Vidar 521 integrating digital voltmeter. In order to scan a particular channel, the program sends an OUT command to the scanning group of the MOC. This then activates a TTL logic circuit that triggers the low level scanner, giving instructions as to what

---

[†] Manufactured by Northern Electric Co. Ltd.

* Pal language (General Electric assembler language)

function to scan (voltage), on what channel (load, for example), and on what range (one volt, for example). The logic circuit then arranges for the signal to bypass the ohms-converter and enter the voltmeter directly. The signal enters the computer at the digital input scanner (DIS) level. An IN command transfers the value of the signal to core memory. With this arrangement, channels cannot be scanned simultaneously. The shortest time possible between two scans is limited by the minimum integrating time of the voltmeter, 1.66 ms, and the time it takes to output the OUT command and generate the IN command. This all adds up to a maximum scan rate of fifty readings per second.

3.3.2 Software

Before presenting the control and data acquisition programs, a brief description of the operation of the GE/PAC 4020 computer will be given, so that the framework within which these programs were written can be appreciated.

Firstly, the GE/PAC 4020 is a process control computer and like most computers of this genre, all real time execution is done according to a system clock. That is, while a test is running, the software and hardware respond to events that are triggered by the system clock. However, since the GE/PAC operates on a time-sharing priority basis, other programs that are running concurrently may delay the scanning during the test. For the faster tests, in which time is critical, it is possible to make the system unavailable to users running from the cardreader or other remote devices. The maximum lockout time allowed by the management of the computing facility is ten minutes.

In addition, the available core size is 24,000 octal words. Therefore, any program written for this system must be smaller than this size. For efficient operation with concurrently running programs the size should be less than 15,000 octal words.

The original software to run the Instron and acquire data was written by Luton. It consisted of three programs that allowed the operator to run regular compression tests as well as interrupted tests (99). In addition, Luton wrote software to calibrate the Instron and to handle the data. The philosophy behind the acquisition programs was to divide the flow curve into two regions. Region I was from 0 to 0.1 true strain and region II was from 0.1 strain to the end of the test, usually at 0.7 or 0.8 strain. In region I, 80 to 120 data pairs were acquired at equal time intervals and, hence, equal strain intervals, provided that the strain rate was slow enough. If the strain rate was too fast, as many points as possible were obtained at the fastest scanning rate. In region II the same number of points were acquired but at a necessarily longer time interval between each reading. This philosophy has worked well (8,99). However, it was decided that since the present work requires an as exact as possible yield stress, and since the flow stress of copper exhibited oscillatory behaviour, the flow curve should be better defined by acquiring more data. Furthermore, the programs of Luton were very large and required up to 85% of the core when running. Therefore they were difficult to use when other users were running concurrently. As a result of these considerations, the author modified the programs to acquire more data and the two large programs were divided into four more manageable ones. The data acquisition philosophy of Luton was adopted, but in the new programs 120 to 160 points are acquired in region I and 360 to 400 points in region II.

3.3.3 Range of the Experimental Equipment

With the specimen size used in this investigation and the range of Instron crosshead speeds described earlier, the range of strain rates of the equipment is 6.7×10^{-6} to 0.67 s^{-1}. However, since the maximum data acquisition rate is only fifty readings per second, the fastest strain rate at which enough data points could be obtained to accurately define the macroscopic yield stress is $4.9\times10^{-2}s^{-1}$. Since the measured loads were always under 500 Kg in the present investigation, there was no danger of overloading the 2,000 Kg load cell.

The amount that a sample can be strained is limited by several factors. The first of these is the range of the displacement transducer which has already been shown to be ± 1 cm. Secondly, the probe on the constant strain rate device is also limited to a similar distance of travel. Therefore, the maximum sample height that can be accommodated in this equipment is two centimetres. The amount of deformation is only limited by the range of the load cell and by the influence of friction on the deformation behaviour of the specimen. It has been found that at strains greater than 0.8, barreling of the specimen becomes serious enough to cause gross inhomogeneity in the deformation.

3.4 EXPERIMENTAL PROCEDURE

Before starting a series of tests, the furnace was brought to temperature and allowed to reach equilibrium. Then the anvils were brought together and the reading of the DCDT was recorded by the computer for later use. With the anvils still in contact, various crosshead microswitches were adjusted so that accidental overloading of the equipment could not occur. In addition, since the anvils were in contact, this corresponds to an infinite amount of strain and therefore a strain rate of zero. Hence, this was used as a calibration point for the constant true strain rate device. The rest of the range of this device was calibrated by using a micrometer screw to simulate the motion of the crosshead. It was found that calibration of the strain rate equipment and the zero position of the DCDT was only necessary when the temperature was changed. This happened because these devices are very stable, even after a period of several days of continuous operation.

To initiate a test, the furnace and Inconel muffle were raised on the crosshead and the glass-coated sample placed on the lower anvil. The chamber was then closed as quickly as possible; and the system was successively evacuated and purged with argon. This procedure was repeated three times before a constant flow of argon was allowed to bubble through the oil trap. During the insertion of the sample, the temperature within the muffle dropped approximately 200 °C. Thirty minutes were allowed for the specimen to reach the test temperature and to stabilize at this temperature. In general, it took 15 to 20 minutes for the temperature to reach the test temperature. About 20 minutes after the sample had been inserted in the furnace the software operations were initiated.

Upon completion of the test, the sample was removed from the muffle via the quench hole in the lower anvil. This allowed specimens to be quenched within one or two seconds after the completion of a test.

3.5 DATA HANDLING

The data accumulated by the acquisition programs consists of the test parameters and an area with the voltage output from the load and displacement transducers, as well as the time at which each reading was taken. The full time stress-true strain curves were obtained by using a data handling program of Luton. By using the calibration factors for the transducers, the uniaxial force and the crosshead displacement were deduced from the raw data. However, since it is not possible to measure the actual displacement of the ram with respect to the lower anvil, the displacement readings had to be corrected for the distortion of the loading members. Previous users of this apparatus (4,5,8,99) have measured this distortion as a function of load, temperature and crosshead velocity. The results of these tests, reproduced from Petkovic-Luton (99), are shown in Figure 3.5. It is evident that the machine distortion, d_m, is not dependent on temperature or the crosshead speed. The data in Figure 3.5 fits an equation of the form:

$$d_m = B(F_o + C)^E - D \qquad 3.1$$

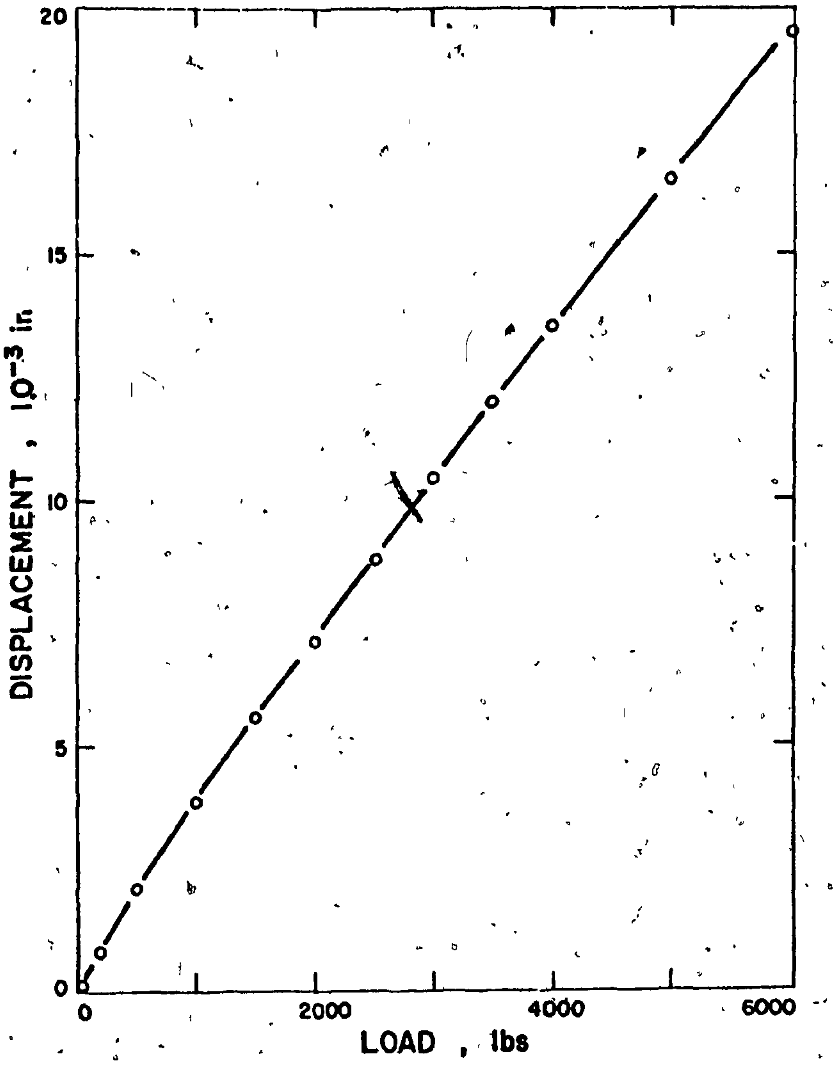

FIGURE 3.5 Elastic distortion of the Instron frame (after Petkovic-Luton (99))

where F_o is the instantaneous load and B, C, D, and E are constants. Therefore, the true instantaneous sample height, h_i, is given by:

$$h_i = h_o - d_{\text{[illegible]}} + d_m \qquad 3.2$$

where h_o is the initial sample height and d_i is the instantaneous crosshead displacement. The true strain, ε, is given by the expression

$$\varepsilon = - \ln\left[h_o/h_i\right] \qquad 3.3$$

and the true stress, σ, by

$$\sigma = F_o/A_i \qquad 3.4$$

where A_i is the cross-sectional area of the compressed sample at an instant i and is calculated from the relation

$$A_i = A_o h_o/h_i \qquad 3.5$$

Here A_o is the cross-sectional area of the undeformed specimen. This equation is based on the assumption that flow is homogeneous during compression.

The second operation of this data handling program was to plot the true stress-true strain data on an on-line California Computers digital Calcomp plotter. The curve was defined by plotting the actual stress-strain data pairs. Two curves were plotted; the full stress-strain curve and an expanded plot of the initial loading region, as shown in Figure 3.6. The yield stress was determined by using the expanded plot. It was defined by the use of the offset method (102) as illustrated schematically in Figure 3.7. The interval OM is the specified offset of 0.002 strain in this case. The line MN is drawn parallel to the initial loading line OA. The stress at which MN intersects the flow curve is defined as the yield stress.

The problem with the above approach is that it is too prone to error. Firstly, as can be seen from Figure 3.6b, there is some scatter in the data. Since the yield is very sensitive to the slope of the loading line, this scatter can lead to an uncertainty of ± 10% in the yield value. Furthermore, human bias can influence the placing of the loading line. Secondly, the load and the strain readings were not taken simultaneously. In the treatment of Luton the time difference was assumed to be negligible. This assumption is correct when the time between each data reading is long, that is, at slow scanning rates. However, at high scanning rates the assumption is not valid and the time difference must be taken into account. Finally, the actual strain rate can be calculated from the strain-time readings, providing additional precision for the data to be used in the activation analysis.

Based on these considerations, the author wrote a program, YIELD, that takes the data from the bulk storage and calculates the actual true strain rate and the yield stress. In addition, plots of the work-hardening versus stress up to the first peak, and an expanded plot of the yield region are drawn. A listing of the program, which is written for the GE/PAC computer, is presented in Appendix I. The sequence of operations that take place are illustrated by the block diagram shown in Figure 3.8.

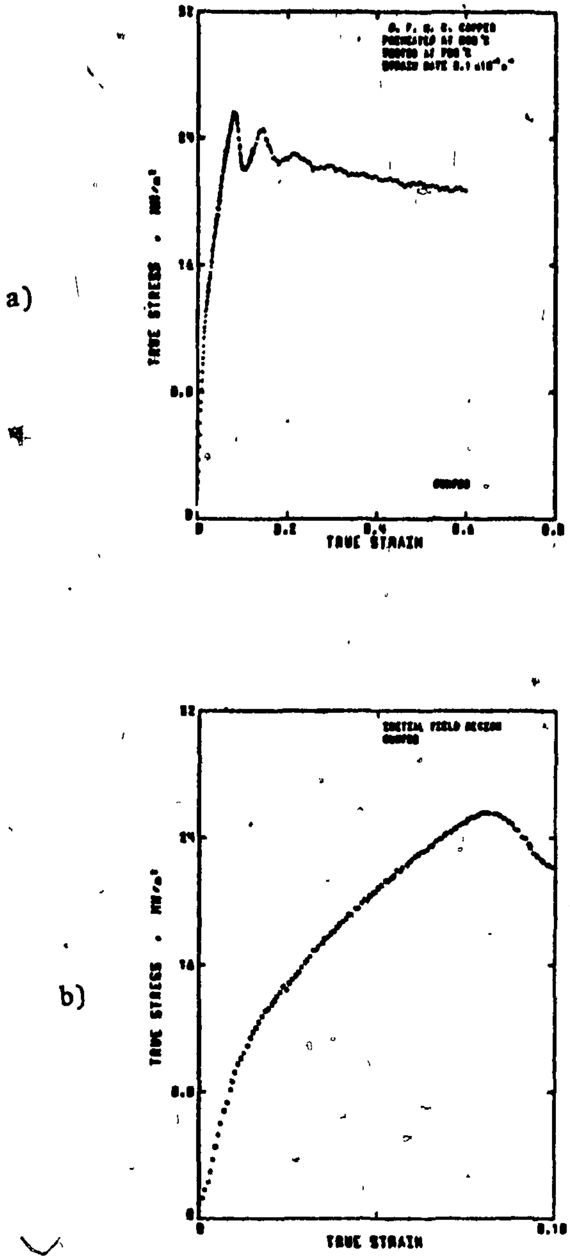

FIGURE 3.6 Typical plots from the data handling program of Luton

a) full stress-strain curve of OFHC copper

b) expanded plot of the initial loading region of plot (a)

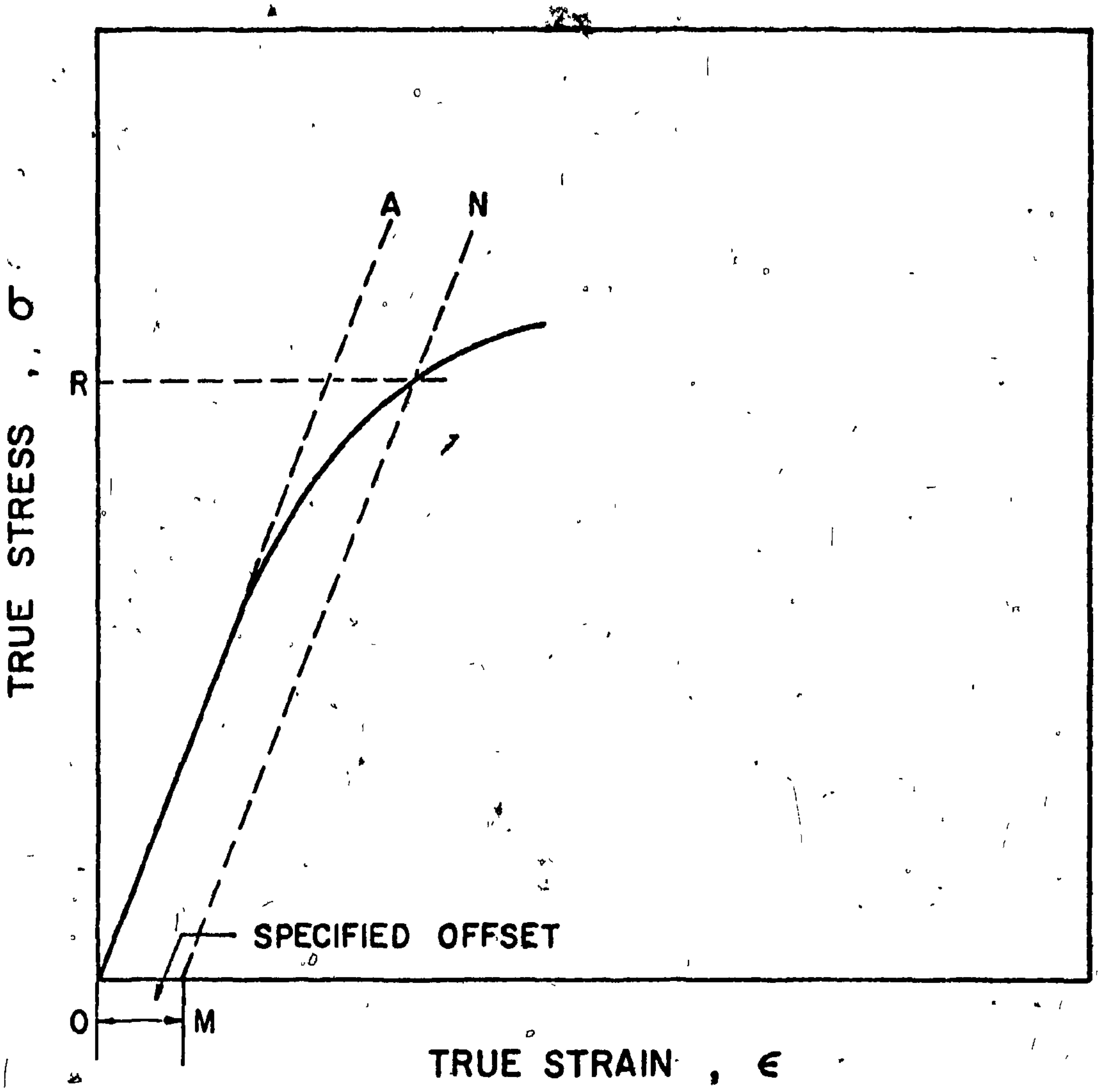

FIGURE 3.7 Schematic representation of the offset method

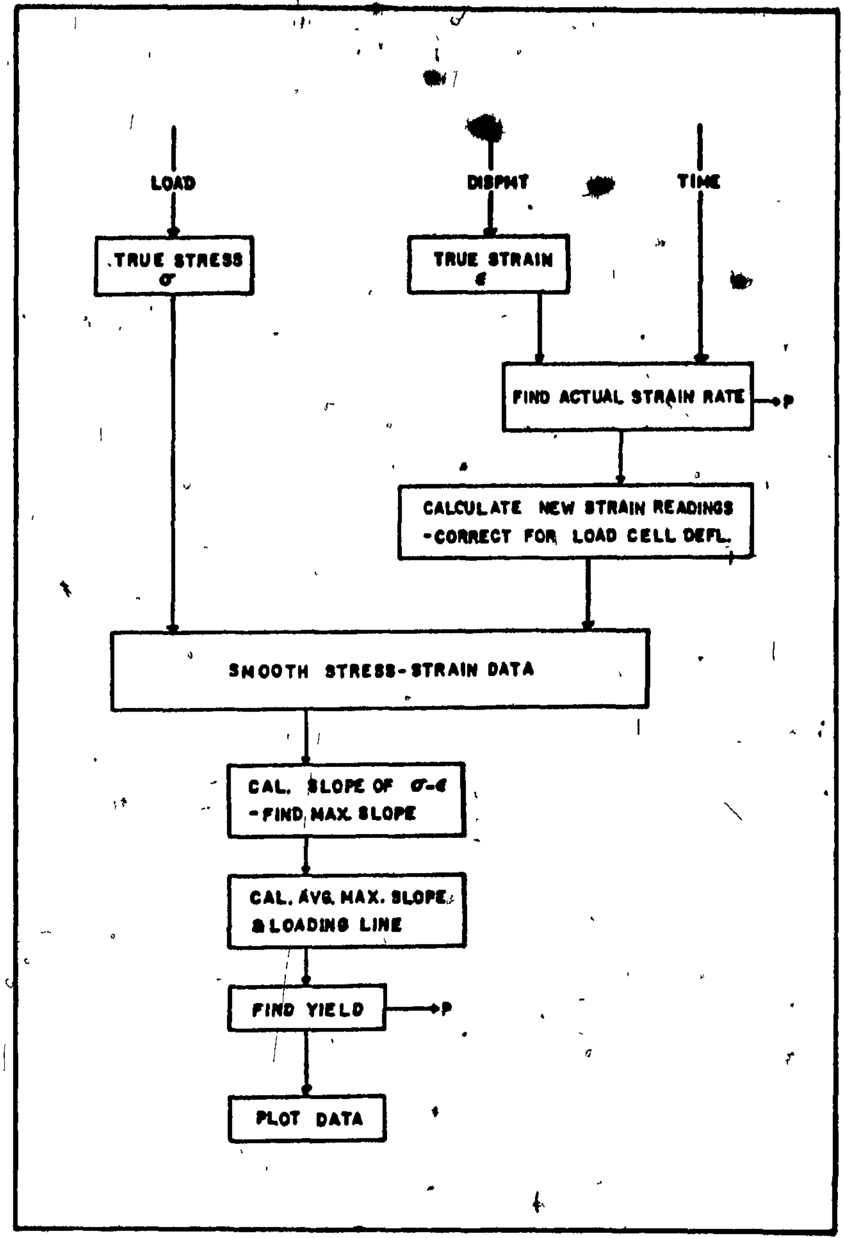

FIGURE 3.8 Block diagram illustrating the operation of the program YIELD

The first operation of YIELD is to smooth the data. Of the two measured variables, only the strain data was amenable to such an operation. Since the tests were performed at constant true strain rate, the strain-time data must form a straight line. Hence a least squares straight line fit was made to the strain versus time data. The smoothed strain data was obtained by putting the time values into the equation of the straight line and calculating the strain. The strain was then corrected for the load cell and machine deflection. The slope of the straight line fit is the actual strain rate and this is output to the printer, P. The load values, however, cannot be smoothed in this manner since the load is the dependent variable and its functional form is unknown. The true stress and true strain values were calculated from the load and displacement data by using Equations 3.3 to 3.5. The stress-strain data was then smoothed by using a three point smoothing routine similar to the IBM scientific subroutine package (SSP) routine SG13. This routine does not influence the trend of the data, but is designed to filter-out abrupt step shifts in the data due to noise. Only the data up to the first peak was considered.

The next task of the program is to determine the most suitable loading line. The logic used to do this is that since only data to the first peak is considered, then the maximum slope must be on the loading line. The computer calculates the slope of the flow curve using a central difference technique similar to that used in the SSP routine DGT3. These slopes, the work hardening, are then plotted against the flow stress on the Calcomp plotter. The slope of the loading line is determined by averaging the three largest values of slope determined by the differentiation routine. The line is completely defined by assuming that it passes through the point of maximum slope. The offset stress is found by simply drawing a line of the same slope at a 0.002 strain offset. The yield is calculated by locating the two data points between which the offset line passes, fitting a line between these points and calculating at what stress the value of this line and the loading line is equal. This value of the stress is the yield stress. The program finally plots the yield region of the stress-strain curve, drawing-in the calculated loading and offset lines. Examples of the work hardening and yield plots are shown in Figure 3.9 and 3.10. It should be noted that the data is the same as that shown in Figure 3.6. By comparing Figures 3.6 and 3.9, it can be seen that the program YIELD accurately determines the yield.

The raw data obtained from approximately 75 compression tests will be presented more formally in the experimental results chapter that follows.

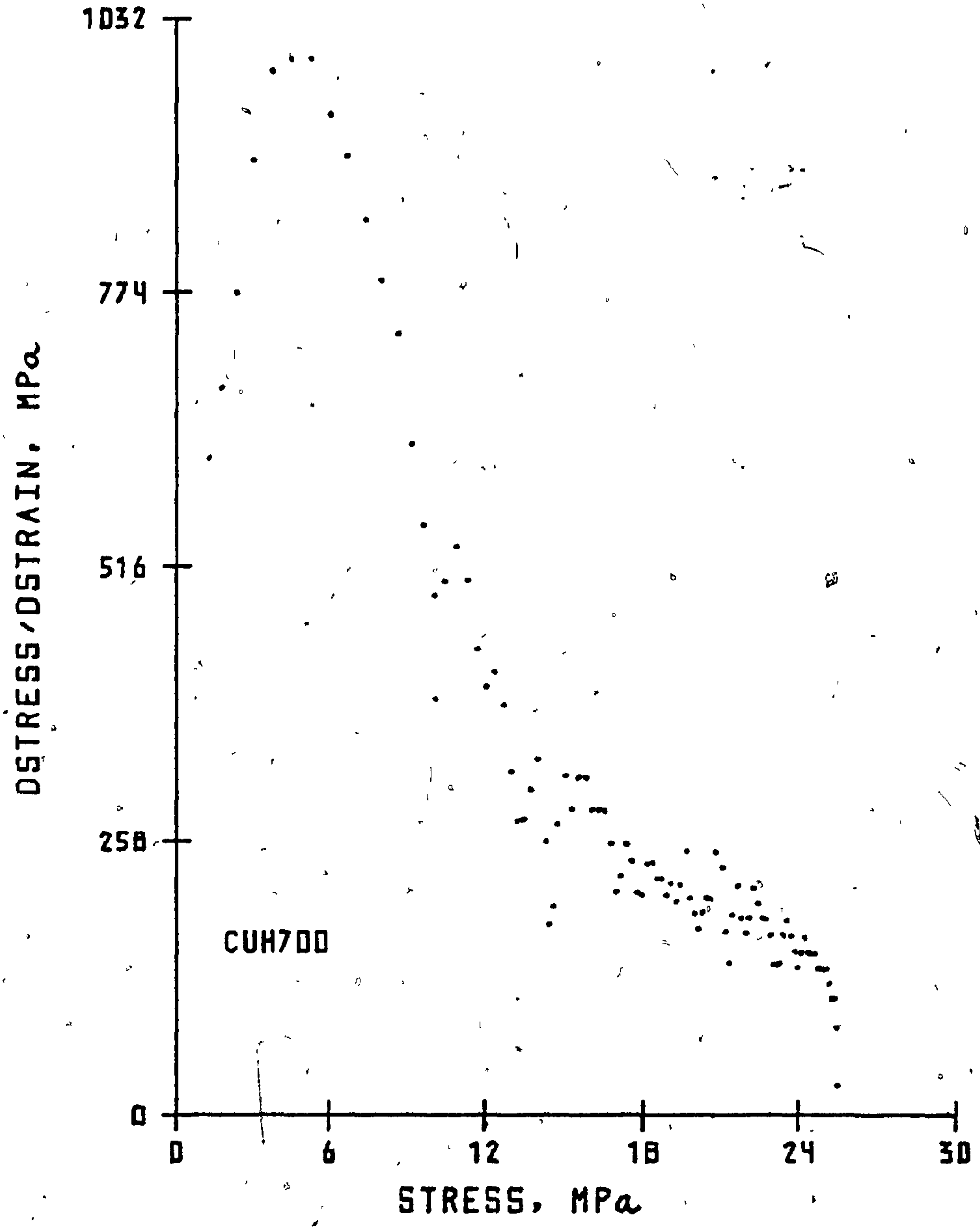

FIGURE 3.9 Plot of the work hardening versus stress as plotted by the digital plotter

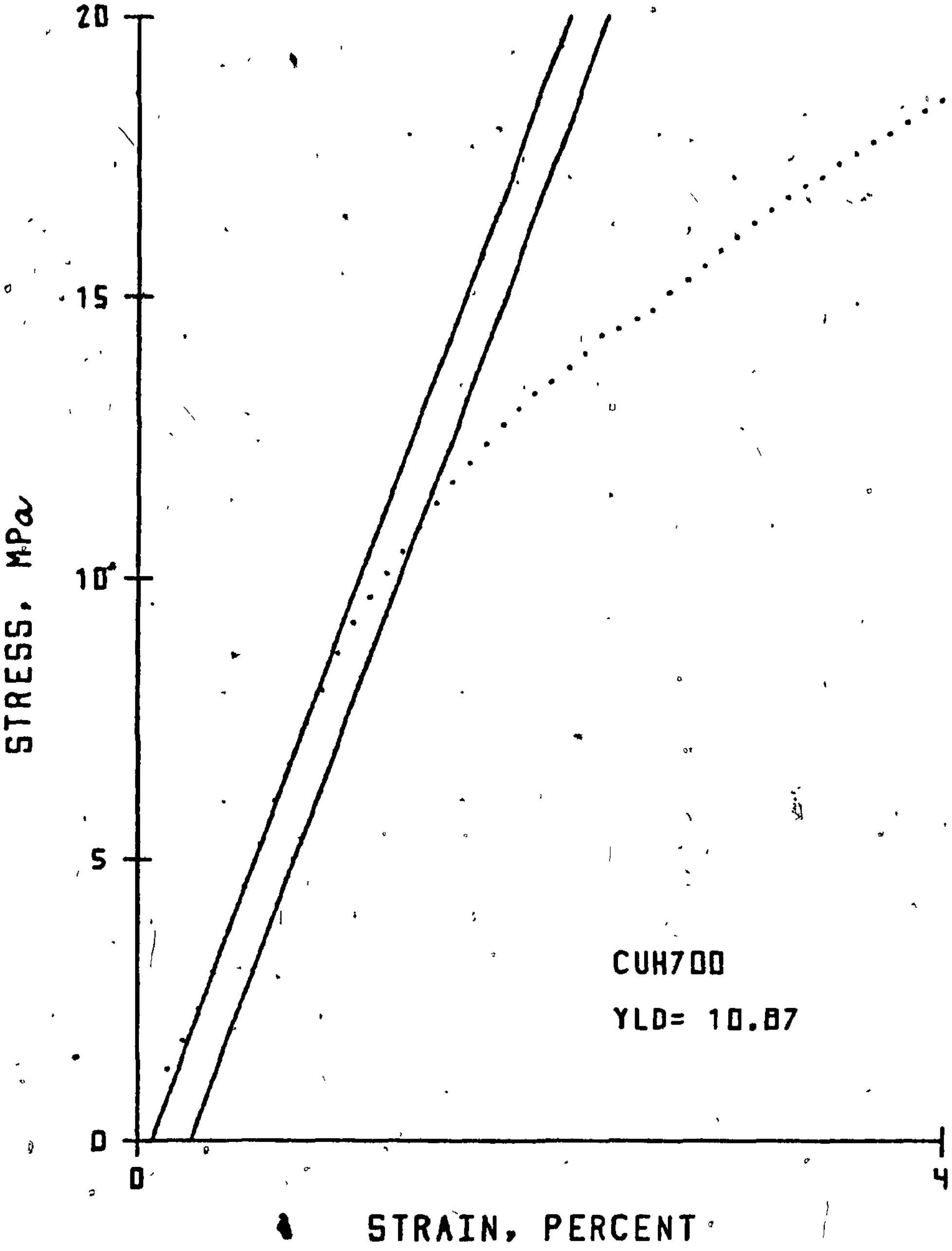

FIGURE 3.10 Yield plot showing the loading and offset lines

CHAPTER 4

EXPERIMENTAL RESULTS

Constant true strain rate compression tests were conducted on OFHC copper at ten different strain rates in the range 5.2×10^{-2} to $5.2\times10^{-5}s^{-1}$. These tests were conducted at constant temperatures in the range 500 to 800°C and at temperature intervals 50°C. Additional experiments were also carried out at 575°C. The upper strain rate limit was imposed by the available equipment. At testing speeds in excess of $5\times10^{-2}s^{-1}$ the data acquisition rate was insufficient to permit an accurate determination of the yield stress. The high temperature and low strain rate limit were principally determined by the limit of resolution of the load cell and the flow stresses developed under these limiting conditions. The lower temperature bound corresponds to a homologous temperature of 0.57 which suggests that at least at the slower strain rates the flow characteristics should be typical of high temperature deformation. The samples were all deformed to a true strain of approximately 0.6. This means that the fastest tests lasted approximately twelve seconds while the slowest tests took almost 3½ hours.

In this chapter the information obtained from these experiments will be presented. The various topics that will be discussed are the characteristics of the true stress-true strain curves, the temperature and strain rate dependence of the yield stress and the determination of the activation parameters.

4.1 CHARACTERISTICS OF THE TRUE STRESS-TRUE STRAIN FLOW CURVES

The influence of the imposed strain rate on the true stress-true strain curves obtained for copper at 700°C, is shown in Figure 4.1. For the sake of clarity only four of the ten curves for this temperature are shown. The effect of temperature on the flow curve at a strain rate of $1.7\times10^{-3}s^{-1}$ is shown in Figure 4.2. The curves at 575 and 800°C are omitted for clarity. All of the flow curves obtained in the present work can be found in Appendix 2 in the form of constant strain rate flow curves at various testing temperatures. It should be noted that at 800°C, tests were only carried out at the five fastest strain rates.

The pronounced peak at high strain rates and the oscillatory behaviour of the flow stress at low strain rates clearly indicates that this material undergoes dynamic recrystallization during straining (1,103). Furthermore, if one examines the typical flow curve shown in Figure 3.6, it can be seen that these curves exhibit three distinct regimes of behaviour. At very low strains, up to one or two per cent strain, the stress increases almost linearly with strain. This is the initial loading region. After this, there is a rather sudden decrease in the slope of the curve followed by a region during which the slope gradually decreases. The net work hardening rate, defined as $d\sigma/d\varepsilon$, finally becomes zero at the first peak. This is called the work hardening region. The third regime of flow occurs at and after the first peak in the stress, and is called the dynamically recrystallized region. In the following three sections, these regimes of flow will be discussed in turn.

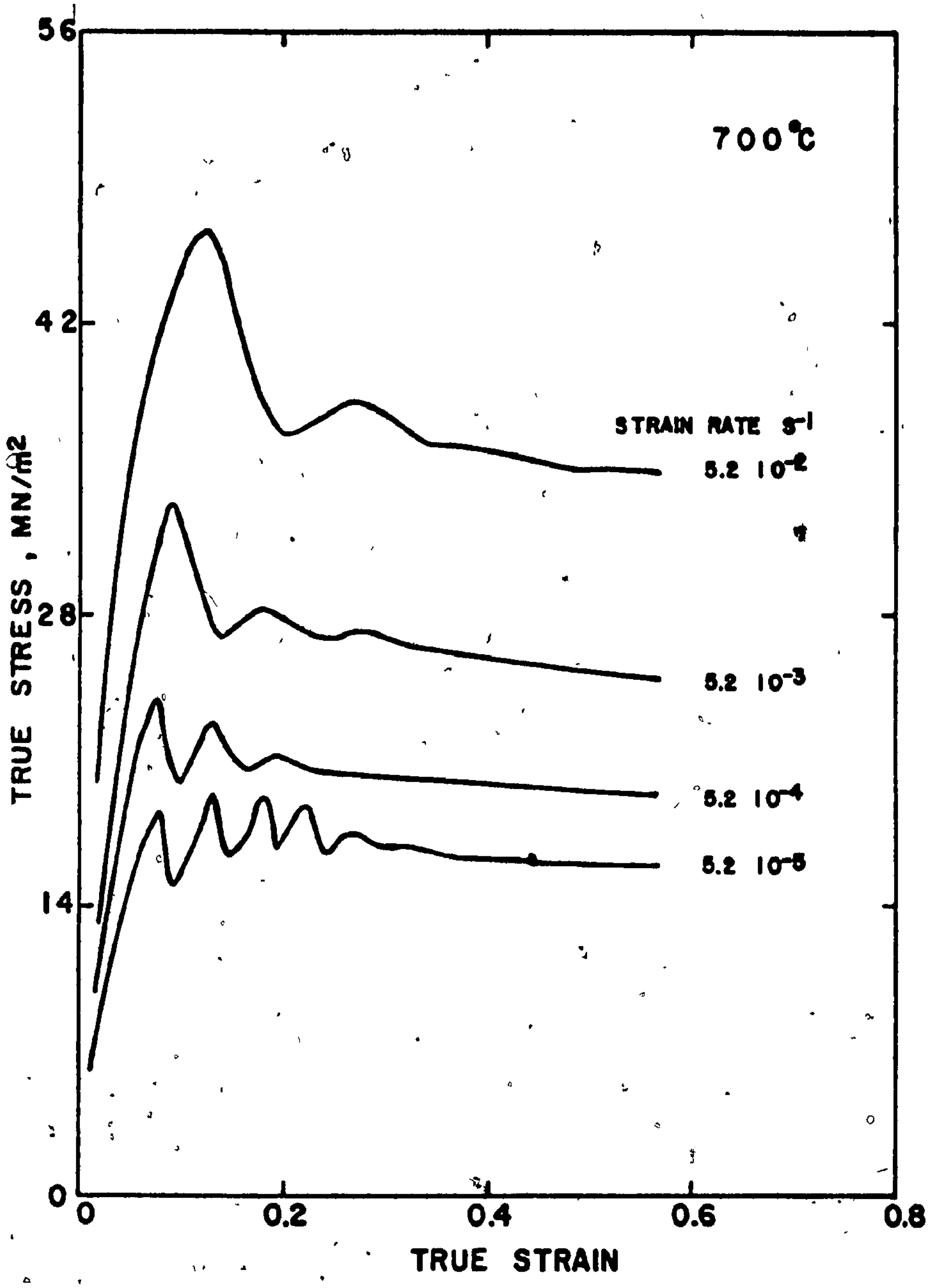

FIGURE 4.1 The influence of strain rate on the flow curves of copper at 700°C

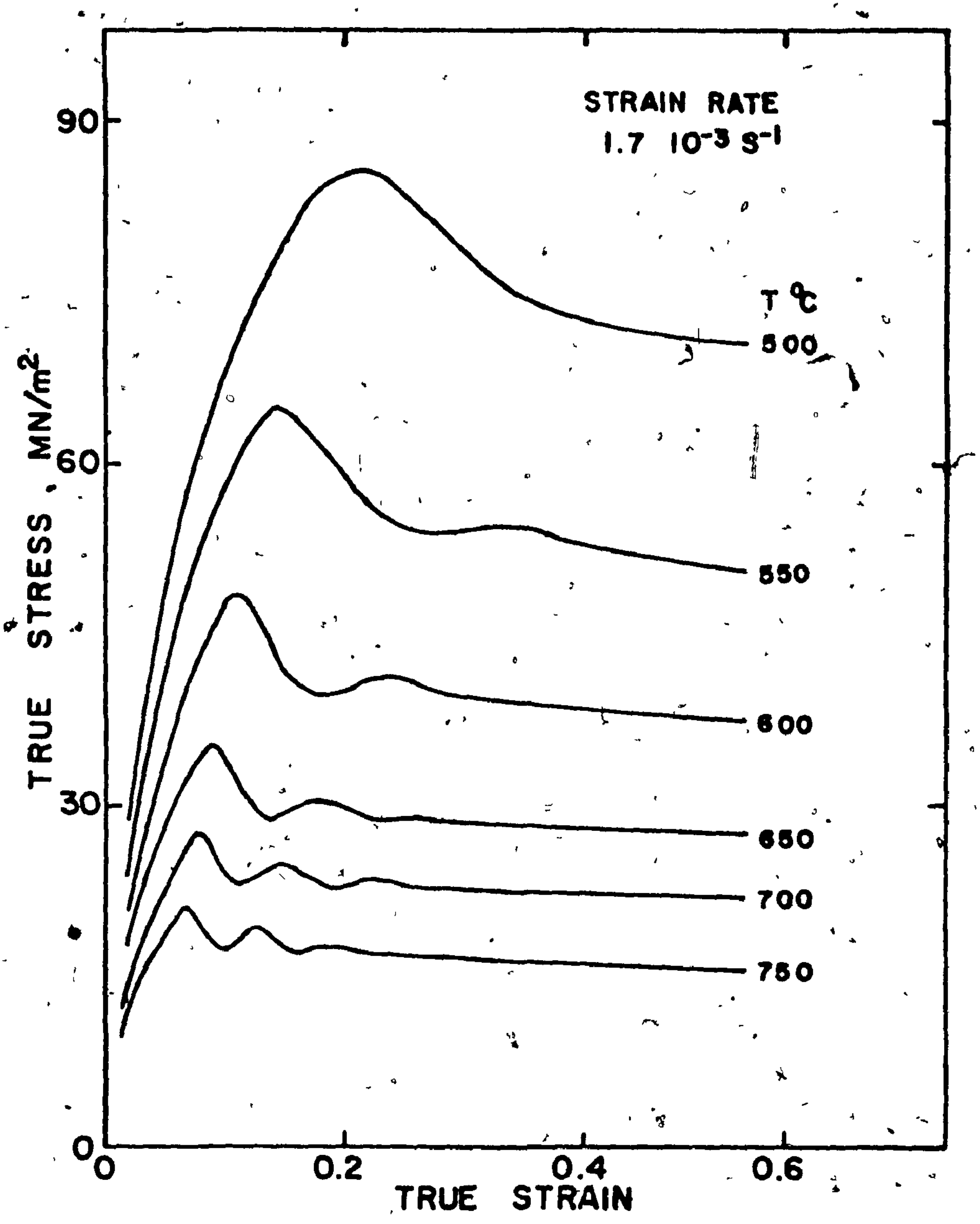

FIGURE 4.2. The influence of temperature on the flow curves of copper at $1.7\times10^{-3}s^{-1}$

4.1.1 The Initial Loading Region

It is clear from the work hardening and yield plots in Figures 3.9 and 3.10, that the initial loading region is actually comprised of three regions. Figure 3.9 is a typical work hardening plot for copper under the present testing conditions. At the start of loading, the work hardening rate increases rapidly up to a peak value and then falls again at the onset of macroscopic plastic flow. The maximum work hardening rate is assumed to be the slope of the initial loading line as was described earlier, in Chapter 3. The slopes of the loading lines vary from about Y/70 at high strain rates and low temperatures, where Y is Young's modulus, to approximately Y/125 at low strain rates and high temperatures.

The behaviour of the flow stress during the initial loading region is due to several factors: microstrain, machine distortion, the sample grooves and the glass lubricant. The large difference between the initial loading slope and the theoretical slope for an elastically strained specimen is, in part, due to the collapse of the sample grooves. The end faces of the specimens were grooved in order to retain the glass lubricant. During the initial loading, the grooves collapse and the lubricant is ejected at the sample-anvil interface. It has been estimated that this can account for one-third of the difference in the slope (4). Part of the remaining discrepancy occurs because the instant the sample is loaded, it becomes plastically strained a small amount. This phenomena is called pre-yield microstrain (73,104). During the initial loading, however, a significant portion of the specimen strain rate is due to the elastic strain rate. As deformation proceeds, the elastic strain rate reduces to zero while the plastic strain rate increases until it is almost equal to the imposed strain rate. At this point, macroscopic yielding occurs and the loading rate drops quickly. Another factor that reduces the loading slope is the distortion of the Instron frame during the initial loading. This distortion causes the initial applied strain rate at the specimen to be lower than the imposed strain rate. At the onset of macroscopic plastic flow the two rates are about equal.

It has been found that the grooves and the lubricant have a negligible influence on the magnitude of the yield stress (5). However, the amount of pre-yield microstrain and the stress level for macroscopic yielding are influenced by the previous thermo-mechanical history of the material. Therefore, as described in Chapter 3, the samples were machined from rods that had all been fully annealed and then cold worked 85%. They were then given the same annealing treatment.

The yield stress was measured by the offset technique that was described earlier in this work. The yield data obtained at different temperatures and strain rates are presented in Appendix III. The strain rates that are listed are the actual imposed rates measured by the program YIELD. This data will be discussed in detail later on in this chapter.

4.1.2 The Work Hardening Region

Although work hardening always occurs during straining, it is not always the dominant process. The regions during which work hardening is dominant can be identified by examining the slope of the true stress-true strain flow curve. If the slope is positive, then hardening is occuring faster than any of the restoration processes.

In this section, the work hardening region referred to starts at the onset of macroscopic plastic flow and terminates just before the first peak in the flow curve.

On yielding, the slope of the flow curve changes abruptly by a factor of about ten. The yield stress, the strain to the peak and the peak stress are strongly temperature and strain rate dependent. Therefore, at high temperatures and low strain rates the hardening region extends only to 0.07 strain, while at high strain rates and low temperatures the region extends to strains of approximately 0.35.

It is evident from the work hardening plot shown in Figure 3.9 that after the onset of yielding the slope of $d\sigma/d\varepsilon$ versus σ decreases as some negative power function of the stress. However, near the peak in the flow stress this slope suddenly decreases to zero. The rapid change in slope can be attributed to the initiation of dynamic recrystallization. This observation is consistent with reports that the critical strain for the start of recrystallization, ε_c, is slightly less than the strain to the peak, ε_p (103).

4.1.3 The Dynamically Recrystallized Region

The dynamically recrystallized region begins at the first peak in the flow stress and continues to the maximum strain. The behaviour of the flow stress observed in this investigation indicates that as the temperature is increased and the strain rate decreased, the number of oscillations in the flow stress increases. At 500°C, for all strain rates, there is only one peak in the flow stress. Whereas, at 750°C and at the slowest strain rate, thirteen peaks in the flow stress were detected in a strain interval of 0.6. There was no indication that the oscillations were being attenuated.

The shape of the recrystallized region of the stress-strain flow curve is determined by the different dependencies of the critical strain for the initiation of recrystallization (ε_c) and the strain for completion of recrystallization (ε_r) on strain rate and temperature (29). At low temperatures and high strain rates ε_r is much greater than ε_c. Consequently, before recrystallization is complete, the regions of the specimen that recrystallized first have reached the critical strain to begin recrystallizing once more. Hence, after the first peak, the recrystallization cycles superimpose and a constant average flow stress is obtained (103). At the other end of the strain rate and temperature range, ε_r is much less than ε_c. Therefore, once recrystallization starts it is completed long before the regions that recrystallized first can work harden to the critical level again. As a result of this, deformation proceeds in waves of repeated recrystallization followed by regions of work hardening. This causes the flow stress to oscillate. The oscillations tend to become damped at high strains because with repeated cycles of recrystallization, the process, throughout the specimen, becomes out of phase.

4.2 TEMPERATURE DEPENDENCE OF THE YIELD STRESS

The temperature dependence of the yield stress is shown graphically in Figure 4.3 and the data are tabulated in Appendix III. The strain rates listed on the figure are the numerical averages of all the measured strain rates at a given temperature and nominal strain rate. These numerical averages and their standard deviations are shown

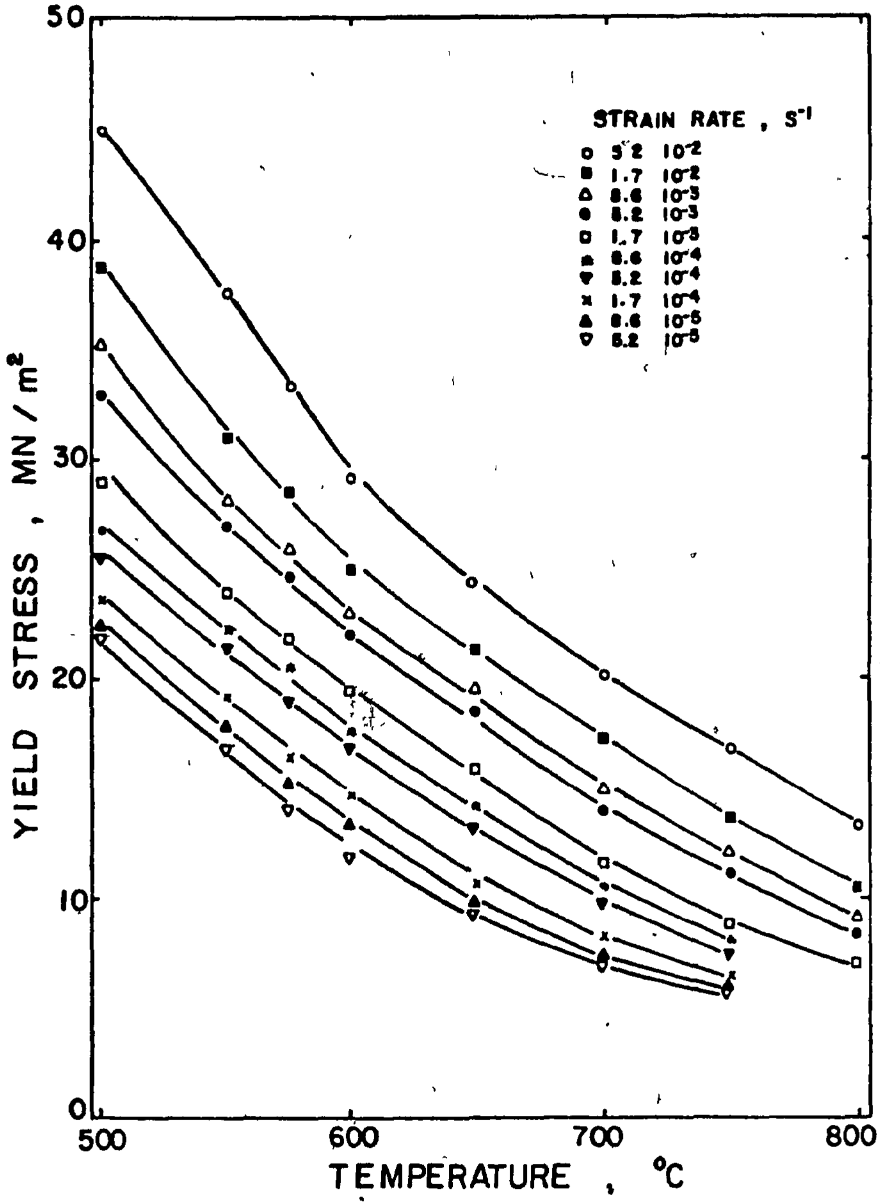

FIGURE 4.3 The temperature dependence of the yield stress of copper

in Table 4.1. It is clear from Figure 4.3 that the yield stress increases monotonically with increasing strain rate and decreasing temperature. All of the curves, except the one at the fastest strain rate, are concave upwards over the entire temperature range. However, at a strain rate of $5.2\times10^{-2}s^{-1}$ there is a point of inflection in the curve at approximately $850^{\circ}K$. At lower temperatures the curve is concave downwards. This effect probably arises due to a transition from thermally activated to athermal flow as the temperature is decreased at the highest strain rate.

4.3 STRAIN RATE DEPENDENCE OF THE YIELD STRESS

The strain rate dependence of the yield stress is shown by a semi-logarithmic plot in Figure 4.4 and by a logarithmic plot in Figure 4.5. From Figure 4.4 it is clear that the strain rate dependence has a very similar form to the temperature dependence of the yield stress. However, in Figures 4.4 and 4.5 the transition from thermally activated to athermal flow is not as pronounced as in Figure 4.3.

4.4 DETERMINATION OF THE ACTIVATION PARAMETERS

In the present work, it is assumed that at the onset of macroscopic plastic flow the internal stress is negligible, and therefore that the effective stress is equal to the yield stress. The reasoning behind this assumption has already been discussed in Chapter 2. Furthermore, since the thermodynamic analysis will be performed in terms of the modulus-reduced shear stress, τ/μ, it is necessary to replot Figures 4.3 and 4.5 in terms of this parameter.

TABLE 4.1

The Average Imposed Strain Rates

Average Strain Rate, s^{-1}	Standard Deviation
5.231×10^{-2}	9.964×10^{-4}
1.735×10^{-2}	2.819×10^{-4}
8.604×10^{-3}	6.479×10^{-5}
5.216×10^{-3}	5.181×10^{-5}
1.694×10^{-3}	2.066×10^{-5}
8.549×10^{-4}	1.032×10^{-5}
5.081×10^{-4}	4.879×10^{-6}
1.713×10^{-4}	3.352×10^{-6}
8.617×10^{-5}	1.171×10^{-6}
5.153×10^{-5}	6.701×10^{-7}

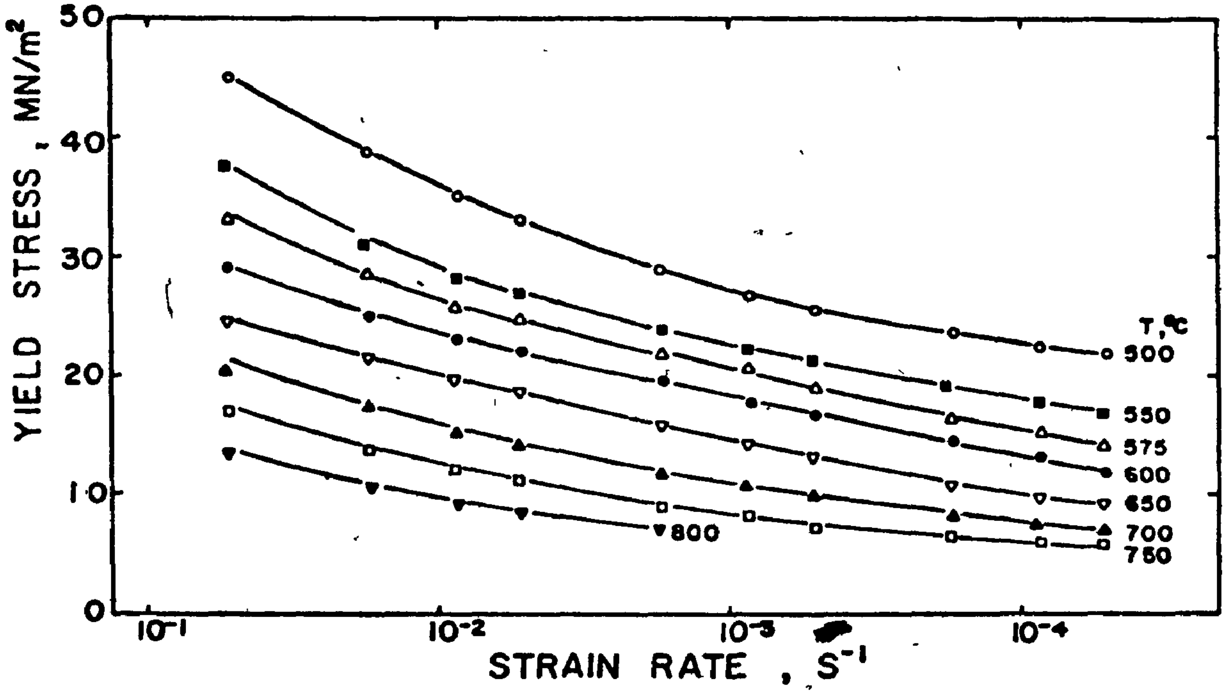

FIGURE 4.4 Semi-logarithmic plot of the strain rate dependence of the yield stress of copper

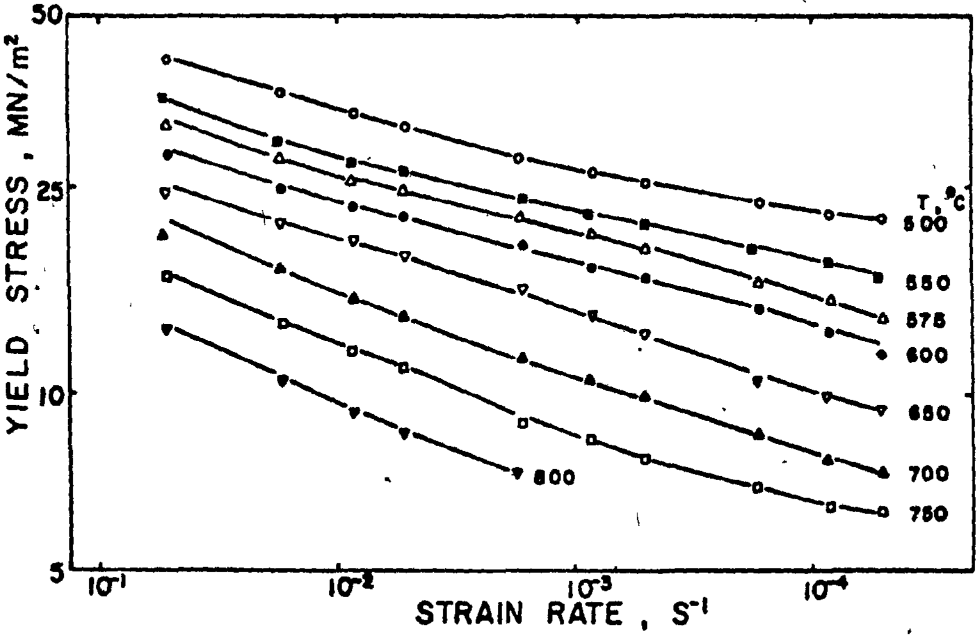

FIGURE 4.5 Logarithmic plot of the strain rate dependence of the yield stress of copper

To convert the compressive yield stress to effective shear stress, the experimentally determined stresses were divided by the average Taylor factor $\overline{M}$, which takes a value of 3.06 for isotropic polycrystalline f.c.c. metals (105). The shear modulus and its temperature dependence was determined from single crystal data as is shown below.

4.4.1 The Shear Modulus of Polycrystalline Copper

The temperature dependence of the elastic constants of copper has been extensively investigated during the past thirty years (107-110,118). Most of the work has been performed on single crystals in the temperature range 4.2 to 800°K (108,109). Overton and Gaffney (108) have measured the temperature dependence of the elastic stiffness coefficients, C_{11}, C_{12} and C_{44}, of copper from 4.2 to 300°K. Chang and Himmel (109) have determined the temperature dependence of these coefficients from 300 to 800°K. These data were used to obtain the curves shown in Figure 4.6. The Voigt, Reuss and Hill Averages were calculated from Equations 2.68, 2.67 and 2.69, respectively. At temperatures above 250°K all of the shear modulli are linear functions of temperature. Since the temperature range of the present investigation is 773 to 1073°K, it is assumed that the linear dependence of the modulii on temperature extends to higher temperatures. This assumption seems reasonable since it is commonly observed that, if there are no changes in crystal structure, the modulus linearly depends on temperature for all temperatures above the Debye temperature, which is 343°K for copper (65).

Least squares straight line fits were made to the linear portions of the curves to allow extrapolation to higher temperatures.

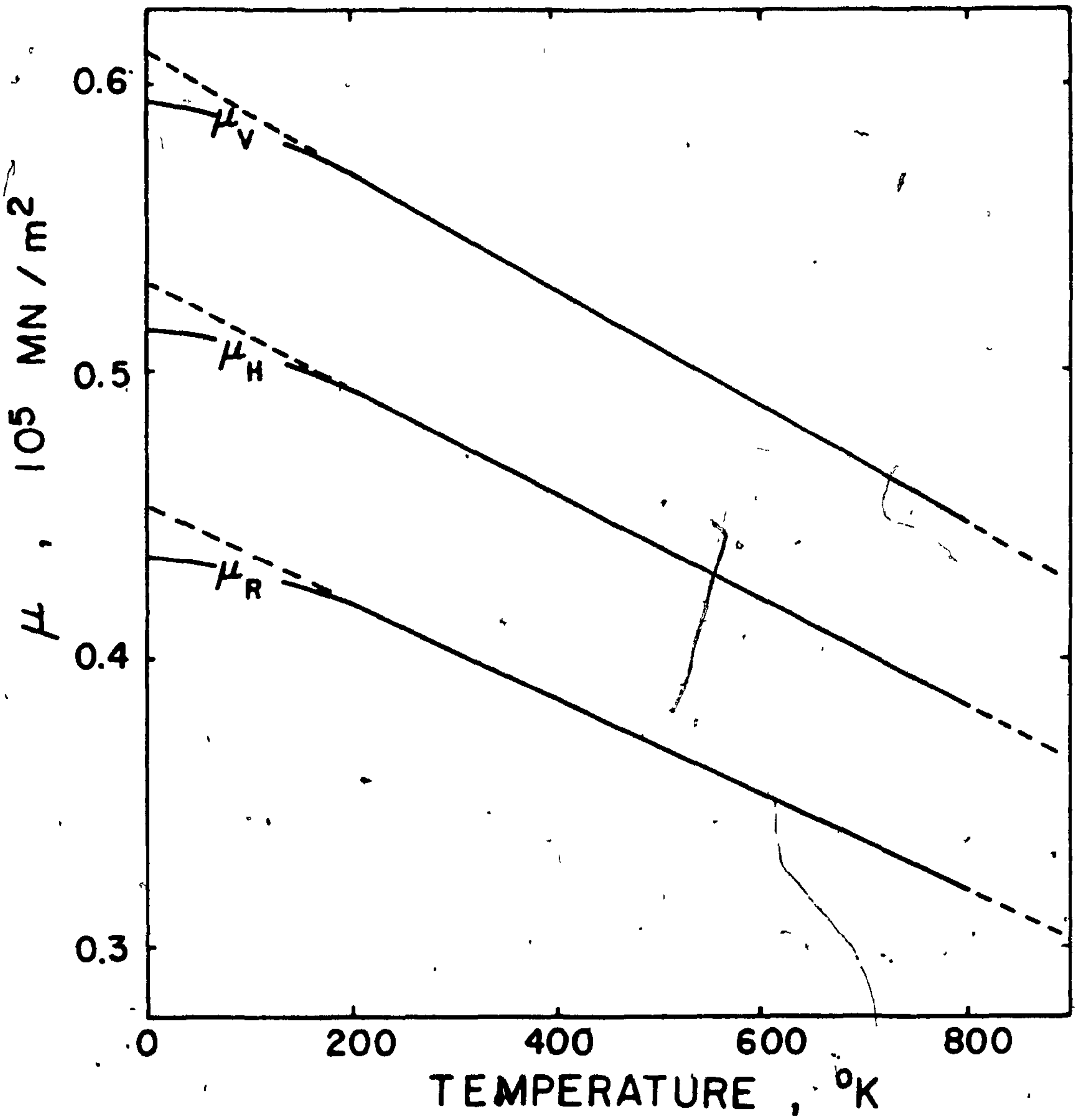

FIGURE 4.6 The temperature dependence of selected shear modulii

The results of these fits are

$$\mu_V = 6.104\text{x}10^4 - 20.357\ T \qquad 4.1$$

$$\mu_R = 4.516\text{x}10^4 - 16.502\ T \qquad 4.2$$

$$\mu_H = 5.310\text{x}10^4 - 18.429\ T \qquad 4.3$$

where the units of the modulii are MN/m^2 and T is the temperature in degrees Kelvin. The correlation coefficients for all of these fits were better than 0.9995, where 1.000 represents a perfect correlation.

In this investigation, only the Hill Average was used for reasons that have been previously discussed in Chapter 2. Using this average and the effective shear stress, the modulus-reduced effective shear stress was calculated. The temperature and strain rate dependence of this parameter is presented below.

4.4.2 The Temperature and Strain Rate Dependence of the Modulus-Reduced Effective Stress

The temperature dependence of the modulus-reduced effective stress is shown in Figure 4.7 and the strain rate dependence is shown in Figures 4.8 and 4.9. In these figures the symbol τ was used to represent the effective stress since we have assumed that the effective and applied stresses are equal. This notation will be used throughout the present work.

In Figure 4.10 the logarithm of the strain rate is plotted for constant values of τ/μ against inverse temperature. The points

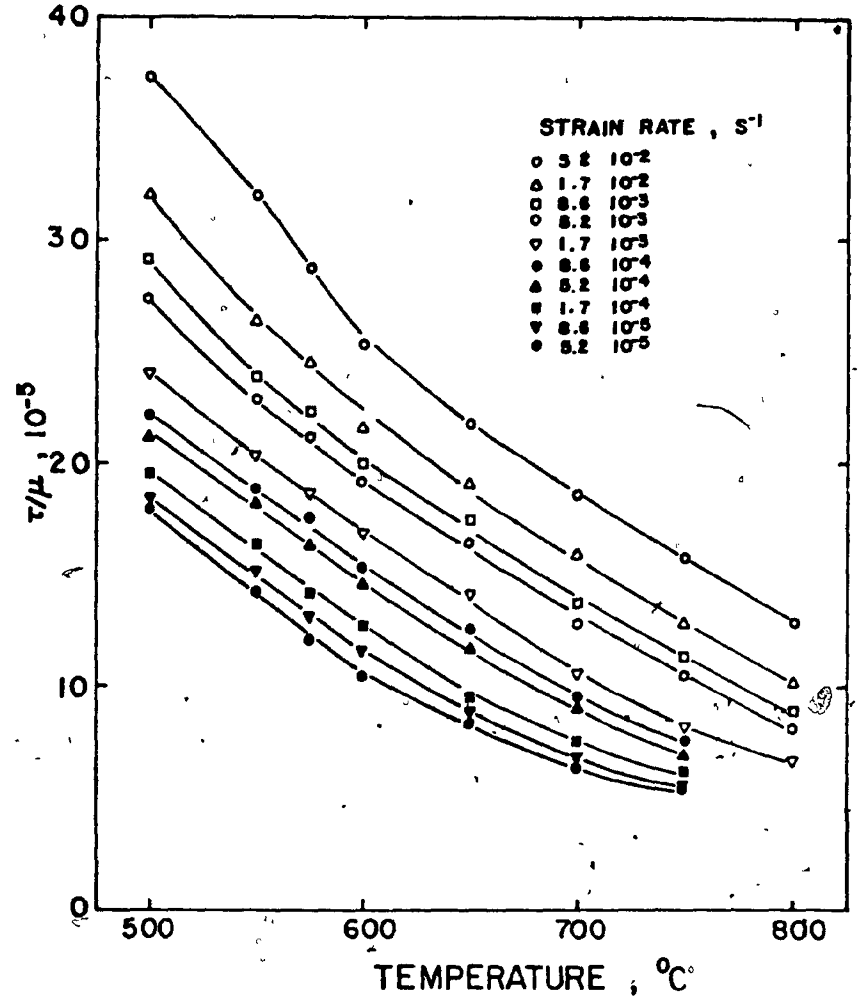

FIGURE 4.7 Temperature dependence of the modulus-reduced yield stress of copper

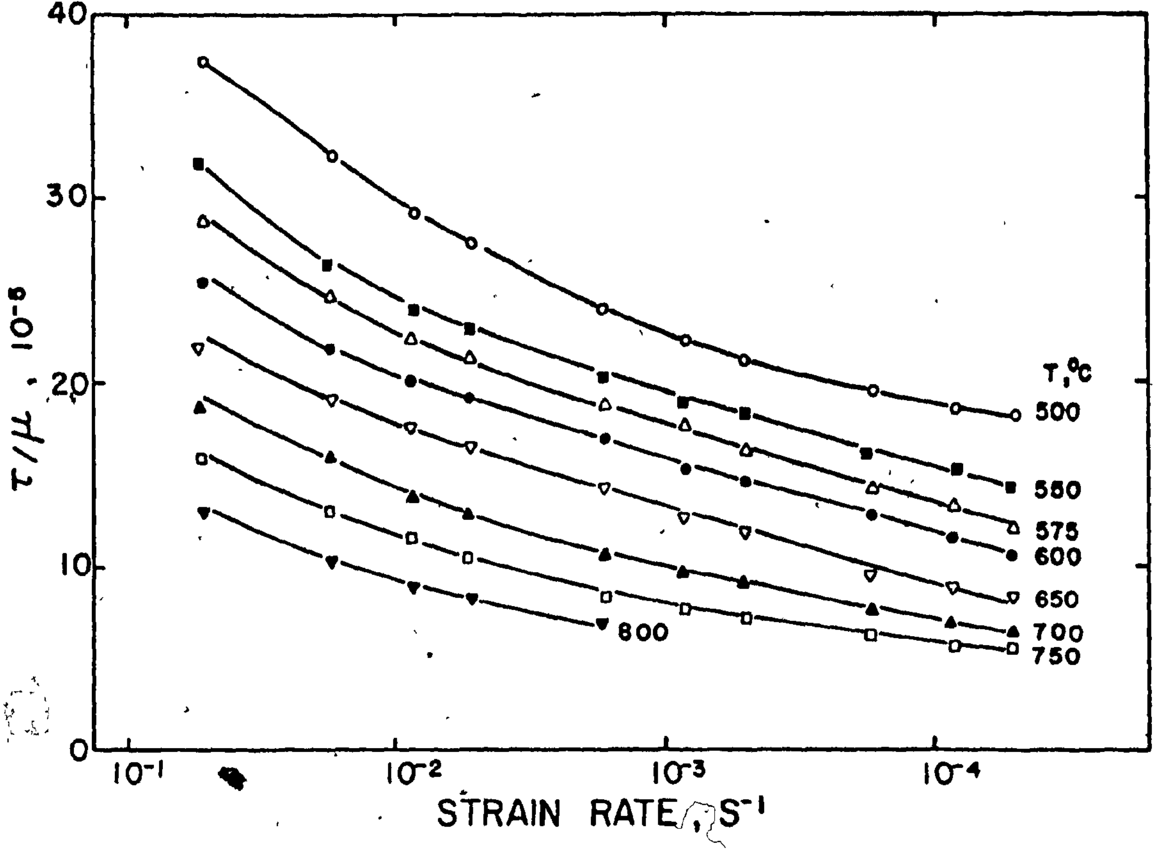

FIGURE 4.8 Semi-logarithmic plot of the strain rate dependence of the modulus-reduced yield stress of copper

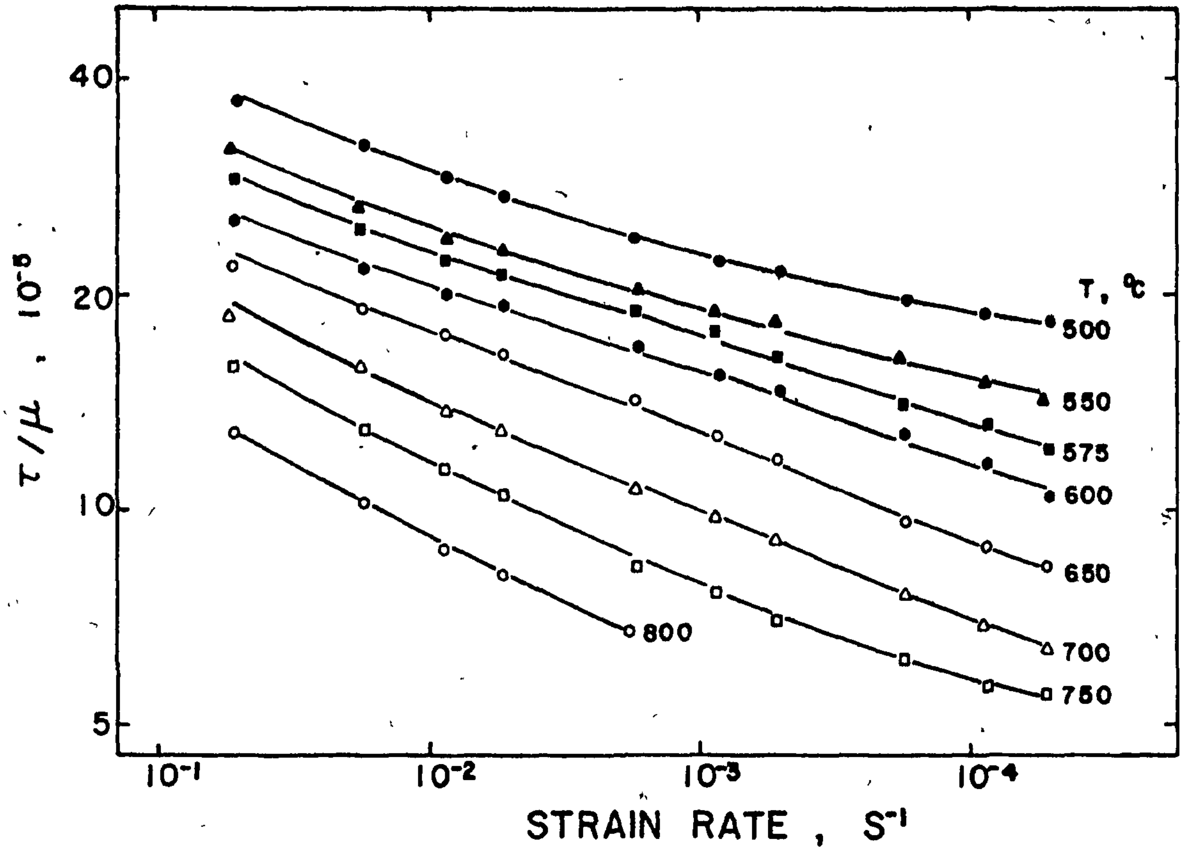

FIGURE 4.9 Logarithmic plot of the strain rate dependence of the modulus-reduced yield stress of copper

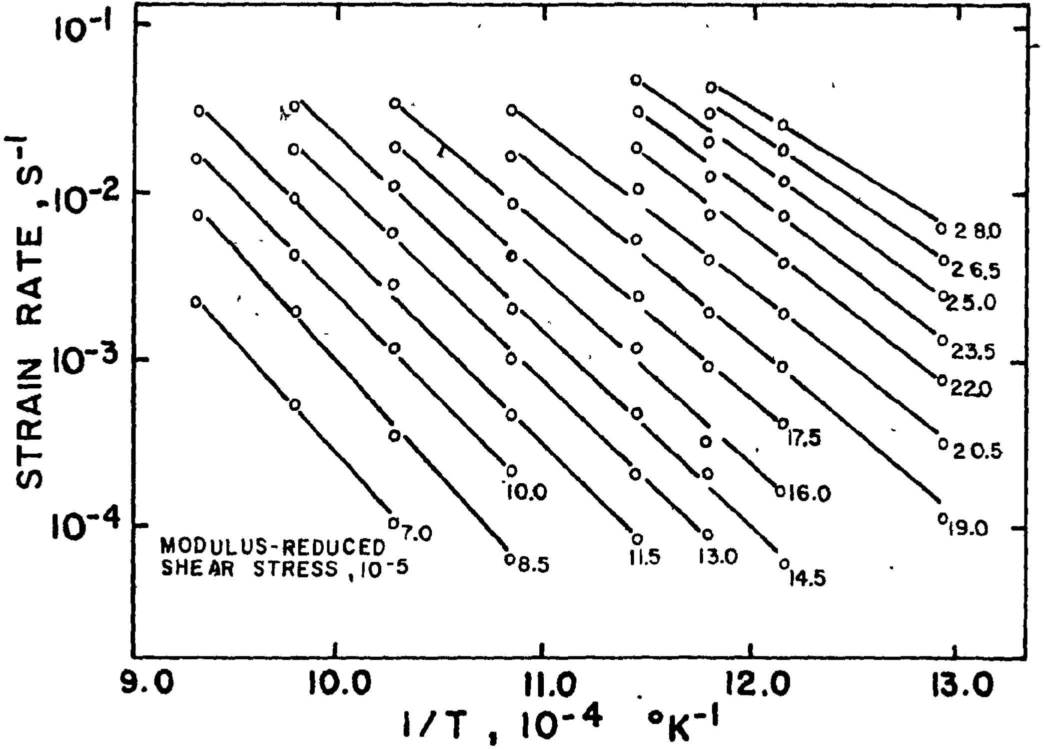

FIGURE 4.10 The inverse temperature dependence of the logarithm of the strain rate at constant values of τ/μ

on this plot represent the intersection of constant τ/μ lines with the smooth lines drawn through the data in Figures 4.7 and 4.8. The data represented graphically in Figure 4.10 is the "raw data" used to calculate the activation parameters and is tabulated in Appendix IV. It should be noted that the constant τ/μ lines are drawn so that they intersect at least three empirical curves within the experimental range. It is felt that at least three points were required to properly define the curves in Figure 4.10. There are two salient features of this plot that are worthy of mention. Firstly, the logarithm of the strain rate varies linearly with inverse temperature at constant τ/μ. This observation indicates that the activation enthalpy, which is directly proportional slope of the lines, is independent of temperature over the temperature range investigated. The second observation is that the slopes of the straight lines decrease with increasing τ/μ.

A computer program was written to analyse the data presented in Figure 4.10 and Appendix IV. Using these data along with the temperature dependence of the shear modulus, the program determines all of the activation parameters. The program, called ACTANL, is listed in Appendix V. In the following sections the scheme of analysis used in this program is presented.

4.4.3 Scheme of Analysis

The theoretical basis of the analytical scheme used in the program ACTANL has been previously presented in Section 2.2.2.3. To initiate the analysis the pre-exponential factor is assumed to be a function of τ/μ only. This permits the direct determination of the activation parameters from experimental data.

The first step in the analysis is to determine the slopes of the lines in Figure 4.10. This is carried out by performing a least squares straight line fit of the form $\ln(\dot{\varepsilon}) = B(1/T) + C$, where B is the slope of the line and C is the intercept. From the values of B, the activation enthalpies, with respect to τ/μ, are derived directly from the relationship

$$\Delta H_{\tau/\mu} = - k(\partial \ln \dot{\varepsilon}/\partial 1/T)_{\tau/\mu} \qquad 4.4$$

and the identity

$$(\partial \ln \dot{\varepsilon}/\partial 1/T)_{\tau/\mu} = B \qquad 4.5$$

The activation free energy, ΔG, is related simply to $\Delta H_{\tau/\mu}$ by the relation

$$\Delta G = (\mu/\mu_o)\Delta H_{\tau/\mu} \qquad 4.6$$

The constant μ_o arises because the shear modulus is a linear function of temperature and of the form: $\mu = \mu_o + T(\frac{d\mu}{dT})$. The activation entropy at constant τ/μ, $\Delta S_{\tau/\mu}$, is related to the free energy in the following manner

$$\Delta S_{\tau/\mu} = - (\Delta G/\mu)(d\mu/dT) \qquad 4.7$$

Using Equation 2.21, stress-strain rate data and the values of ΔG determined with the aid of Equation 4.6, the corresponding values of

$\dot{\varepsilon}_o$ are determined. These values can then be examined in order to check whether the assumption that $\dot{\varepsilon}_o = \dot{\varepsilon}_o(\tau/\mu)$ was valid.

The values of the activation volume, V*, are determined from the relationship

$$V^* = (kT/\mu)((\partial \ln\dot{\varepsilon}/\partial\tau/\mu)_T - (\partial \ln\dot{\varepsilon}_o/\partial\tau/\mu)_T) \qquad 4.8$$

Since the values of the pre-exponential have already been determined, then all that is required to calculate V* are the slopes of the ln $\dot{\varepsilon}$ versus τ/μ data at constant temperature. This is performed by way of the SSP subroutine DDGT3. Furthermore, in order to smooth the values of V*, an equation of the form $\ln(V^*) = B - C(\tau/\mu) - D(\tau/\mu)^2 - E(\tau/\mu)^3$ is fitted to the values of V* using the least squares method.

Finally, in order to compare the values of the activation parameters with published values, it is necessary to compute the parameters with respect to the effective stress only. This is carried out by using the equations

$$\Delta H_\tau = \Delta H_{\tau/\mu} - V^*T(\tau/\mu)(d\mu/dT) \qquad 4.9$$

and

$$\Delta S_\tau = (\Delta H_\tau - \Delta G)/T \qquad 4.10$$

Using this scheme of analysis the program ACTANL calculated the activation parameters. These parameters are presented below.

4.4.4 Activation Enthalpy

The τ/μ dependence of the activation enthalpy is shown in Figure 4.11. In this figure three curves are presented. The lowest curve is for $\Delta H_{\tau/\mu}$ at all temperatures. It is clear that it is strongly dependent on τ/μ, especially at high and low values of τ/μ. The two uppermost curves show the values of ΔH_τ determined from Equation 4.9 for the highest and lowest temperatures. ΔH_τ is larger than $\Delta H_{\tau/\mu}$ because the compatability term on the right-hand side of Equation 4.9, $V^*T(\tau/\mu)(d\mu/dT)$, is negative since $d\mu/dT < 0$. At $\tau/\mu = 0$, $\Delta H_{\tau/\mu}$ must be equal to ΔH_τ for all temperatures. For $\tau/\mu > 0$, ΔH_τ is slightly temperature dependent as is shown in Figure 4.11.

4.4.5 Activation Entropy

The τ/μ dependence of the activation entropy is shown in Figure 4.12. It is clear that both $\Delta S_{\tau/\mu}$ and ΔS_τ are strongly τ/μ dependent especially at low values of τ/μ. The ΔS_τ values are approximately 32 to 35 J/mole^{o}K higher than the $\Delta S_{\tau/\mu}$ values over the entire τ/μ range.

The ΔS_τ values were calculated from Equation 4.10 using the values of ΔH_τ determined in the previous section. Since ΔH_τ is greater than $\Delta H_{\tau/\mu}$, then it follows that ΔS_τ is greater than $\Delta S_{\tau/\mu}$. Unlike ΔH_τ, ΔS_τ is not temperature dependent when plotted against τ/μ. The values of ΔS_τ range from 130.3 to 80.8 J/mol^{o}K. From these values, it can be seen that at high temperatures the activation entropy makes an appreciable contribution to the activation free energy. For example, at 1073^{o}K and $\tau/\mu = 7.0\text{x}10^{-5}$, $\Delta H_\tau = 308.8$ KJ/mol and $\Delta S_\tau = 130.3$ J/mol^{o}K. Therefore, $T\Delta S_\tau = 139.8$ KJ/mol and $\Delta G = 169$ KJ/mol. If ΔS_τ had been neglected then ΔG would have been 308.8 KJ/mol.

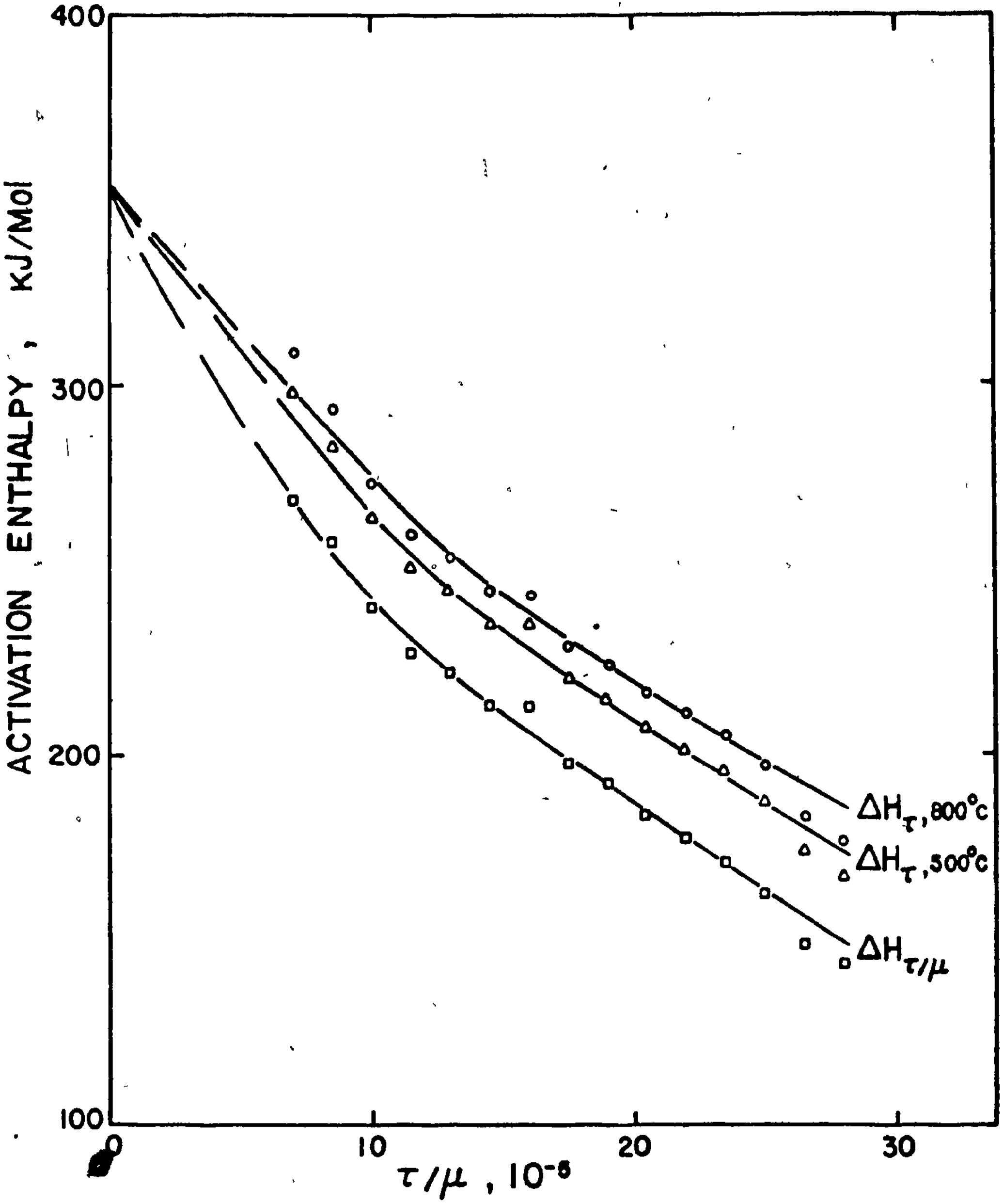

FIGURE 4.11 Dependence of the activation enthalpy of copper on the modulus-reduced effective stress

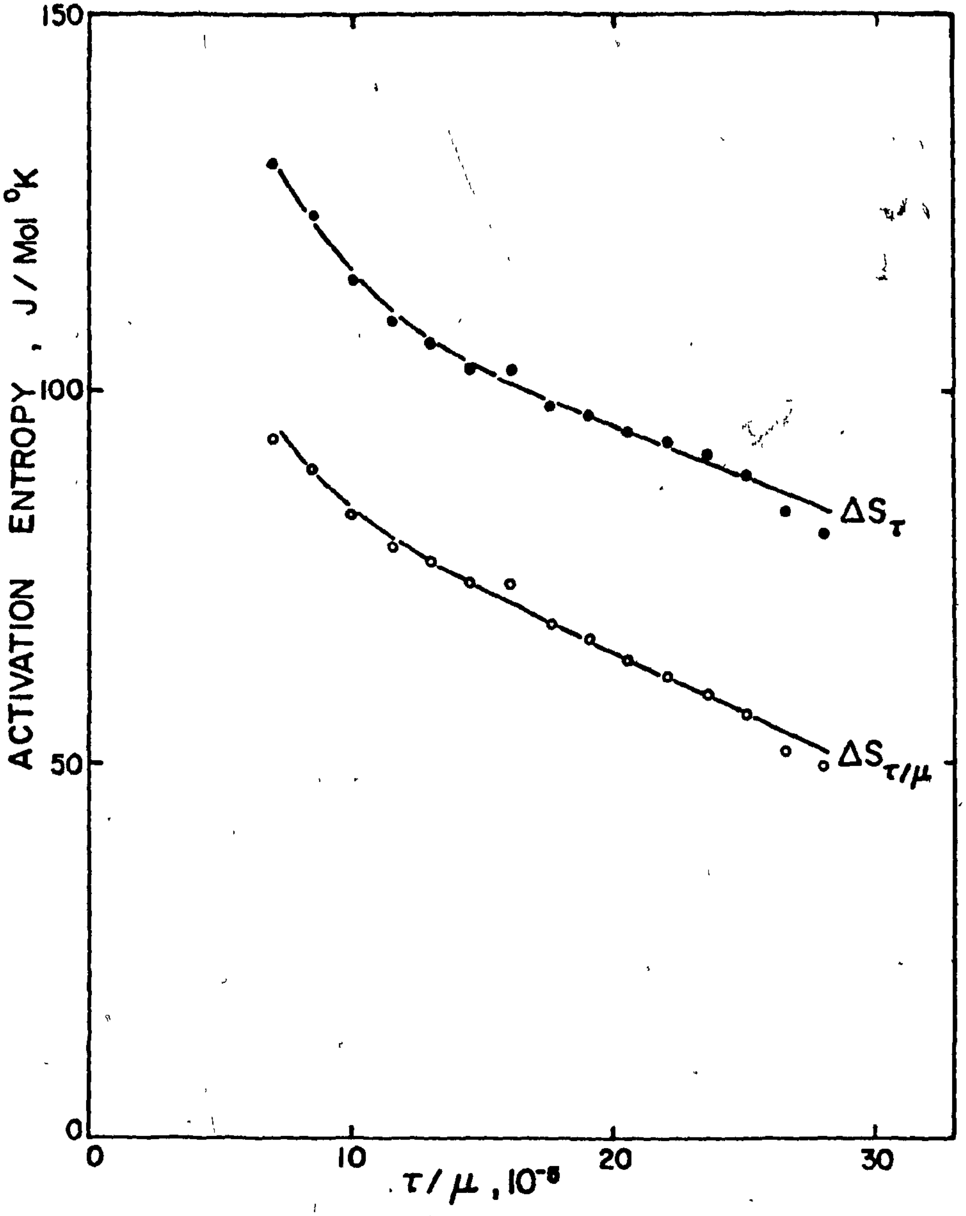

FIGURE 4.12 The modulus-reduced effective stress dependence of the activation entropy of copper

4.4.6 Activation Free Energy

The modulus-reduced activation free energy, $\Delta G/\mu$, was calculated from Equation 4.6 and its dependence on τ/μ is shown in Figure 4.13. This dependence is similar to the dependence of $\Delta H_{\tau/\mu}$ on τ/μ as described earlier. The units of $\Delta G/\mu$ in Figure 4.13 are b^3/atom, where b is the Burgers vector which has a value of 25.6 nm for copper (106). The smooth curve drawn through the data points is discussed in the following chapter.

4.4.7 The Pre-exponential Factor

The temperature and τ/μ dependence of the logarithm of the pre-exponential factor, $\ln(\dot{\varepsilon}_o)$, is shown in Table 4.2. There are two important observations to be made about these data. Firstly, at any value of τ/μ, $\ln(\dot{\varepsilon}_o)$ is approximately constant, that is, $\ln(\dot{\varepsilon}_o)$ is not dependent on temperature. Secondly, at a constant temperature, the value of $\ln(\dot{\varepsilon}_o)$ appears to be independent of τ/μ. Hence, from these observations, it is clear that the pre-exponential factor has a constant value which is independent of stress and temperature. This is the trivial case of $\dot{\varepsilon}_o \propto (\tau/\mu)^m$. At values of τ/μ greater than 2.5×10^{-4} the pre-exponential factor appears to take values that are smaller than those obtained at lower τ/μ levels. This upper limit probably indicates the commencement of the transition between thermally activated and athermal flow. The average value of $\ln(\dot{\varepsilon}_o)$ is 12.77 with a standard deviation of 0.512. Therefore, $\dot{\varepsilon}_o$ takes a mean value of $3.52\times10^5 s^{-1}$.

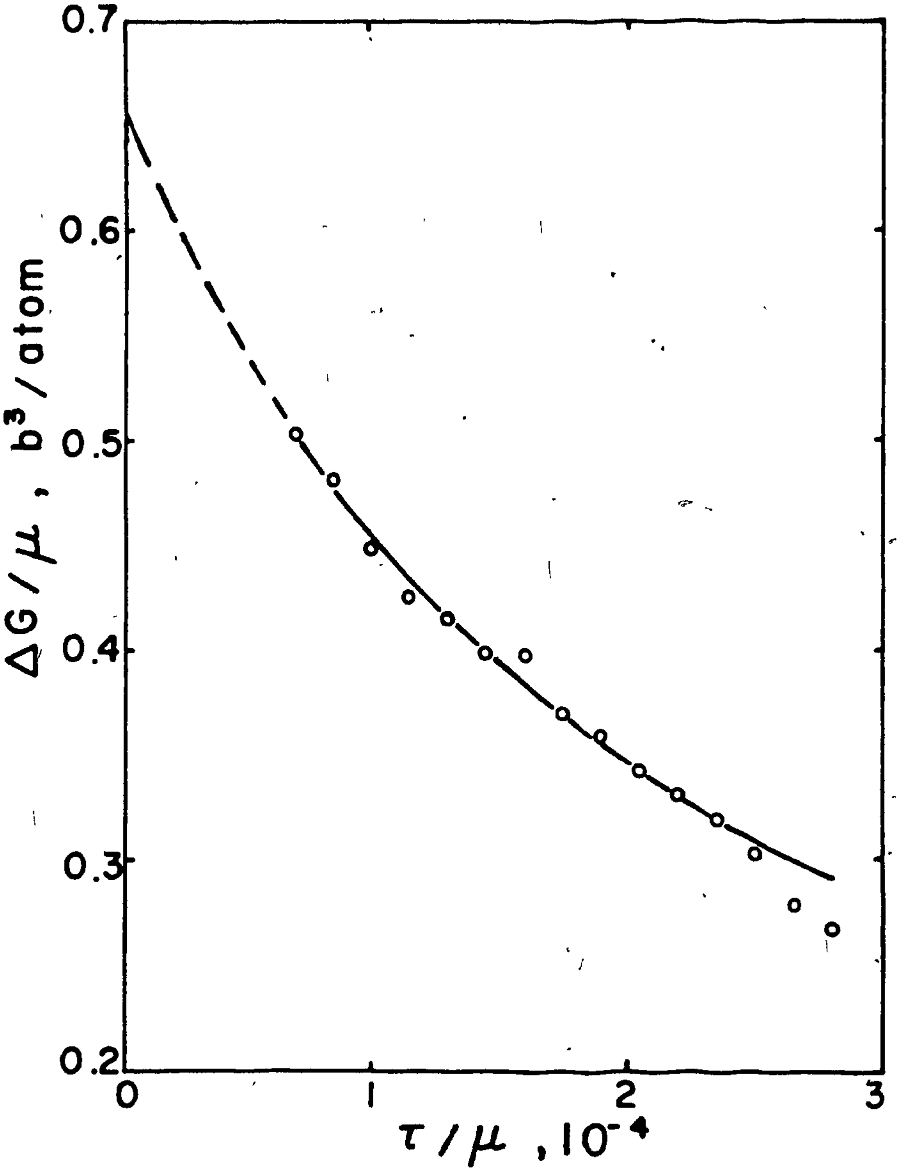

FIGURE 4.13 Dependence of the activation free energy of copper on the modulus-reduced effective stress

TABLE 4.2

The Temperature and τ/μ Dependence of $\ln(\dot{\varepsilon}_o)$

	Temperature °C							
τ/μ, 10^{-5}	500	550	575	600	650	700	750	800
7.0	-	-	-	-	-	12.88	12.76	12.88
8.5	-	-	-	-	13.17	13.13	13.16	13.17
10.0	-	-	-	-	12.67	12.68	12.68	12.67
11.5	-	-	-	12.48	12.55	12.53	12.55	12.47
13.0	-	-	12.84	12.87	12.88	12.86	12.85	-
14.5	-	12.77	12.85	12.94	12.92	12.89	12.77	-
16.0	-	13.47	13.59	13.66	13.62	13.48	-	-
17.5	12.94	12.74	12.82	13.01	12.94	12.81	-	-
19.0	13.19	12.95	13.02	13.23	13.09	-	-	-
20.5	13.02	12.79	12.85	13.06	12.91	-	-	-
22.0	13.04	12.89	12.89	13.07	-	-	-	-
23.5	12.90	12.88	12.76	12.94	-	-	-	-
25.0	12.55	12.51	12.41	12.60	-	-	-	-
26.5	11.49	11.56	11.47	-	-	-	-	-
28.0	11.28	11.32	11.27	-	-	-	-	-

4.4.8 Activation Volume

Since the pre-exponential factor is a constant, the right-hand term on the right-hand side of Equation 4.8 is zero and therefore the activation volume can be obtained easily. The temperature and τ/μ dependence of the activation volume is shown in Figure 4.14. It can be seen that at constant τ/μ levels V* is not a function of temperature. It is, however, a particularly strong function of τ/μ at low values of τ/μ. The smooth curve drawn through the data is the empirical curve that was described earlier.

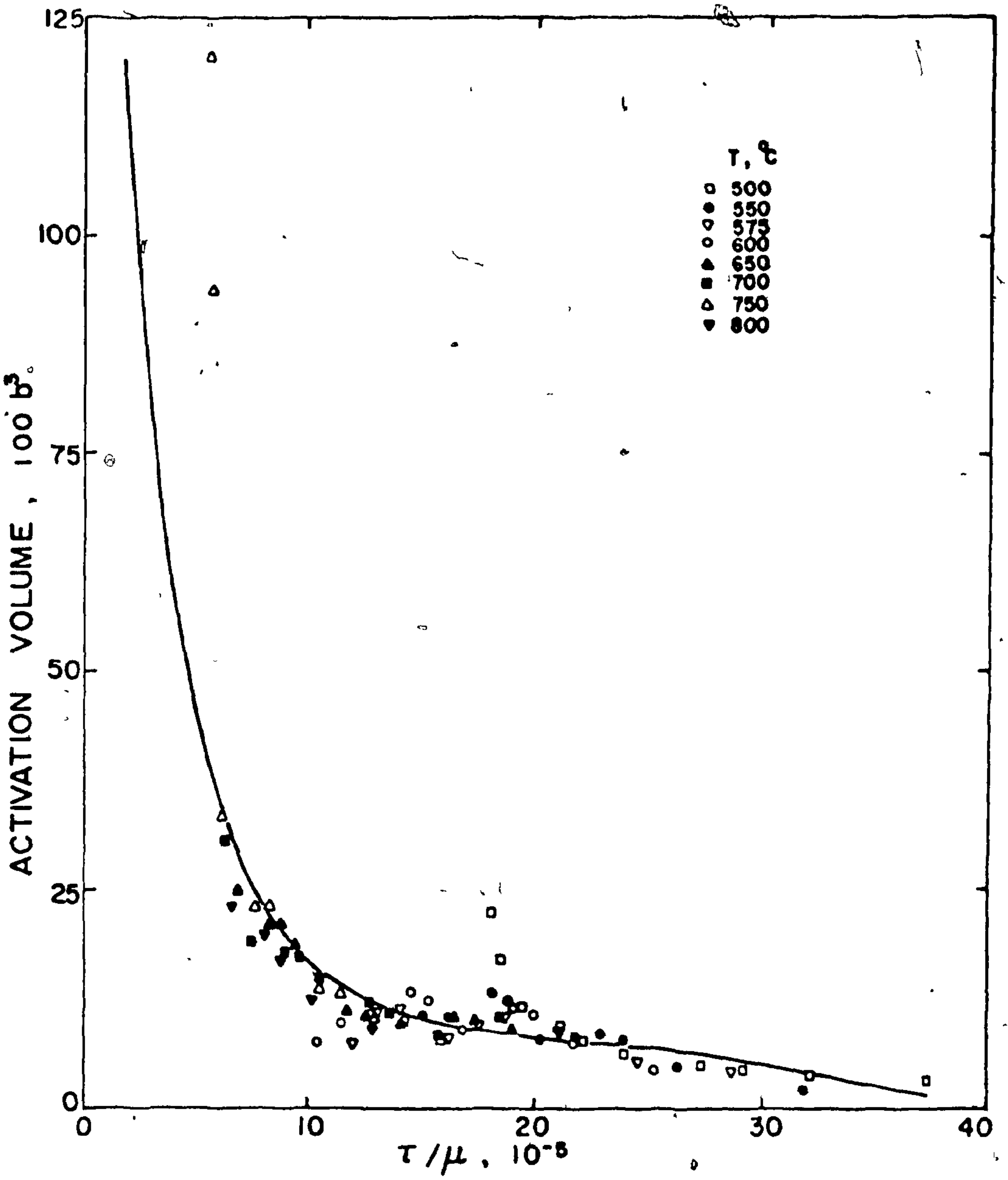

FIGURE 4.14 Dependence of the activation volume of copper on the modulus-reduced effective stress

CHAPTER 5

DISCUSSION

In the preceeding chapter a set of results pertaining to the temperature and strain rate dependence of the yield stress of copper were presented. Furthermore, the activation parameters calculated from these results were also described. In the present chapter, these data will be analysed and models will be proposed to explain the observed behaviour of the activation free energy and the pre-exponential factor. However, before going into the details of these models, we will present a brief discussion of the applicability of the analysis.

5.1 DISCUSSION OF THE METHOD OF ANALYSIS

The analytical scheme used in this work has been described in Chapter 4. The first feature of this analysis that should be noted, is that there was minimum smoothing of the experimental data. In order to obtain the data shown in Figure 4.10, smooth curves were drawn through the experimental data points as is illustrated in Figure 4.8. However, these curves were drawn to allow interpolation between the points and they did not influence the trend of the data. It is clear from Figure 4.10 that the ln $\dot{\varepsilon}$ versus 1/T data, at constant τ/μ, fits a family of straight lines very well. The points tend to be randomly scattered about the lines, indicating that the least squares straight line fit to the data is justified. The activation enthalpy and free energy were calculated directly from the slopes of these lines. The activation volume, on the other hand, was determined from the experimental data of Figure 4.8 by fitting a Lagrangian interpolation polynomial, of degree two, to three consecutive data points, where the derivative was determined at the mid-point.

In discussing the analytical scheme it is of primary importance to know exactly under what conditions the scheme is applicable. Some factors which limit the applicability of the analysis used here are discussed below.

5.1.1 Applicability of the Analysis

The activation parameters were determined from the experimental data by making several assumptions that limit the generality of the analytical scheme. Some of these assumptions are: (i) only one dislocation mechanism is rate controlling; (ii) the obstacles are linear elastic; (iii) the pre-exponential factor is a single-valued function of τ/μ; and (iv) the internal stress is negligible at the onset of macroscopic yielding. These assumptions will be discussed in turn in the following paragraphs.

In order to determine the activation parameters a strain rate equation of the form

$$\dot{\varepsilon}(T,\tau/\mu) = \dot{\varepsilon}_0(T,\tau/\mu)\exp(-\Delta G(T,\tau/\mu)/kT) \qquad 5.1$$

was used. This equation is essentially the same as Equation 2.21, except here, part of the temperature dependence of the parameters is included in the τ/μ term. The use of this equation implicitly assumes that a single type of activation process is rate controlling.

Otherwise, the strain rate would be given by a sum of terms with each term representing a separate thermally activated process. In order to simplify the analysis, a single glide obstacle mechanism was assumed to be rate controlling. If there were, in fact, several rate controlling processes, then ΔG in Equation 5.1 would actually be the proper average of the free energies of activation associated with the individual obstacles (111).

The analysis presented in Chapters 2 and 4 is only applicable to linear elastic obstacles. That is, it only applies to obstacles for which the back stress is not a function of the effective stress, and when the back stress has the same temperature dependence as the shear modulus. This latter statement implies that the dislocation-obstacle interactions are probably described by the theory of linear elasticity. It is further assumed that the obstacles are rigid.

The pre-exponential factor is taken to be a single-valued function of τ/μ. This assumption is checked by an inductive approach. In other words, if the data is in agreement with such a dependence then the procedure is justified. Further support for the validity of this assumption is that several of the terms which reasonably enter the pre-exponential are generally believed to be functions of only τ/μ. For example, the dislocation segment length (40) and the mobile dislocation density (112-114) appear to uniquely depend on τ/μ.

Finally, it is assumed that at the onset of macroscopic yielding the internal stress is much less than the applied stress. This assumption has already been discussed in Chapter 2.

Within this framework we will now discuss the values and functional dependencies of the derived activation parameters, as well as the physical interpretation of these results.

5.2 THE ACTIVATION PARAMETERS

The parameters obtained from the activational analysis described above will now be discussed in turn.

5.2.1 The Activation Volume

The activation volumes determined by numerical differentiation of the stress-strain rate data were depicted in Figure 4.14. This data was fitted to an equation of the form $V^* = B \exp\{- CX - DX^2 - EX^3\}$, where $X = (\tau/\mu)(5\text{x}10^3)$ and V^* is the activation volume in units of $100\ b^3$. The functional form of this equation is the same as that used by Surek et al (64). It has no physical significance. It is clear from Figure 4.14 that V^* is a function of τ/μ only. The values of the empirical constants were found to be

$$B = 5.44,\ 100\ b^3 \qquad D = -\ 175.53$$

$$C = 40.96 \qquad E = 271.33$$

where C, D and E are dimensionless. This empirical fit is represented by the smooth line drawn in Figure 4.14. It is evident that although the fitting procedure is effective in the middle range of experimental τ/μ values, $0.7\text{x}10^{-4} \leqslant \tau/\mu \leqslant 2.8\text{x}10^{-4}$, the functional form is less valid at the end points. However, the activation analysis was only carried out in this mid-range of τ/μ values. At $\tau/\mu = 2.8\text{x}10^{-4}$ the smoothed value of V* is 592 b^3 while at $\tau/\mu = 0.7\times10^{-4}$ it is 2826 b^3. We will return to these values of V* later in this chapter where the most likely rate controlling dislocation mechanisms are discussed.

5.2.2 The Activation Free Energy

The functional dependence of the activation free energy on τ/μ has been presented previously in Figure 4.13. It can be seen from this figure that extrapolation of the data to $\tau/\mu = 0$ is difficult because there are no points near zero. However, since it is necessary to know the value of ΔG at $\tau/\mu = 0$, in order to identify the rate controlling mechanism, an attempt was made to extrapolate the data to zero stress. This was achieved by fitting a series of equations to the data using the computer program CURVE[†]. The "best fit" was found to be of the form: $\Delta G = -C + (X + D)/(E + B(X + D))$, where $X = (\tau/\mu)\times10^4$ and ΔG is the activation free energy in units of μb^3/atom. The values of the constants are

$$B = 1.022 \text{ atom}/\mu b^3 \qquad D = 3.758$$

$$C = 0.980 \text{ atom}/\mu b^3 \qquad E = -1.548 \text{ atom}/\mu b^3$$

where D is dimensionless. The total RMS error in this correlation is 1.04%. This is demonstrated in Figure 4.13, where the smooth line

---

[†] This program was written by Professor D. Pfeiffer, Department of Mechanical Engineering, McGill University, Montreal. This program fits fifteen different functions to the data and chooses the "best fit" on the basis of a standard deviation criterion.

represents this equation. This expression was then used to determine the value of ΔG at $\tau/\mu = 0$, ΔG^o, which was found to be 0.66 μb^3/atom. This extrapolation to zero stress is shown by the dotted portion of the curve in the figure. Using the temperature dependence of μ given by Equation 4.3 we obtain $\Delta G^o(T) = 3.494\text{x}10^4 - 12.126\ T$, $\text{MNb}^3/\text{m}^2\text{atom}$ and therefore $\Delta G^o(0) = 351$ kJ/mol. ΔG^o is the total reversible work required to overcome an obstacle without the aid of an external stress. It is an intrinsic quantity that describes the interaction between the dislocation and the obstacle. We will return to this value later where the rate controlling barriers are identified.

In Figure 4.13 it can be seen that at high values of τ/μ the data tends to fall below the fitted curve. This probably arises because of the commencement of the transition from thermally activated to athermal flow.

5.2.3 The Activation Enthalpy

Smooth curves were drawn through the activation enthalpy data shown in Figure 4.11. These curves were extrapolated to $\tau/\mu = 0$. From Equation 4.9 it is clear that at $\tau/\mu = 0$, $\Delta H_{\tau/\mu} = \Delta H_{\tau} = \Delta H^o$ for all temperatures. ΔH^o was found to be approximately 350 kJ/mol. Therefore, $\Delta H^o \approx \Delta G^o(0)$, which is a necessary condition for internal consistency of the analysis. Furthermore, this value of ΔH^o can be compared with the previous values of the activation enthalpy that have been published in the literature.

The activation enthalpies that can be found in the literature have been obtained in three ways: the activation enthalpy for self-diffusion, for creep and for hot working. Landon et al (174), Garafalo (36) and Honeycombe (175) have determined ΔH_{SD}, self-diffusion, for copper to be in the range 184-234 kJ/mol, while numerous workers have found ΔH_C, creep, to be in the range 197-234 kJ/mol (36,174-176). The activation enthalpy for hot working, ΔH_{HW}, is approximately 301 kJ/mol (25). It is evident that the activation enthalpy determined here is much larger than ΔH_{SD} or ΔH_C, but is reasonably close to the hot working value. Since the ΔH_{HW} was determined from steady state hot torsion data, it is not strictly comparable with the enthalpy found in the present work as it includes a restoration component that arises from dynamic recrystallization.

The activation entropy has already been discussed in Chapter 4 and the pre-exponential factor will be dealt with later on in this chapter. Before going on to do this we will discuss the influence of some extraneous factors, such as grain boundary sliding and the presence of impurities, and their effects on the activation parameters.

5.2.4 Extraneous Factors

All of the specimens used in this investigation had the same initial grain size of 0.24 mm and the same composition as shown in Table 3.1. It is important, however, to consider the possible influence these two factors may have had on the mechanical behaviour of this metal.

It was mentioned in Chapter 3 that grain boundary sliding occurs during high temperature deformation. The amount of sliding depends on grain size, deformation rate and the extent of deformation (the amount of strain). We have pointed out that the grain size was made as large as possible to minimize sliding. Furthermore, the mechanical data used in the analysis was the yield stress, and therefore the amount of plastic strain is small, of the order of 0.001 strain. Since grain boundary sliding occurs in order to accommodate strain within the grains, this means that the likelihood of sliding occuring is negligible, even at very low strain rates.

In the OFHC copper used in this investigation there are approximately 0.08 wt% impurities, this is a typical impurity level for this material (177). The three major impurities are lead (0.013 wt%), iron (0.030 wt%) and phosphorous (0.020 wt%). In addition, it is clear from Table 3.1 that almost all of the impurities are positive metallic atoms and hence they are probably present in the copper matrix as substitutional or interstitial atoms, or they are located at the grain boundaries. It is unlikely that precipitates are present since there are very few atoms the metallic atoms could precipitate with. For example, in tough pitch copper, 0.04 wt% oxygen, some of the oxygen is present as the Cu_2O precipitate. However, at oxygen levels below 0.0035 wt% this precipitation is unlikely to occur. In the copper used in this work the oxygen level was only 0.0004 wt%.

Although there probably are no precipitates present, it is possible that the impurities could influence the mechanical properties of the copper. Since we are especially interested in ascertaining how these impurities would influence thermally activated flow, it is important to know whether they would contribute to the long or short range stress fields. The impurities that are substitutional or interstitial atoms would have short range stress fields. But, since the activation enthalpy is so much greater than the self-diffusion enthalpy, it is probable that such obstacles would be relatively transparent to the dislocations. That is, these atoms would be dragged along by the dislocations. The impurities at the grain boundaries would probably have long range stress fields and therefore would not interfere with the thermally assisted motion of the dislocations. However, grain boundaries can act as a source or sink of dislocations and therefore play a major role in determining deformation behaviour. If this is indeed the case then the segregation of impurity atoms to the grain boundaries could significantly influence the deformation behaviour.

5.3 THE PRESENT RESULTS IN TERMS OF RECOVERY-CREEP AND DISLOCATION GLIDE MODELS

So far, we have described the temperature and strain rate dependence of the yield stress, and have presented the activation parameters that characterize the deformation mechanism. This information will now be used to propose a model that explains the observed high temperature behaviour of OFHC copper.

The purpose of the present section is to examine the applicability of the various models for high temperature deformation to the present data.

5.3.1 Dislocation Climb Models

Dislocation climb models require that since climb is diffusion controlled, then the activation enthalpy must be of the same magnitude as ΔH_{SD} and the activation volume must be of the order of

1 b^3 (70). In this investigation, V^* was found to vary from 600 to 2800 b^3 over the τ/μ range of $2.8\text{x}10^{-4}$ to $0.7\text{x}10^{-4}$, respectively, and ΔH^o is much greater than ΔH_{SD}. In addition, climb models predict that the enthalpy is independent of stress, whereas we have found ΔH to be strongly stress dependent. Furthermore, climb theories were postulated to explain steady state creep behaviour and cannot be extended, without modification, to explain yield behaviour of a hot worked metal. Therefore, based on these facts we can say that the dislocation climb model is not applicable to the present investigation.

5.3.2 Jogged Screw Dislocation Models

The measured activation volumes are in reasonable agreement with the requirements of the jogged screw dislocation models. However, since jog dragging is diffusion controlled, once more the activation enthalpy should be that for self-diffusion, ΔH_{SD}, and independent of stress. From the previous section we know that ΔH^o is much greater than ΔH_{SD} in this case. Therefore, we can conclude that neither the climb nor the jogged screw dislocation models are applicable in the case of the high temperature deformation of copper.

5.3.3 Network Recovery Models

The network recovery models (see Section 2.1.3.2) agree well with the microstructural observations made on hot deformed materials. Work hardening can be equated with the contraction of the dislocation network, while recovery can be regarded as arising from network expansion. Such a concept can be used as a basis for the understanding of the observed behaviour in the transient region of the flow curves. In this way, the barriers to dislocation motion can be considered to be the nodes in the three-dimensional dislocation network; and the rate controlling step to be the unpinning of these nodes. In order to determine whether or not such a model is applicable to the present results, the properties of dislocation nodes will be considered in more detail below.

5.4 THE NETWORK RECOVERY THEORY AS A MECHANISTIC MODEL

When a dislocation, gliding along its slip plane, encounters a forest dislocation the elastic stress fields of these dislocations interact and the dislocations form a junction. These interactions are either attractive or repulsive, depending on the magnitude of the Burgers vectors of the dislocations and the angles between the intersecting dislocation lines. These junctions can obviously act as barriers to dislocation glide and can furthermore be overcome by the cooperative action of the effective stress and thermal fluctuations. Due to the flexible nature of the dislocation line, attractive junctions are approximately four times stronger than repulsive junctions (119). Therefore, the unpinning of attractive junctions is more likely to be rate controlling at high temperatures, especially since the repulsive junctions are commonly invoked as the barriers to glide at low temperatures (135). Consequently, attention will now be focussed on attractive junctions.

5.4.1 The Attractive Junction

An illustration of the formation of an attractive junction is shown in Figure 5.1 for unextended straight dislocations. The stress field of LL' interacts with MM' over a relatively short length that increases as ϕ decreases (120). Upon completion of the intersection process jogs are generally formed. If the elastic stress fields are such that the dislocations attract each other, then extra work has to be done to separate the dislocations after they have been drawn together. This attraction constitutes an additional component of the energy well. Furthermore, there is a particularly large reduction in energy at the attractive junction when a dislocation reaction occurs that reduces the total length of dislocation line. A typical reaction of this type is shown in Figure 5.1 (c) and 5.1 (d) for the intersection of two screw dislocations. Here the dislocations b_1 and b_2 react to form a third dislocation NN' with a Burgers vector b_3. The configuration shown in Figure 5.1 (d) is called a node (121). The types of dislocation reactions that give a local reduction in energy have been well catalogued for cubic materials (122-125). In addition, nodes have been observed by using electron microscopy (126-128).

In order for a dislocation to be unpinned from an attractive junction, the junction must be unzipped along PP' (see Figure 5.1 (d)). However, in low stacking fault metals such as copper the dislocations tend to be dissociated. These dislocations form extended nodes within the partial PP'. Hence, at elevated temperatures, it is to be expected that the overcoming of the extended nodes in the network would be rate controlling. These extended nodes are more complicated than the ones discussed above and will therefore be dealt with below.

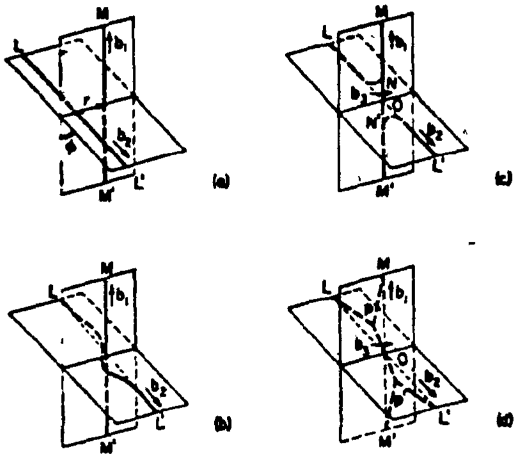

FIGURE 5.1 An illustration of the formation of an attractive junction (after Hull (119))

a) dislocation LL' moves towards MM'
b), c), and d) LL' and MM' react to form a new dislocation PP'

5.4.2 Extended Nodes

Extended nodes were first observed by Whelan (129) and later by Swann (130). More recently, these nodes have been observed by Ruff (131), Gallagher and Washburn (132) and Gallagher (133). A schematic representation of an attractive junction formed from two dissociated dislocations is shown in Figure 5.2. Sastry et al (134) and Tangri and Sastry (135) have shown that the unpinning of such a junction is probably the rate controlling mechanism in the high temperature deformation of Zr-Sn alloys (134) and nickel (135). According to Sastry et al there are three components to the energy required to overcome such an obstacle. These are illustrated in Figure 5.2 and are the intersection energy, ΔG_i, the constriction energy, ΔG_c, and the recombination energy, ΔG_r.

The intersection energy is the energy required to reunite two threefold nodes (the distance XY in Figure 5.2), ~~and~~ therefore to allow unpinning of the node. Saada (136) has shown that this energy is given by

$$\Delta G_i = \beta \mu b^2 \Delta \ell \qquad 5.2$$

where $\Delta \ell$ is the length of the combined dislocation between the two nodes and β is a constant with a range of values but is assumed to be 0.1 (134). In Chapter 2 it was noted that thermal fluctuations can only act coherently over small distances, hence widely separated nodes would be athermal in nature. The stress required for the uncombined portions of the mobile dislocations to bow out around the junction, τ_{BOW}, is given by

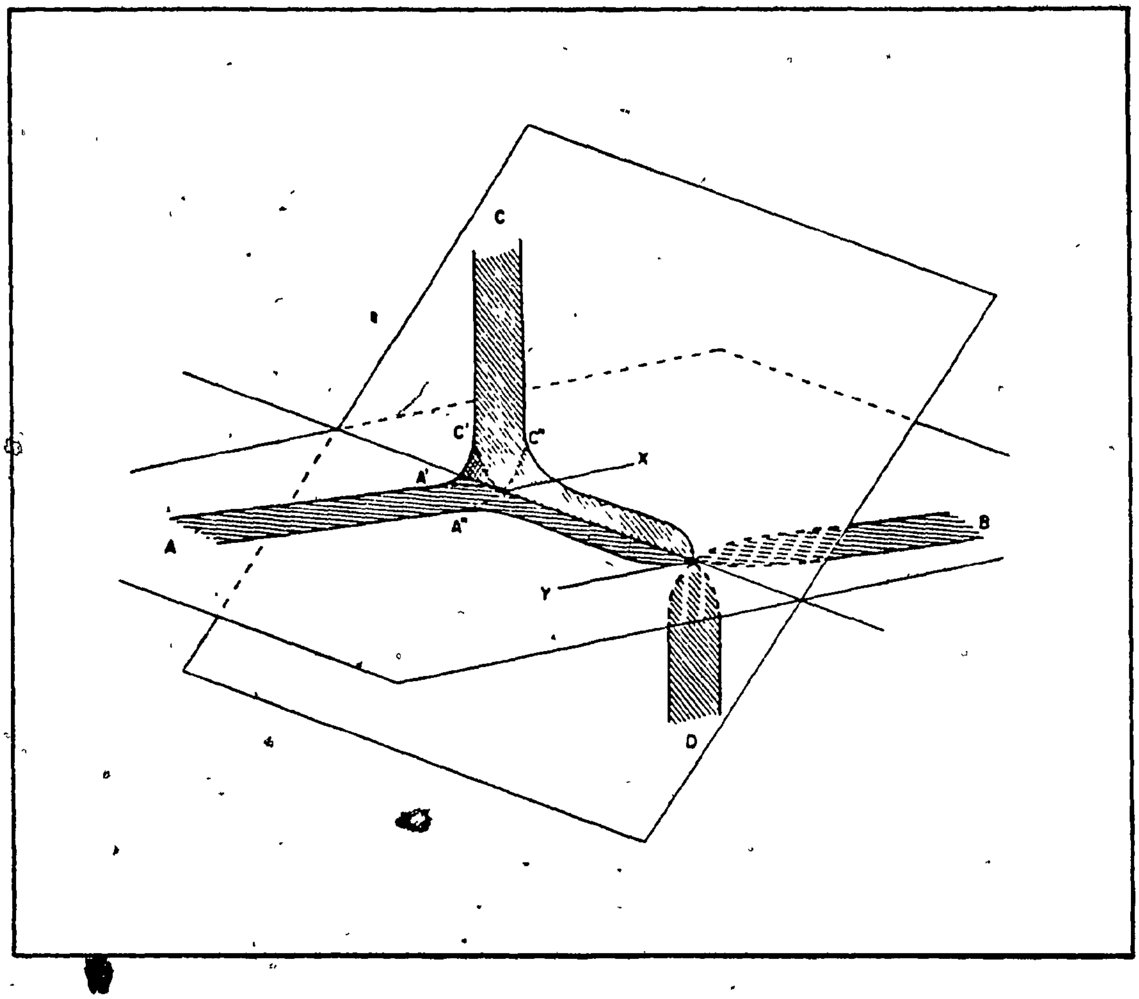

FIGURE 5.2 A schematic representation of the attractive junction for the case of two dissociated dislocations (after Sastry et al. (134)).

$$\tau_{BOW} = \frac{E\mu b}{\ell} \qquad 5.3$$

Here E is a constant with a value between 0.1 and 2, and ℓ is the average length of the forest segments. Saada (136) has shown that $\Delta\ell$ decreases with stress and is of the order of $\ell/20$ at bow-out. But at elevated temperatures the developed stress is well below τ_{BOW} and bow-out does not, in general, occur. In the presence of a stress, therefore, the threefold nodes are separated by a distance of the order of $\ell/20$. For short forest segments, this means that $\Delta\ell$ will not be more than a few Burgers vectors in length. If thermal fluctuations are of sufficient magnitude, then, for such short segment lengths, thermally activated unpinning of the junctions is possible. The magnitude of such fluctuations is given by Equation 5.2. Setting $\Delta\ell$ equal to 3b (say), we obtain

$$\Delta G_i = 0.3\mu b^3 \qquad 5.4$$

It should be noted that this value of ΔG_i represents the magnitude of the thermal fluctuation required to replace bowing by intersection when the dislocations are perfect. To this energy must be added the constriction and recombination energies of the partials.

The constriction energy is associated with the area C'A'X in Figure 5.2. Stroh (137) has calculated this energy to be approximately

$$\Delta G_c = 0.016 r\mu b^2 (\ell n(r/b))^{1/2} \qquad 5.5$$

where r is the stacking fault width.

The recombination energy, associated with the areas C"XY and A"XY in Figure 5.2, has been calculated to be (138)

$$\Delta G_r = \Delta \ell \frac{\mu b^3}{32} \ln\left(\frac{r}{b}\right) \qquad 5.6$$

The total activation energy for the unpinning of an attractive junction is then given by

$$\Delta G_T = \Delta G_i + \Delta G_c + \Delta G_r + \Delta G_j \qquad 5.7$$

The term, ΔG_j, is due to the jog that is left behind in each intersecting dislocation after they have intersected. McLean (38,139) has discussed the jog resistance for the case of attractive junctions. He considers that only one-half of the jog energy has to be supplied during breaking. The value of ΔG_j is approximately $0.04\ b^3$. Since this term is much less than the other terms that comprise ΔG_T it will be neglected.

In conclusion, therefore, ΔG_T is given by

$$\Delta G_T = 0.30\mu b^3 + 0.016 r\mu b^3 (\ln(r/b))^{1/2} + \Delta \ell \frac{\mu b^2}{32} \ln\left(\frac{r}{b}\right) \qquad \ldots\ldots 5.8$$

Before an estimate of the magnitude of ΔG_T can be made, it is necessary to determine the value of r, the stacking fault width.

5.4.3 The Stacking Fault Width in Copper

The stacking fault width can be calculated from the stacking fault energy, Λ, by using the method of Heidenreich and Shockley (140,141). They proposed that a dislocation in a f.c.c. lattice dissociates into two partial dislocations, Shockley partials, separated by a stacking fault. The dislocation reaction is as follows:

$$\frac{1}{2}a\left[01\bar{1}\right] \rightarrow \frac{1}{6}a\left[\bar{1}2\bar{1}\right] + \frac{1}{6}a\left[11\bar{2}\right]$$

where a is the lattice parameter. The Burgers vectors of all three dislocations lie in the same (111) plane. There are two forces acting upon the partials, the force of repulsion due to the fact that they have the same sign, and the force of attraction due to the stacking fault energy. When the partials are separated by a distance, r, the force of repulsion per unit length of each is approximately $a^2\mu/24\pi r$. This repulsive force is, in turn, balanced by the stacking fault energy. Hence, at equilibrium we may write

$$\Lambda = \frac{a^2\mu}{24\pi r}$$

or $\qquad\qquad\qquad\qquad\qquad\qquad\qquad\qquad\qquad\qquad$ 5.9

$$r = \frac{a^2\mu}{24\pi\Lambda}$$

For copper, the lattice parameter, a, is 36.15 nm and μ is 5.146×10^4 MN/m^2, the Hill Average value at 0°K. The value of the stacking fault energy, however, is not known precisely. Table 5.1 lists the values of Λ for copper and the methods of determination in chronological order, starting

TABLE 5.1

The Stacking Fault Energy for Copper

Method	Λ, mJ/m^2	Reference
2 x coherent twin energy	~ 40	143
2 x coherent twin energy	~ 42	144
τ_3	163	145,146
τ_3	102 → 165	147
extrapolated node data	~ 40	148
2 x coherent twin energy	~ 24	149
recalculated node data	70 ± 10	150
normalized fault probability	67 ± 17	151
absence of extended nodes	$\gtrsim 31$	152
τ_3	50	153
tetrahedra stability (scaled)	78	154
tetrahedra stability	73 ± 15	155
faulted dipoles	$\lesssim 59$	156
faulted dipoles	150 ± 30	157
tetrahedra stability	58.5	158
normalized fault probability	70 ± 15	159
extrapolated node data	48 ± 10	160
weak beam electron microscopy	41 ± 9	161,162

with the earliest determination of the stacking fault energy. Although there is a wide range of values for Λ, the most recent results seem to fall randomly about some mean value, except for the value of Λ of 150 mJ/m^2 determined by Steeds (157). Gallagher (163) has stated that the consensus of these findings is that the stacking fault energy for copper is approximately 55 mJ/m^2. Consequently, this value is used to calculate the stacking fault width. Substituting in Equation 5.9 we obtain $r \approx 6.4$ b.

We are now in a position to calculate the total energy required to unpin an attractive junction in copper.

5.4.4 The Rate Controlling Mechanism

Setting the stacking fault width equal to 6.4 b and $\Delta\ell = 3$ b, we obtain $\Delta G_T = 0.61 \mu b^3$/atom. This value agrees very well with the value of $0.66 \mu b^3$/atom obtained for ΔG^o from the experimental data. It should be noted that the value obtained for ΔG_T is only approximate since the values for r and $\Delta\ell$ could only be estimated. Furthermore, the value of ΔG^o is also very rough since the extrapolation of the experimental data to zero stress is only an approximation. Despite this, the fact that ΔG_T and ΔG^o are in such good agreement does imply that the rate controlling mechanism of high temperature flow in copper is the thermally activated unzipping of attractive junctions.

As shown earlier, this mechanism was suggested by assuming that the network recovery models apply to the hot working of copper. Another argument for this mechanism is an argument of omission. None of the other models are compatable with the activation parameters that have been determined.

Having determined the rate controlling obstacle, it is now necessary to attempt to explain the behaviour of the pre-exponential factor in terms of a dislocation model that is consistent with the node unpinning model for the activation free energy.

5.5 A MODEL FOR THE PRE-EXPONENTIAL FACTOR

There are two salient features about the experimental values of the pre-exponential factor. These are (i) the pre-exponential is not dependent on τ/μ or temperature; and (ii) this constant value of the pre-exponential is approximately $3.5\text{x}10^5 s^{-1}$.

We can estimate the consistency of the value of $\dot{\varepsilon}_o$ from Equation 2.21, that is

$$\dot{\varepsilon}_o = \rho_m \frac{b\nu A}{M\ell} \qquad 5.10$$

The mobile dislocation density, ρ_m, can be estimated from this equation by making some assumptions about the terms in this expression. Firstly, we assume that A, the area swept out by a dislocation segment, ℓ, after a successful activation event, is equal to ℓ^2 (64). Therefore, Equation 5.10 becomes

$$\rho_m = \dot{\varepsilon}_o \frac{M}{b\nu\ell} \qquad 5.11$$

There are two ways of determining the attempt frequency, ν, that lead to different values of ρ_m.

Friedel (40) has assumed that the pinned segment attempts to surmount the obstacle with a frequency of $\nu_D b/\ell$, where ν_D is the Debye frequency. Substituting these terms into Equation 5.11, we obtain

$$\rho_m = \dot{\varepsilon}_o \frac{M}{b^2 \nu_D} \qquad 5.12$$

Using the value of $\nu_D = 10^{13} s^{-1}$, the average value of $\dot{\varepsilon}_o$, $3.5 \times 10^5 s^{-1}$, corresponds to a mobile dislocation density of approximately $1.6 \times 10^{12} m^{-2}$.

Kocks et al (65), on the other hand, have used another approach to estimate the attempt frequency. They have pointed out that the limits of ν are the atomic frequency, ω, and the dislocation ground state frequency, $\omega b/4\ell$. The atomic frequency is defined as the ratio of the speed of sound in a material to the Burgers vector of the material. For copper, ω is $8.4 \times 10^{-2} s^{-1}$ (65). Granato et al (166) have shown that ν is a property of the obstacle and the dislocation line tension, but not of the obstacle spacing. Kocks et al have used these findings to show that ν generally has the following range of values:

$$\frac{\omega}{1000} \leqslant \nu \leqslant \frac{\omega}{100} \qquad 5.13$$

or, typically, $10^{10} \leqslant \nu \leqslant 10^{11} s^{-1}$. Assuming that $\ell \sim 1/\sqrt{\rho_m}$ and using these values for ν, we obtain a range of values for ρ_m : $1.8 \times 10^9 \leqslant \rho_m \leqslant 1.8 \times 10^{11} m^{-2}$.

The value of ρ_m determined by using Friedel's assumption is somewhat higher than the density one would expect for a well annealed polycrystal. However, the range of values obtained by using Kock's method give a more reasonable value for the mobile dislocation density. In addition, from a mechanistic viewpoint, Kock's method is more precise than Friedel's. The finding that the mobile dislocation density at the onset of macroscopic yielding is approximately the same as that in a well annealed polycrystal, supports our contention that the internal stress is negligible at the onset of macroscopic yielding. Furthermore, this finding agrees with the observed stress and temperature independence of the pre-exponential factor, because a constant $\dot{\varepsilon}_0$ implies a constant ρ_m. This proposition is plausible when one considers that all of the specimens had the same thermo-mechanical treatment prior to testing.

The model leading to Equation 5.10 is appropriate for cases where changes in the applied stress are expected to lead to different substructures, and therefore to different total and mobile dislocation densities (64). This situation arises in steady state creep and hot working. The present data, however, applies to the yield stress. Therefore, it is better to consider a pre-exponential model that is based upon a dislocation structure which is approximately constant at the onset of macroscopic yielding.

5.5.1 A Pre-Exponential Model Based on a Distribution of Dislocation Segment Lengths

A model for the pre-exponential factor, based on a distribution of dislocation segment lengths, was proposed by Surek et al (64) and subsequently by Immarigeon (5). This model was used to explain the τ/μ dependence of the pre-exponential factor observed in the hot working of zirconium (64) and Armco iron and silicon steel (5). However, this model can be used to explain the behaviour of the pre-exponential factor determined in the present investigation, as will be shown below.

Following the example of Immarigeon, we assume that the dislocations in the copper at the onset of macroscopic yielding are arranged in a manner similar to a Frank net (165). It is further assumed that this network can be described by a population of link lengths occurring in a spectrum of link lengths. The final assumption is that the strain rate is produced by a density of mobile dislocations, ρ_m, which depends on the distribution of segment lengths and on the effective stress. Now, according to this model, at an arbitrary value of the effective stress only a narrow range of segment lengths will be thermally activatable. The upper limit of the length, ℓ_{max}, is defined by the minimum length that can bow out between the local obstacles without the aid of thermal activation. Generally, ℓ_{max} is proportional to the inverse of the modulus-reduced effective stress. Hence, the higher the stress the lower the value of ℓ_{max}. In principle, all segment lengths less than ℓ_{max} can be thermally activated. However, at lengths below some value, ℓ_{min}, the segments are so short that the wait time for thermal activation is excessively long. These very short segments can therefore be considered immobile. Hence, the mobile dislocation density is due to those segments with lengths, ℓ, such that: $\ell_{min} \leqslant \ell \leqslant \ell_{max}$. The dislocation density available for thermal activation is given by the expression

$$\rho_m = \int_{\ell_{min}}^{\ell_{max}} \ell\xi(\ell)d\ell \qquad 5.14$$

where $\xi(\ell)$ is the number of link lengths per unit volume and per unit interval of segment length. Therefore, $\xi(\ell)d\ell$ is the number of segment lengths per unit volume with lengths between ℓ and $\ell + d\ell$. It should be noted that according to this model, the total dislocation density, ρ_T, is given by:

$$\rho_T = \int_0^{\infty} \ell\xi(\ell)d\ell \qquad 5.15$$

The density of activatable sites, N, is $N = \rho_m/\ell$, and given that $dN/d\rho_m = 1/\ell$ then it follows that

$$N = \int_{\ell_{min}}^{\ell_{max}} \xi(\ell)d\ell \qquad 5.16$$

Immarigeon has approximated this integral with the expression

$$N = \overline{\xi}(\ell^*)\Delta\ell^* \qquad 5.17$$

where $\overline{\xi}(\ell^*)$ is the average distribution factor which is given by:

$$\overline{\xi}(\ell^*) = \frac{1}{\Delta\ell^*}\int_{\ell_{min}}^{\ell_{max}} \xi(\ell)d\ell \qquad 5.18$$

Here $\Delta\ell^*$ is the difference between ℓ_{max} and ℓ_{min}, and ℓ^* is the average segment length of those segments that are longer than ℓ_{min} and shorter than ℓ_{max}.

The equation for the pre-exponential factor, Equation 5.10, can be rewritten as

$$\dot{\varepsilon}_o = N \frac{Ab\nu}{M} \qquad 5.19$$

where all the terms have the usual meaning. The area swept out after activation, A, is equal to $\ell^*\ell_{av}$, where ℓ_{av} is the average segment length in the network. Using the value of ν obtained by Kocks et al (65), we obtain

$$\dot{\varepsilon}_o \simeq \overline{\xi}(\ell^*)\Delta\ell^*\ell^*\ell_{av} \frac{b10^{11}}{M} \qquad 5.20$$

The quantity $\ell_{av}10^{11}b/M$ can be regarded as constant since it is assumed that the overall structure and network length distribution, at the commencement of plastic flow, remains essentially the same as the unstressed material. Therefore, in order for $\dot{\varepsilon}_o$ to be constant, $\overline{\xi}(\ell^*)\Delta\ell^*\ell^*$ must also be independent of stress and temperature. In order to see how this could arise we will now consider the stress and temperature dependence of each of these terms.

From Equation 5.18 it is clear that any stress dependence of $\overline{\xi}(\ell^*)$ will arise because of the stress dependence of ℓ^* (5). Statistical treatments of obstacle-dislocation interactions (167-169) show that ℓ^* takes a stress dependence of the form

$$\ell^* \propto (\tau/\mu)^{-c} \qquad 5.21$$

where $c < 1$.

Friedel (167) has argued that as the stress increases, the dislocation contacts more obstacles thereby reducing ℓ^*. Such an analysis leads to a value of 1/3 for the stress exponent, c. Kocks (168,169), in a more complex analysis, found that c increases from 1/3 to 4/5 as the obstacle strength increases. Finally, for athermal obstacles, c is equal to 1.

The dependence of $\bar{\xi}(\ell^*)$ on ℓ^* is similar to that of $\xi(\ell)$ on ℓ. It has been found from internal friction studies (170) that $\xi(\ell)$ and ℓ are related by an expression of the form:

$$\xi(\ell) \propto \left(\frac{1}{\ell}\right)^{i} \qquad 5.22$$

where i ranges from 3 to 5. This relationship has been confirmed by observations made of the link length distribution using electron microscopy (171,172). However, these studies indicate that i varies from a value of 2.5 in unstressed materials to a value of 6 or 8 at large values of strain. Since, in the present work, only the macroscopic yield stress was considered, a value of i = 3 was considered appropriate.

The stress dependence of $\bar{\xi}(\ell^*)$ can be derived from that of ℓ^*, and is found to be

$$\xi(\ell^*) \propto (\tau/\mu)^{j} \qquad 5.23$$

where $j = c.i$.

In order to completely describe the τ/μ dependence of the pre-exponential, it is only left to determine the stress dependence of $\Delta\ell^*$. It is assumed that this dependence has the form

$$\Delta\ell^* \propto (\tau/\mu)^n \qquad 5.24$$

Since $\Delta\ell^* = \ell_{max} - \ell_{min}$, an approximate value of n can be obtained by investigating the stress dependencies of ℓ_{max} and ℓ_{min}. ℓ_{max} is the critical segment length above which the segment bows out under the action of the effective stress only. It is related to the stress by an Orowan type expression (173)

$$\ell_{max} = Db(\tau/\mu)^{-1} \qquad 5.25$$

where b is the Burgers vector and D is a numerical constant of about 0.5. ℓ_{min} is the minimum length for which the wait time for thermal activation is not excessively long. It is difficult to estimate the stress dependence of ℓ_{min}. However, we know that $\ell_{max} > \ell_{min}$ for all τ/μ, and that as the temperature decreases and the strain rate increases the flow stress becomes athermal. When the flow is completely athermal, ℓ_{max} and ℓ_{min} must be equal to zero. That is, when τ/μ takes a value so that plastic flow is athermal then $\Delta\ell^* = 0$. It is clear, therefore, that n in Equation 5.24 must be negative. Furthermore, the stress dependence of ℓ_{min} must be less than the dependence of ℓ_{max} so that, if ℓ_{min} is represented by the following function

$$\ell_{min} \propto (\tau/\mu)^{-f} \qquad 5.26$$

then 0 < f < 1. Consequently, it is reasonable to assume that $\Delta\ell^*$ has a similar stress dependence as ℓ_{max}, that is, n should be approximately equal to -1.

From Equations 5.20, 5.21, 5.23 and 5.24, it is possible to estimate the stress dependence of the pre-exponential factor. That is,

$$\dot{\varepsilon}_o \propto (\tau/\mu)^m \qquad 5.27$$

where $m = c.i - c + n$ which is equal to $c(i - 1) + n$. If $1/3 < c < 4/5$, $i \approx 3$ and $n \approx -1$ we obtain $m = 2c - 1$, that is, $-1/3 < m < 3/5$. This range of values of m is compatable with a constant pre-exponential factor.

The analysis of the present experimental data has shown that m is close to zero. This result is clearly consistent with a node unpinning model where the pre-exponential factor is determined by the properties of a distribution of dislocation segment lengths.

CHAPTER 6

CONCLUSIONS

Uniaxial compression tests have been carried out on polycrystalline OFHC copper in the temperature range 500 to 800°C and at constant true strain rates ranging from 5.2x10^{-2} to 5.2x10^{-5}s^{-1}. The temperature and strain rate dependence of the macroscopic yield stress data, obtained from these experiments, has been interpreted in terms of the thermally assisted motion of dislocations over localized elastic obstacles. This study has led to a number of conclusions regarding the high temperature deformation behaviour of copper.

1. The true stress-true strain curves of copper are typical of a metal that recrystallizes dynamically. The oscillations in flow stress, observed at high strains, increase with increasing temperature and decreasing strain rate. The strain to the first peak and the width of this peak decreases with increasing temperature and decreasing strain rate.

2. At the start of loading the flow curves exhibited an interval of initial loading, the extent of which is strain rate and temperature dependent. The end of this region is marked by an abrupt change in the work hardening rate. The slope of the flow curve decreases by a factor of approximately ten at this point. The high temperature yield stress, as defined by the 0.2% strain offset, is strongly temperature and strain rate sensitive.

3. The yield stress data were reduced by a method of activation analysis for linear elastic obstacles in terms of the modulus-reduced effective stress. The analytical scheme leads to activation free energies and volumes that are functions of the modulus-reduced effective stress only, as required for such obstacles. Of particular interest are the following observations:

(i) The pre-exponential factor in the rate equation is constant and independent of temperature and the modulus-reduced stress.

(ii) The activation enthalpy is strongly dependent on the modulus-reduced stress. In the absence of stress, this enthalpy is much greater than the activation enthalpy for self-diffusion.

(iii) The activation volume varies from approximately 600 b^3 at $\tau/\mu = 2.8\times10^{-4}$ to 2800 b^3 at $\tau/\mu = 0.7\times10^{-4}$.

(iv) In the absence of stress, the activation free energy is 0.66 μb^3/atom.

These observations preclude the possibility of the rate controlling mechanism being dislocation climb or the dragging of jogs in screw dislocations.

4. It is concluded from the above observations that the obstacle to dislocation glide that is rate controlling is the thermally activated unpinning of attractive junctions. It is shown that such a process requires thermal fluctuations of approximately 0.61 μb^3/atom in the absence of stress.

5. The stress and temperature independent pre-exponential factor is consistent with a node unpinning model for dislocation glide where the behaviour of the pre-exponential term is determined by the properties of a distribution of dislocation segment lengths.

REFERENCES

1. J.J. Jonas, C.M. Sellars and W.J. McG. Tegart: Met. Reviews, 130, (1969), 1.

2. O.D. Sherby and P.M. Burke: Progr. Mater. Sci., 13, (1968), 325.

3. D. McLean: Rep. Progr. Physics., 29, (1966), 1.

4. M.J. Luton: Ph.D. Thesis, McGill University, Montreal, (1971).

5. J-P.A. Immarigeon: Ph.D. Thesis, McGill University, Montreal, (1974).

6. R. Lagneborg: Met. Reviews, 165, (1972), 130.

7. A.S. Norwick: Acta. Met., 3, (1955), 312-321.

8. B. Heritier: Ph.D. Thesis, McGill University, Montreal, (1976).

9. J.J. Jonas, D.R. Axelrad, and J.L. Uvira: Proc. Internat. Conf. on "Strength of Metals and Alloys", Tokyo, Sept. (1967); Trans. Japan Inst. Metals, (1968), 9, Suppl., 257.

10. R.A. Reynolds and W.J. McG. Tegart: J. Iron Steel Inst., 200, (1962), 1044.

11. J.L. Uvira and J.J. Jonas: Trans. Met. Soc. A.I.M.E., 242, (1968), 1619.

12. D.M. Keane, C.M. Sellars and W.J. McG. Tegart: Mém. Sci. Rev. Mét., 65, (1968), 255.

13. C. Rossard and P. Blain: Rev. Mét., 55, (1958), 573; Publ. IRSID (174a), (1957).

14. C. Rossard and P. Blain: Mém. Sci. Rev. Mét., 56, (1959), 286; Publ. IRSID (174), Part II, (1958).

15. R. Tamhankar, J. Plateau and C. Crussard: Rev. Mét., 55, (1958), 383.

16. C. Crussard and R. Tamhankar: Trans. Met. Soc. A.I.M.E., 212, (1958), 718.

17. C. Rossard and P. Blain: Mém. Sci. Rev. Mét., 57, (1960), 173.

18. C. Rossard: D.Sc. Thesis, Univ. Paris, 1960; Métaux. Corrosion-Ind., 35, (1960), 102, 140, 190.

19. G.A. Redfern and C.M. Sellars: "Deformation under Hot-Working Conditions", Special Rep. No.108, p.29, London (Iron Steel Inst.), (1968).

20. A.T. English and W.A. Backofen: Trans. Met. Soc. A.I.M.E., 230, (1964), 396.

21. J.J. Jonas, H.J. McQueen and W.A. Wong: Ref.19, p.49.

22. H.J. McQueen, W.A. Wong and J.J. Jonas: Canad. J. Physics, 45, (1967), 1225.

23. D. Hardwick and W.J. McG. Tegart: J. Inst. Metals, 90, (1961-62), 17; Mem. Sci. Rev. Met., 58, (1961), 869.

24. W.A. Wong, H.J. McQueen and J.J. Jonas: J. Inst. Metals, 95, (1967), 129.

25. C.M. Sellars and W.J. McG. Tegart: Mém. Sci. Rev. Mét., 63, (1966), 731.

26. J. Cotner and W.J. McG. Tegart: J. Inst. Metals, 97, (1969), 73.

27. G. Gagnon: Ph.D. Thesis, McGill University, Montreal, (1968).

28. W.D. Nix: Acta Met., 15, (1967), 1079.

29. M.J. Luton and C.M. Sellars: Acta. Met., 17, (1969), 1033-1043.

30. J.P. Sah, G.J. Richardson and C.M. Sellars: J. Australian Inst. Metals, 14, (1969), 392.

31. E. Shapiro and G.E. Dieter: Met. Trans., 1, (1970), 1711.

32. J. Weertman: J. Appl. Phys., 28, (1957), 362.

33. J. Weertman: J. Appl. Phys., 26, (1955), 1213.

34. J.E. Dorn: "Progress in Understanding High-Temperature Creep" (H.W. Gillette Memorial Lecture, 1962), (1962), Philadelphia, Pa. (Amer. Soc. Test. Mat.).

35. J.E. Dorn: "Energetics in Metallurgical Phenomena", Vol.I, p.241, New York (Gordon and Breach), (1965).

36. F. Garofalo: "Fundamentals of Creep and Creep-Rupture in Metals", New York (Macmillan), (1965).

37. C.R. Barrett and W.D. Nix: Acta. Met., 13, (1965), 1247.

38. D. McLean: Rep. Prog. Phys., 29, (1966), 1.

39. R. Lagneborg: Metal.Sci. J., 3, (1969), 56.

40. J. Friedel: "Dislocations", Pergamon Press, London, (1964).

41. A. Seeger: "Dislocations and Mechanical Properties of Crystals", Wiley, New York, (1959).

42. H. Conrad: J. Iron Steel Inst., 198, (1961), 364.

43. G.B. Gibbs: Mat. Sci. Engr., 4, (1969), 313-328.

44. A.H. Cottrell: "Dislocations and Plastic Flow in Crystals", Clarendon Press, Oxford, (1953).

45. A. Seeger: Phil. Mag., 46, (1955), 1194.

46. A. Seeger: Proc. 2nd Geneva Conf. PUAE 6, (1958), 250.

47. J.C. Slater: "Introduction to Chemical Physics", McGraw Hill, New York, (1939).

48. D. Turnbull and J.S. Fisher: J. Chem. Phys., 17, (1949), 71.

49. B. Escaig: Cry. Lat. Def., 1, (1970), 189.

50. R. Becker: Physick Zeitz, 26, (1925), 919.

51. H. Eyring: J. Chem. Phys., 4, (1936), 283.

52. W. Kauzmann: Trans. AIME, 143, (1941), 57.

53. F. Seitz and T.A. Read: J. Appl. Phys., 12, (1941), 100, 170, 470, 538.

54. Z.S. Basinski: Phil. Mag., 4, (1959), 393.

55. G. Schoeck: Phys. Stat. Sol., 8, (1965), 499.

56. G.B. Gibbs: Phys. Stat. Sol., 5, (1964), 693.

57. G.B. Gibbs: Phys. Stat. Sol., 10, (1965), 507.

58. G.B. Gibbs: Phil. Mag., 16, (1967), 97.

59. G.B. Gibbs: Phil. Mag., 22, (1970), 701.

60. J.C.M. Li: Trans. AIME, 233, (1965), 219.

61. J.C.M. Li: "Dislocation Dynamics", p.87 (A.R. Rosenfield, et al., Eds.), McGraw Hill, New York, (1968).

62. J.P. Hirth and W.D. Nix: Phys. Stat. Sol., 35, (1969), 177.

63. T. Surek, M.J. Luton and J.J. Jonas: Phil. Mag., 27, (1973), 425.

64. T. Surek, M.J. Luton and J.J. Jonas: Phys. Stat. Sol., 57, (1973), 647.

65. U.F. Kocks, A.S. Argon and M.F. Ashby: "Thermodynamics and Kinetics of Slip", Pergamon Press, Oxford, (1975).

66. Z.S. Basinski: Acta Met., 5, (1967), 684-686.

67. H. Conrad and H. Wiedersich: Acta Met., 8, (1960), 128-130.

68. J.C.M. Li: Can. J. Phys., 45, (1967), 493-509.

69. J.W. Christian and B.C. Masters: Proc. Roy. Soc. London, 281, (1964), 240-257.

70. A.G. Evans and R.D. Rawlings: Phys. Stat. Sol., 34, (1969), 9.

71. J.J. Jonas and M.J. Luton: Met. Trans., 2, (1971), 3492-3495.

72. J.J. Jonas, M.J. Luton and T. Surek: Met. Trans., 3, (1972), 2295-2297.

73. M.J. Luton and J.J. Jonas: Can. Met. Quart., 11, (1972), 79-90.

74. C. Alstetter: "Thermal and Athermal Deformation", in Energetics in Metallurgical Phenomena, Vol.IV, Ed. W.M. Mueller, Gordon and Breach, New York, (1968), 7.

75. J-P.A. Immarigeon and J.J. Jonas: Acta Met., 22, (1974), 1235-1247.

76. T. Surek, L.G. Kuon, M.J. Luton and J.J. Jonas: John E. Dorn Symp. on Rate Proc. in Plastic Deform., ASM, Cleveland, (1974), 629-655.

77. R.A. Swalin: "Thermodynamics of Solids", J. Wiley and Sons, Inc., New York, (1962), 27-29.

78. J.D. Fast: "Entropy", McGraw-Hill, New York, (1962).

79. H.B. Callen: "Thermodynamics", Wiley Inc., (1960).

80. J.P. Hirth: "Fundamental Aspects of Dislocation Theory", National Bureau of Standards (U.S.A.), Washington (D.C.), (1970), Spec. Publ. 317, p.1111.

81. J.J. Jonas: Acta Met., 17, (1969), 397-405.

82. W. Voigt: "Lehrbuch der Kristallphysik", Teubner, Leipzig, (1928).

83. C. Zener: "Elasticity and Anelasticity of Metals", University of Chicago Press, Chicago, (1948), 11.

84. W.J. McG. Tegart: "Elements of Mechanical Metallurgy", Macmillan Company, New York, (1966).

85. C. Zener: Ref.83, pp.12-15.

86. A. Reuss: Z. Angew. Math. Mech., 9, (1929), 55.

87. W. Voigt: Ref.82, p.716.

88. D.J. Abson and J.J. Jonas: J. Nucl. Mat., 42, (1972), 73.

89. R. Hill: Proc. Phys. Soc. (London) A65, (1952), 349-354.

90. C. Rossard: Rev. Met., 65, (1968), 181-195.

91. M.M. Farag, C.M. Sellars and W.J. McG. Tegart: "Deformation under Hot Working Conditions" (Special Rep. No.108), Iron and Steel Inst., London, (1968), 60-67.

92. D. Hanson and M.A. Wheeler: J. Inst. Metals, 45, (1931), 229.

93. R. King, R.W. Cahn and B. Chalmers: Nature, Lond., 161, (1948), 682.

94. F.W. Rhines, W.E. Bond and M.A. Kissel: Trans. ASM, 48, (1956), 919.

95. F. Wineberg: Trans. AIME, 212, (1958), 808.

96. R.P. Carreker, Jr. and W.R. Hibbard, Jr.: Acta Met., 1, (1953), 654-663.

97. W.J. McG. Tegart: Ref. 84, p.166.

98. A.S.T.M. Standards, Pt.31, (1972), 428.

99. R.A. Petkovic-Luton: Ph.D. Thesis, McGill University, Montreal, (1975).

100. M.J. Luton, J-P.A. Immarigeon and J.J. Jonas: J. Phys. E.: Sci. Instr., 7, (1974), 862-864.

101. H.J. McQueen and J.J. Jonas: "Metal Forming: Interrelation between Theory and Practice", Ed. A.L. Hoffmanner, Plenum Publishing Corp., New York, (1970), 393-428.

102. Standard Methods of Compression Testing of Metallic Materials at Room Temperature, ASTM Standard, E9-67.

103. H.J. McQueen and J.J. Jonas: Recovery and Recrystallization During High Temperature Deformation in "Plastic Deformation of Materials", Ed. R.J. Arsenault, Academic Press, N.Y., (1975), 393-493.

104. M.J. Luton and J.J. Jonas: Proc., 2nd Int. Conf. Strength Metals and Alloys (Asilomar, 1970), ASM, Metals Park, 1100-1105.

105. G.I. Taylor: J. Inst. Met., 62, (1938), 307.

106. M.R. Staker and D.L. Holt: Acta Met., 20, (1972), 575.

107. W. Koster: Z. Metallk., 39, (1948), 145.

108. W.C. Overton and J. Gaffney: Phys. Rev., 98, (1955), 969-977.

109. Y.A. Chang and L. Himmel: J. App. Phys., 37, (1966), 3567-3572.

110. G. Simmons and H. Wang: "Handbook of Single Crystal Elastic Constants and Calculated Aggregate Properties, 2nd Ed.", M.I.T. Press, Cambridge, Mass., (1971), 56.

111. W. Frank: Phys. Stat. Sol., 26, (1968), 197.

112. C.R. Barrett and W.D. Nix: Acta Met., 13, (1965), 1247.

113. A.A. Solomon: Ph.D. Thesis, Stanford University, (1968).

114. J.L. Lytton, C.R. Barrett and O.D. Sherby: Trans. AIME, 233, (1965), 1399.

115. U.F. Kocks: Ref. 76, pp.356-383.

116. J-P. Immarigeon: Masters Thesis, McGill University, Montreal, (1970).

117. J-P. Immarigeon and J.J. Jonas: Acta Met., 19, (1971), 1053-1061.

118. H.B. Huntington: Solid St. Phys., 7, (1958), 213.

119. D. Hull: "Introduction to Dislocations", Pergamon Press, Oxford, (1965), p.150.

120. W. Carrington, K.F. Hale and D. McLean: Proc. Roy. Soc. A, 259, (1968), 203.

121. F.R.N. Nabarro: "Theory of Crystal Dislocations", Clarendon Press, Oxford, (1967).

122. J.P. Hirth: J. Appl. Phys., 14, (1961), 439.

123. L.J. Teutonico: Phys. Stat. Sol., 16, (1966), 457.

124. B. Gale: "Relation between Structure and Mechanical Properties of Metals", H.M.S.O., London, (1963), p.100.

125. C.S. Hartley: Phil. Mag., 14, (1966), 7.

126. J.M. Hedges and J.W. Mitchell: Phil. Mag., 44, (1953), 223.

127. S. Amelinckx: Nuovo Cim. Suppl., 7, (1958), 569.

128. E.C.H. Silk and R.S. Barnes: Acta Met., 9, (1961), 558.

129. M.J. Whelan: Proc. Roy. Soc.A, 249, (1958), 114.

130. P.R. Swann: "Electron Microscopy and Strength of Crystals", Wiley, New York, (1963), 131.

131. A.W. Ruff: Met. Trans., 1, (1970), 2391.

132. P.C.J. Gallagher and J. Washburn: Phil. Mag., 14, (1966), 971.

133. P.C.J. Gallagher: Phys. Stat. Sol., 16, (1966), 95.

134. D.H. Sastry, M.J. Luton and J.J. Jonas: Phil. Mag., 30, (1974), 115.

135. K.K. Tangri and D.H. Sastry: Phil. Mag., 32, (1975), 513.

136. G. Saada: Acta Met., 8, (1960), 841.

137. A.N. Stroh: Proc. Phys. Soc. Lond. B, 67, (1954), 427.

138. J.R. Dorn and J.B. Mitchell: "High Strength Materials", Ed. V.F. Zackay, Wiley, New York, (1965), 510.

139. D. McLean: "Mechanical Properties of Metals", Wiley, London, (1962), 103.

140. W. Shockley: Phys. Rev., 73, (1948), 1232.

141. R.D. Heidenreich and W. Shockley: "Strength of Solids", p.57.

142. R.A. Robie, P.M. Bethke and K.M. Beardsley: U.S. Geological Survey, Bulletin 1248.

143. R. Fullman: J. Appl. Phys., 22, (1951), 448.

144. J.C. Fisher and C.G. Dunn: "Imperfections in Nearly Perfect Crystals", Wiley, New York, (1952), p.317.

145. A. Seeger, R. Berner and H. Wolf: Z. Physik, <u>155</u>, (1959), 247.

146. R. Berner: Z. Naturforsch, <u>A15</u>, (1960), 689.

147. P. Haasen and A. King: Z. Metallk., <u>51</u>, (1960), 722.

148. A. Howie and P.R. Swann: Phil. Mag., <u>6</u>, (1961), 1215.

149. M.C. Inman and A.R. Kahn: Phil. Mag., <u>6</u>, (1961), 932.

150. P.R. Thornton, T.E. Mitchell and P.B. Hirsch: Phil. Mag., <u>7</u>, (1962), 1349.

151. L.F. Vassamillet and T.B. Massalski: J. Appl. Phys., <u>34</u>, (1963), 3398.

152. P.C.J. Gallagher: Ph.D. Thesis, Cambridge University, England, (1964).

153. E. Peissker: Acta Met., <u>13</u>, (1965), 419.

154. M.H. Loretto, L.M. Clarebrough and R.L. Segall: Phil. Mag., <u>11</u>, (1965), 459.

155. J. Jøssang and J.P. Hirth: Phil. Mag., <u>13</u>, (1966), 657.

156. F. Haussermann and M. Wilkens: Phys. Stat. Sol., <u>18</u>, (1966), 609.

157. J.W. Steeds: Phil. Mag., <u>16</u>, (1967), 771.

158. L.M. Clarebrough, P. Humble and M.H. Loretto: Can. J. Phys., <u>45</u>, (1967), 1135.

159. H.M. Otte: J. Appl. Phys., <u>38</u>, (1967), 217.

160. P.C.J. Gallagher and Y.C. Liu: Acta Met., <u>17</u>, (1969), 127.

161. W.M. Stobbs and C.H. Sworn: Phil. Mag., <u>24</u>, (1971), 1365.

162. D.J.H. Cockayne, M.L. Jenkins and I.L.F. Ray: Phil. Mag., <u>24</u>, (1971), 1383.

163. P.C.J. Gallagher: Met. Trans., <u>1</u>, (1970), 2429.

164. R.W.K. Honeycombe: "The Plastic Deformation of Metals", Arnold, London, (1968), 225.

165. F.C. Frank: Proc. Phys. Soc. A, <u>62</u>, (1950), 131.

166. A.V. Granato, K. Lucke, J. Schlipf and L.J. Teutonico: J. Appl. Phys., <u>35</u>, (1964), 2732.

167. J. Friedel: Ref.40, p.225.

168. U.F. Kocks: Can. J. Phys., 45, (1967), 737-755.

169. U.F. Kocks: Phil. Mag.[illegible]3, (1966), 541-566.

170. W.P. Mason: J. Acoust. Soc. Am., 28, (1956), 1207-1218.

171. J.B. Bilde-Sorensen: Acta Met., 21, (1973), 1495.

172. A. Oden, E. Lind and R. Lagneborg: Proc. Conf. Creep Strength in Steel and High Temperature Alloys, Sheffield, (1972).

173. E. Orowan: Symp. on Internal Stresses in Metals, Inst. of Metals, London, (1948), 451.

174. P.R. Landon, J.L. Lytton, L.A. Shepard and J.E. Dorn: Trans. ASM, 51, (1959), 900.

175. R.W.K. Honeycombe: Ref.164, p.368.

176. P. Feltham and J.D. Meakin: Acta Met., 7, (1959), 614.

177. M.R. Staker and D.L. Holt: Acta Met., 20, (1972), 569.

APPENDIX I

Listing of the Data Handling Computer Program YIELD

```
JOB, START=10303
JOB, REMOVE, YIELD
JOB, COMPILE, YIELD, NOLIST
C          ***************************************************************
C          ***************************************************************
C
C                                  *********
C                                  * YIELD *
C                                  *********
C
C          ***************************************************************
C          ***************************************************************
C
C
C
C
C          ***************************************************************
C          THIS PROGRAM TAKES DATA FROM THE DISC SCRATCH FILE AREA AND
C          PRODUCES A YIELD PLOT OF THE DATA.  THIS IS ACCOMPLISHED BY
C          CALCULATING THE ACTUAL APPLIED STRAIN RATE FROM THE DATA.
C          THEN THE STRAINS ARE RECALCULATED ON THE BASIS OF THE NEW RATE
C          THE TIME DIFFERENCE IN THE LOAD .. STRAIN READINGS IS ACCOUNTED
C          FOR
C          ***************************************************************
C
C
        DOUBLE PRECISION DTIME, DSTRN, SUMX, SUMY, SUMX2, SUMXY, EDOTAP, EINT
        DIMENSION C( 4 ), NOTEST( 2 ), TSTNUM( 20 )
C
      DIMENSION BLKSZE( 1 ), DATAD( 1 ), NTYPE( 1 ), TESTNO( 2 ), PRETT( 1 ), TESTT( 1 ),
     1SRT( 2 ), MATER( 8 ), CHST( 1 ), RTNSPD( 1 ), LSCALE( 1 ), DSCALE( 1 ), LOFFST( 1 ), DO
     2FFST( 1 ), H( 1 ), D( 1 ), EI( 1 ), ET( 1 ), DELAY( 1 ), TESTAR( 1 ), DESTAR( 1 ), RESTAR(
     31 ), NDATE( 3 ), RLJ( 1 ), LONGDL( 1 ), NRESLT( 1 ), RESULT( 1938 ), DUMMY( 9 )
C
      DIMENSION STATBL( 128 )
      INTEGER BLKSZE, DATAD, TESTNO, PRETT, TESTT, SRT, TESTAR, DESTAR, RESTAR, R
     1LJ, STATBL, TSTNUM
      REAL LSCALE, LOAD, LOFFST, LFAC
        LOGICAL ISSW
      DATA C/3. 947563E-03, 8.968124E-01, 3. 484678E-04, 5 613456E-02/, LFAC/2
     +. 13603E4/, DFAC/0. 894579/
      CALL FAC1( IP, IR )
        IP1=IP+1024
1       CALL MSGREP( IP1, IR, 22, 22HTAPE = 1 ,  TEST = 2 ? , IANS, 10 )
        IF( IANS GT. ITWO )GO TO 1
        GO TO ( 2, 3 ), IANS
        ENTER PAL
$2      LDA TAPCAT
        BRU *+2
$3      LDA TESCAT
```

[redacted]

```
         RBK 23
         STA STATIN
         SPB DTRC02        TRANS STATUS FILE INTO PGM
         LDK STATIN        LABEL OF THE TRANSFER DESCRIPTOR
         SPB DELC30        DELAY 1/5TH AND REPEAT IN TRANSFER FAILS
        LEAVE PAL
    4    CALL MSGTYP( IP1, 9, 9HLISTING ? )
        CALL ANSWER( IR, IANS, IERR )
        GO TO ( 5, 4, 4, 1000 ), IERR
      5 GO TO ( 30, 6 ), IANS
      6 NTEST = 1
         CALL MSGTYP( IP1, 13, 13HTEST NUMBER ? )
      7 CALL INRC10( IR, 2, NOTEST, ICHAR )
        IF( ICHAR. GE. 0 ) GO TO 8
        IERR = -ICHAR
        GO TO ( 9, 9, 1000 ), IERR
      8 IF( ICHAR. EQ. 0 ) GO TO 10
        IF( ICHAR. NE. 6 ) GO TO 9
        TSTNUM( NTEST ) = NOTEST( 1 )
        TSTNUM( NTEST+1 ) = NOTEST( 2 )
        NTEST = NTEST + 2
        IF( NTEST. GT. 20 ) GO TO 10
      9 CALL MSGTYP( IP1, 7, 7HNEXT ? )
        GO TO 7
     10 NTEST = NTEST - 1
        CALL MSGTYP( IP, 12, 12HDATA REQUEST )
        ENTER PAL
         LXK 0, 7
         LDA TSTNUM, 7
         STA NOTEST
         LDA TSTNUM+1, 7
         STA NOTEST+1
         LDA IP
         SPB OURC20
         LDK MSG1
         BRU $1000
         INX 2, 7
         LDA 7
         SUB NTEST
         T[illegible]23
         BTS *-12
        LEAVE PAL
     11 CALL MSGTYP( IP1, 16, 16HIS REQUEST OK ? )
        CALL ANSWER( IR, IANS, IERR )
        GO TO( 12, 11, 11, 1000 ), IERR
     12 IF( IANS EQ. 2 ) GO TO 6
        DO 400 JJ = 1, NTEST, 2
        NOTEST( 1 ) = TSTNUM( JJ )
        NOTEST( 2 ) = TSTNUM( JJ+1 )
        GO TO 32
```

```
       13 WRITE( IP, 14 )NOTEST
       14 FORMAT( 1H , 12HTEST NUMBER , 2A3, 12H NOT ON FILE )
          GO TO 400
          ENTER PAL
$30        LXK 0, 7
           LDA $STATBL+3, 7    ASSIGN THE FIRST 3 CHARS.
           STA NOTEST          OF TEST NAME TO NOTEST.
           LDA STATBL+4, 7     ASSIGN THE SECOND 3 CHARS.
           STA NOTEST+1        OF THE TEST NAME TO NOTEST+1
           LDA IP
           SPB OURC20          WRITE OUT THE TEST NAME
           LDK MSG1
           BRU $1000
           INX 5, 7
           LDA 7
           SUB STATBL+/177     CHECK IF ALL TESTS HAVE BEEN
           TOD 23              LISTED
           BTS *-12            IF NOT  WRITE OUT THE NEXT
           BRU $6              OTHERWISE GO TO  NEW REQUEST
$32        LXK 0, 7
           LDA STATBL+3, 7     CHECK IF THE
           SUB NOTEST          FIRST 3 CHARACTERS OF TEST NUMBER
           TZE                 CORRESPOND TO THE REQUESTED NUMBER
           BTS *+7             IF SO CHECK THE NEXT 3 CHARACTERS
           INX 5, 7            OTHERWISE INDEX 7 BY 5
           LDA 7
           SUB STATBL+/177     CHECK WHETHER ALL RECORDS HAVE
           TOD 23              BEEN CHECKED
           BTR $13             IF SO WRITE THAT REQUIRED TEST NOT ON FILE
           BRU *-9             OTHERWISE READ NEXT TEST NUMBER
           LDA STATBL+4, 7     CHECK IF THE
           SUB NOTEST+1        SECOND 3 CHARACTERS CORRESPOND
           TZE
           BTR *-9             IF NOT INDEX 7 AND CONTINUE SEACH
           LDA STATBL+1, 7     OTHERWISE THE TEST DATA IS FOUND SO
           STA DATAIN          STORE ADDRESS OF START OF FILE
           LDA STATBL, 7
           STA DATAIN+1        STORE SIZE OF DATA BLOCK.
           SPB DTRC02          TRANSFER REQUESTED DATA INTO PROGRAM
           LDK DATAIN          LABEL OF TRANSFER DESCRIPTOR
           SPB DELC30          DELAY 1/5TH AND REPEAT IF TRANSFER FAILS
           LEAVE PAL
       50 CONTINUE
C
C          *****************************************************************
C          CALCULATE STRESS, STRAIN, TIME AND THE MAXIMUM STRESS
C
C          X=TIME
C          Y=STRAIN
C          Z=LOAD
```

[redacted]

```
C       *****************************************************************
C
        IF( ISSW( 21 ))GO TO 61
62      CALL MSGTYP( IP, 20, 20HCUT-OFF STRESS( MPA )? )
        CALL KFREAD( IR, 1, DEDUC, 3, IERR )
        GO TO ( 61, 62, 62, 999 ), IERR
61      SUMX=0 0D0
        SUMY=0. 0D0
        SUMX2=0. 0D0
        SUMXY=0. 0D0
        SUMW=0. 0
        SUMR=0 0
        SUMWR=0 0
        SUMR2=0. 0
        NN=NRESLT( 1 )
        MK=0
        K=0
        N=-1
        IF( DSCALE( 1 ) GT 1. 0 )N=1
        DEDUC=( 3. 14159*D( 1 )**2 )*DEDUC/27. 57904
        DO 100 J=1, NN, 3
        IF( N GT 0 )GO TO 60
        LOAD=( RESULT( J )-LOFFST( 1 ) )*LSCALE( 1 )/1000. 0
        DISPMT=( RESULT( J+1 )-DOFFST( 1 ) )*DSCALE( 1 )
        GO TO 65
60      LOAD=( RESULT( J )-LOFFST( 1 ) )*LFAC/LSCALE( 1 )/1000 0
        DISPMT=( RESULT( J+1 )-DOFFST( 1 ) )*DFAC/DSCALE( 1 )
65      IF( LOAD. LT DEDUC )GO TO 100
        MK=MK+1
        K=( MK-1 )*3+1
       IF( ( RESULT( K+2 )-RESULT( K-1 ) ) GT 60. )RESULT( K+2 )=RESULT( K+2 )-53410
        RESULT( K+2 )=RESULT( J+2 )+0 04
        TTIME=RESULT( K+2 )
        RESULT( K )=LOAD
        HO=H( 1 )-DISFMT
        STRN=ALOG( H( 1 )/HO )
        DTIME=TTIME
        DSTRN=STRN
        SUMX=SUMX+DTIME
        SUMY=SUMY+DSTRN
        SUMXY=SUMXY+DSTRN*DTIME
        SUMX2=SUMX2+DTIME*DTIME
        IF( MK EQ 1 )GO TO 100
        IF( ( RESULT( K )-RESULT( K-3 ) ) LT. -0. 010 )GO TO 101
        IF( STRN GT 0 3 )GO TO 101
100     CONTINUE
C
C       *****************************************************************
C       STRAIN=EINT+EDOTAP*TIME
C       LOAD=( ALOAD/TTIME )+BLOAD
```

[redacted]

```
C      NOTE   THE STRAIN FIT WAS MADE TO THE UNCORRECTED
C      DATA ,THAT IS, IT WAS NOT CORRECTED FOR THE
C      DEFLECTION OF THE LOAD CELL.
C      THE TRUE STRAIN WAS THEN RECALCULATED USING DEL....
C      RESULT( N )=STRESS
C      RESULT( N+1 )=STRAIN
C      RESULT( N+2 )=TTIME
C      ******************************************************************
C
  101  EINT=( SUMX*SUMXY-SUMX2*SUMY )/( ( SUMX**2 )-SUMX2*MK )
       EDOTAP=( SUMY-EINT*MK )/SUMX
       EINTER=EINT
       EDOT=EDOTAP
       XLN=ALOG( EDOT )
       MK=MK*3 0
       BMAX=0. 0
       DO 201  IN=1, MK, 3
       STRAIN=EDOT*RESULT( IN+2 )+EINTER
       LOAD=RESULT( IN )
       DEL=C( 1 )*( LOAD+C( 4 ) )**C( 2 )-C( 3 )
       RATIO=H( 1 )/EXP( STRAIN )
       HI=RATIO+DEL
       RESULT( IN+1 )=ALOG( H( 1 )/HI )
       AI=3 14159*H( 1 )*D( 1 )**2/4 0/HI
       RESULT( IN )=LOAD*6 89476/AI
       IF( RESULT( IN ). GT. BMAX )BMAX=RESULT( IN )
       JIN=IN-3
 201   CONTINUE
C
C      ******************************************************************
C      SMOOTH THE STRESS-STRAIN CURVE
C      SEE  SSP  SUBROUTINE SG13
C      ******************************************************************
C
       DO 116 I=7, JIN, 3
       XM=0 3333333*( RESULT( I-5 )+RESULT( I-2 )+RESULT( I+1 ) )
       YM=0. 3333333*( RESULT( I-6 )+RESULT( I-3 )+RESULT( I ) )
       T1=RESULT( I-5 )-XM
       T2=RESULT( I-2 )-XM
       T3=RESULT( I+1 )-XM
       XM=T1*T1+T2*T2+T3*T3
       IF( XM )38, 38, 39
 39    XM=( T1*( RESULT( I-6 )-YM )+T2*( RESULT( I-3 )-YM )+T3*( RESULT( I )-YM ) )/XM
 38    IF( I-7 )36, 36, 35
 36    HH=XM*T1+YM
 35    RESULT( I-6 )=HH
 116   HH=XM*T2+YM
       RESULT( JIN-3 )=HH
       RESULT( JIN )=XM*T3+YM
C
```

```
C       **************************************************************
C       THIS SECTION FITS A STRAIGHT LINE TO THE INITIAL LOADING
C       CURVE.    IT THEN CALCULATES THE STRAIN AT STRESS=0. 0.
C       THIS VALUE OF STRAIN ( TINT ) IS THEN SUBTRACTED
C       FROM ALL RESULT( I+1 ) VALUES.
C       **************************************************************
C
        DO 34 II=1, 13, 3
        W=RESULT( II )
        R=RESULT( II+1 )
        SUMW=SUMW+W
        SUMR=SUMR+R
        SUMWR=SUMWR+W*R
        SUMR2=SUMR2+R*R
34      CONTINUE
        TINT=( SUMR*SUMWR-SUMR2*SUMW )/( ( SUMR**2 )-SUMR2*5. 0 )
        SLOPE=( SUMW-TINT*5. 0 )/SUMR
        TINT=-TINT/SLOPE
        DO 93 I=1, JIN, 3
        RESULT( I+1 )=RESULT( I+1 )-TINT
93      CONTINUE
C
C       **************************************************************
C       CALCULATE THE WORK HARDENING RATE USING A PROGRAM SIMILAR TO .
C       THE  SSP  SUBROUTINE DGT3
C       **************************************************************
C
        AMAX=0. 0
        A=RESULT( 2 )
        B=RESULT( 1 )
        DY2=RESULT( 5 )-A
        DY2=( RESULT( 4 )-B )/DY2
        DO 17  I=7, JIN, 3
        A=RESULT( I+1 )-A
        IF( A. EQ. 0. 0 )GO TO 17
        A=( RESULT( I )-B )/A
        B=RESULT( I+1 )-RESULT( I-2 )
        IF( B. EQ. 0. 0 )GO TO 17
        DY1=DY2
        DY2=( RESULT( I )-RESULT( I-3 ) )/B
        DY3=A
        A=RESULT( I-2 )
        B=RESULT( I-3 )
        IF( I-7 )15, 15, 16
15      RESULT( 3 )=DY1+DY3-DY2
16      RESULT( I-1 )=DY1+DY2-DY3
        IF( RESULT( I-1 ). GT. AMAX )GO TO 303
        GO TO 17
303     AMAX=RESULT( I-1 )
        INT=I-3
```

```
17      CONTINUE
        RESULT( JIN+2 )=DY2+DY3-DY1
C
C       *****************************************************************
C       CALCULATE THE YIELD STRESS
C       *****************************************************************
C
        AVG=( RESULT( INT+5 )+AMAX+RESULT( INT-1 ) )/3. 0
        BB=RESULT( INT )-AVG*RESULT( INT+1 )
        DO 981  I=1, JIN, 3
        X=RESULT( I+1 )
        Y=AVG*( X-0. 002 )+BB
        IX=I
        IF( Y. GT. RESULT( I ) )GO TO 982
981     CONTINUE
        WRITE( IP, 756 )
756     FORMAT( 1H , 40HERROR*** OFFSET DOES NOT INTERCEPT CURVE )
        GO TO 999
982     SLP=( RESULT( IX )-RESULT( IX-3 ) )/( RESULT( IX+1 )-RESULT( IX-2 ) )
        X1=RESULT( IX-2 )
        Y1=RESULT( IX-3 )
        X=( SLP*X1-Y1-0. 002*AVG+BB )/( SLP-AVG )
        YIELD=AVG*X-0 002*AVG+BB
        WRITE( IP, 989 )TESTNO, YIELD, XLN, EDOT
989     FORMAT( 1H , 2A3, 3X, 4HYLD=, F6. 2, 3X, 9HLN( EDOT )=, F6. 3, 6H EDOT=, E10 3 )
        WRITE( IP, 979 )AVG
979     FORMAT( 1H , 10HW H. SLOPE=, E9. 3 )
C
C       *****************************************************************
C       DRAW THE AXIS
C       *****************************************************************
C
        IF( ISSW( 12 ) )GO TO 133
403     CALL MSGTYF( IP, 5, 5HPLOT? )
        CALL ANSWER( IR, IANS, IERR )
        GO TO ( 402, 403, 403, 999 ), IERR
402     IF( IANS. EQ. 2 )GO TO 400
203     CALL MSGTYP( IP, 11, 11HYIELD PLOT? )
        CALL ANSWER( IR, IANS, IERR )
        GO TO ( 204, 203, 203, 999 ), IERR
204     IF( IANS EQ 2 )GO TO 205
1004    CALL MSGTYP( IP, 25, 25HX-AXIS (PERCENT STRAIN ) ? )
        CALL KFREAD( IR, 0, IDX, 3, IERR )
        GO TO ( 1003, 1004, 1004, 999 ), IERR
1003    XIDX=FLOAT( IDX )/100. 0
        DO 1001  II=1, JIN, G
        NON=II
        IF( RESULT( II+1 ). GT. XIDX )GO TO 1002
1001    CONTINUE
1002    CALL PLOT( 0, 0, 0 )
```

```
      CALL PLOT( 2, 0. , -12. )
      CALL PLOT( 4, 0, 0 )
      CALL PLOT( 0, 0, 0 )
      CALL PLOT( 2, 0, 1. 76 )
      CALL PLOT( 4, 0, 0 )
      CALL PLOT( 0, 0, 0 )
      NXD=1
      XP=5. 906
      XN=0. 0
      YP=7. 874
      YN=0. 0
      NYD=4
      IVX=0
      IVY=0
      IDY=IFIX( RESULT( NON )/4. 0 )+1
      SX=1. 0
      SY=1. 0
      NLX=15
      NLY=15
      SLX=1. 3
      SLY=1. 3
      CALL LAXIS( XP, XN, YP, YN, NXD, NYD, IVX, IVY, IDX, IDY, SX, SY, NLX, NLY, SLX,
     +SLY, 15HSTRAIN, PERCENT, 15HSTRESS, MPA     )
C
C     ***************************************************************
C     PLOT THE DATA
C     ***************************************************************
C
      JX=1
 7004 X=RESULT( JX+1 )*100. 0*XP/FLOAT( IDX*NXD )
      Y=RESULT( JX )*7. 874/FLOAT( IDY*4 )
      IF( X GT. XP )GO TO 7003
      CALL PLOT( 2, X, Y )
      CALL SYMPLT( 1, . 25, . 25, 2 )
      JX=JX+3
      IF( JX GT. K )GO TO 7003
      GO TO 7004
 7003 CALL PLOT( 2, 3. 543, 1. 181 )
      XT=XP+5. 906
      CALL LETTER( 2, 1. 1, 1. 1, TESTNO, 6 )
      CALL PLOT( 2, 3. 543, 0. 787 )
      CALL LETTER( 2, 1. 1, 1. 1, 4HYLD=, 4 )
      CALL NUMBR( 2, 1. 1, 1. 1, 6, 2, YIELD )
      Y=0. 0
      X=( Y-BB )/AVG
      X=X*590. 6/FLOAT( IDX )
      CALL PLOT( 2, X, Y )
      Y=AVG*X IDX+BB
      IYP=IFIX( RESULT( NON )/4. 0 )+1
      Y=Y*7. 874/FLOAT( IYP*4 )
```

```
            IF( Y. GT. 7. 874 )GO TO 309
            CALL  PLOT( 3, 5. 906, Y )
            GO TO 310
      309   Y=FLOAT( IYP*4 )
            X=( Y-BB )/AVG
            X=X*590. 6/FLOAT( IDX )
            CALL  PLOT( 3, X, 7. 874 )
      310   X=-( BB/AVG )+0 002
            X=X*590. 6/FLOAT( IDX )
            CALL  PLOT( 2, X, 0. 0 )
            ~~Y=AVG*( XIDX-0. 002 )+BB~~
            Y=Y*7 874/FLOAT( IYP*4 )
            IF( Y. GT. 7. 874 )GO TO 305
            CALL  PLOT( 3, 5. 906, Y )
            GO TO 306
      305   Y=FLOAT( IYP*4 )
            X=( ( Y-BB )/AVG )+0. 002
            X=X*590 6/FLOAT( IDX )
            CALL  PLOT( 3, X, 7. 874 )
      306   CALL  PLOT( 2, 0. , 0. )
            CALL  PLOT( 2, XT, 0. )
            CALL  PLOT( 4, 0, 0 )
      C
      C     *****************************************************************
      C     PROGRAM SEGMENT TO DRAW THE AXIS FOR THE WORK HARDENING PLOT
      C     *****************************************************************
      C
      205   CALL  MSGTYP( IP, 20, 20HWORK-HARDENING PLOT? )
            CALL  ANSWER( IR, IANS, IERR )
            GO TO ( 207, 205, 205, 999 ), IERR
      207   IF( IANS EQ 2 )GO TO 400
      133   CALL  PLOT( 0, 0, 0 )
            XP=5 906
            XN=0. 0
            YP=7. 874
            YN=0. 0
            NXD=5
            NYD=4
            IVX=0
            IVY=0
            IF( ISSW( 21 ) )GO TO 335
            IF( ISSW( 20 ) )GO TO 333
            GO TO 334
      333   CALL  MSGTYP( IP, 21, 21HTYPE MAX X THEN MAX Y )
            CALL  KFREAD( IR, 1, XAX, 1, YAX, 3, IER )
            GO TO( 338, 333, 333, 999 ), IER
      338   EMAX=XAX
            AMAX=YAX
            GO TO 334
      335   IDX=IFIX( XAX/NXD )+1
```

[redacted]

```
        IDY=IFIX( YAX/NYD )+10
        GO TO 336
334     IDX=IFIX( BMAX/NXD )+1
        IDY=IFIX( AMAX/NYD )+10
336     SX=1.0
        SY=1. 0
        NLX=15
        NLY=20
        SLX=1 3
        SLY=1. 3
        CALL LAXIS( XP, XN, YP, YN, NXD, NYD, IVX, IVY, IDX, IDY, SX, SY, NLX, NLY, SLX,
      +SLY, 15HSTRESS,  MPA      , 20HDSTRESS/DSTRAIN,  MPA )
C
C       ****************************************************************
C       PLOT THE WORK HARDENING DATA
C       ****************************************************************
C
        JIN=JIN-3
        DO 301 J=1, JIN, 3
        X=RESULT( J )*XP/FLOAT( IDX*NXD )
        Y=RESULT( J+2 )*YP/FLOAT( IDY*NYD )
        IF( Y LT 0 0 )GO TO 301
        IF( Y GT. YP )GO TO 301
        CALL PLOT( 2, X, Y )
        CALL SYMPLT( 1,  25,  25, 2 )
        IF( ( BMAX-RESULT( J ) ). LT 0 05 )GO TO 302
301     CONTINUE
302     CALL PLOT( 2, 0 394, 1 181 )
        XT=XP+5 906
        CALL LETTER( 2, 1  1, 1  1, TESTNO, 6 )
        CALL PLOT( 2, 0 , 0  )
        CALL PLOT( 2, XT, 0  )
        CALL PLOT( 4, 0, 0 )
 400   CONTINUE
 999    CALL MSGTYP( IP, 17, 17HYIELD IS NOW OFF' )
 1000  CALL FAC2( IP, IR )
        STOP
        ENTER FAL
STATIN  BSS 1
        FOR 0, /200
        DEL 0, STATEL
DATAIN  BSS 1
        BSS 1
        DEL 0, BLKSZE
ENDAD1  EQL /7205700
MSG1    DEL 0, FMT1
        DEL 0, NOTEST
FMT1    BCD 6, 2, 1, 0, 0
        CON D, -1
TEMP    BSS 1
```

```
TAPCAT CON G, TAPKAT
TAFKAT EQL /7146100
TESCAT CON G, TESKAT
TESKAT EQL /7205700
DELC30 LIB
OURC20 LIB
              LEAVE PAL
              END
              SUBROUTINE ANSWER( IR, IANS, IERR )
              DATA IYES/3HYES/, INO/3HONO/, I/3H000/
              IANS=IREFLY( IR, 256, IERR )+I
              GO TO ( 10, 50, 50, 50 ), IERR
   10         IF( IANS NE IYES )GO TO 20
              IANS=1
              GO TO 50
   20         IF( IANS NE INO )GO TO 30
              IANS=2
              GO TO 50
   30         IERR=2
   50         RETURN
              END
JOB, RELEASE, YIELD
JOB, END
```

APPENDIX II

The Temperature and Strain Rate Dependence of the Flow Curves of Copper

(COMPUTER PLOTS)

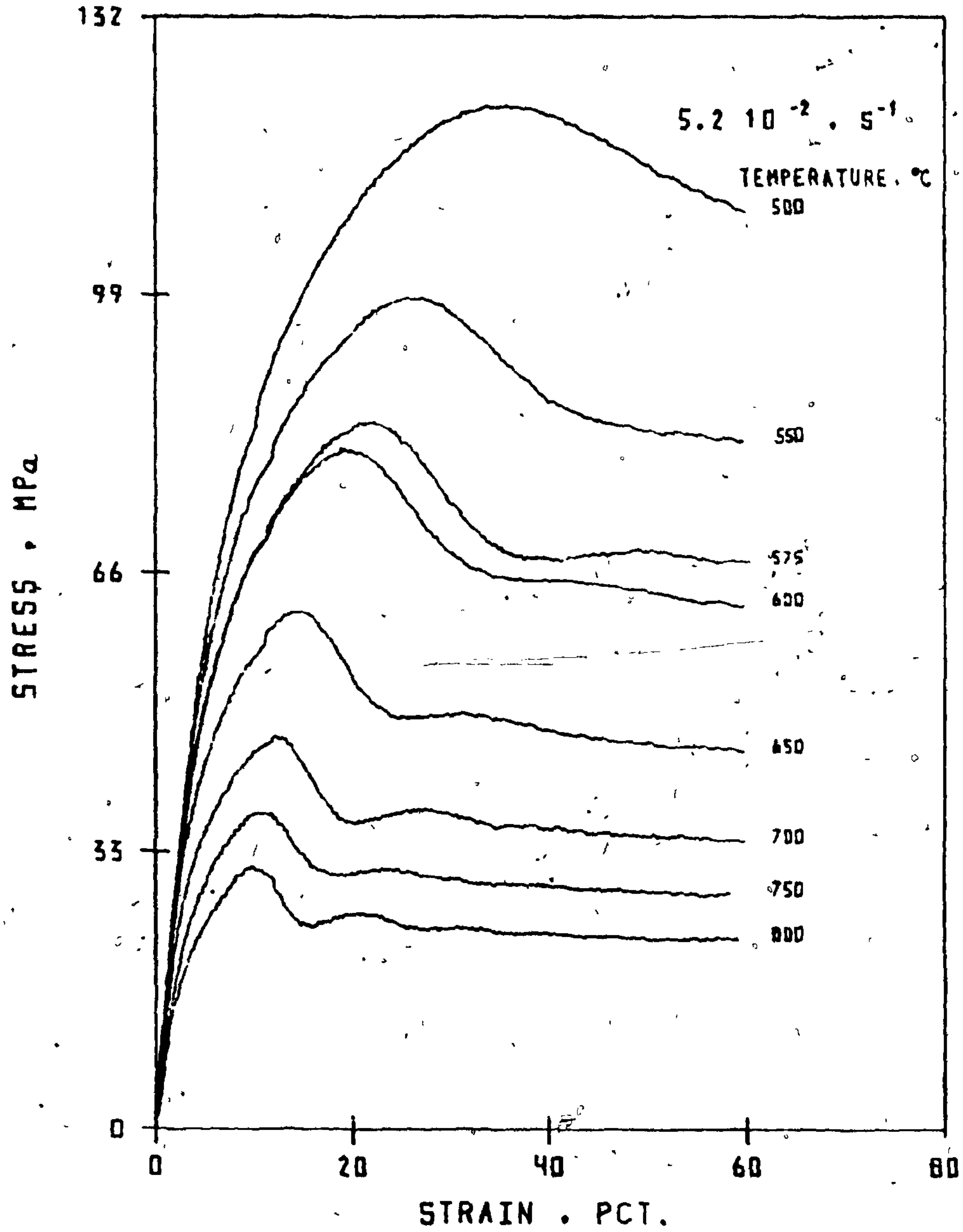

132
99
66
33
0
STRESS . MPa
0
20
40
60
80
STRAIN . PCT.
5.2 10 -2 . S-1
TEMPERATURE . °C
500
550
575
600
650
700
750
800

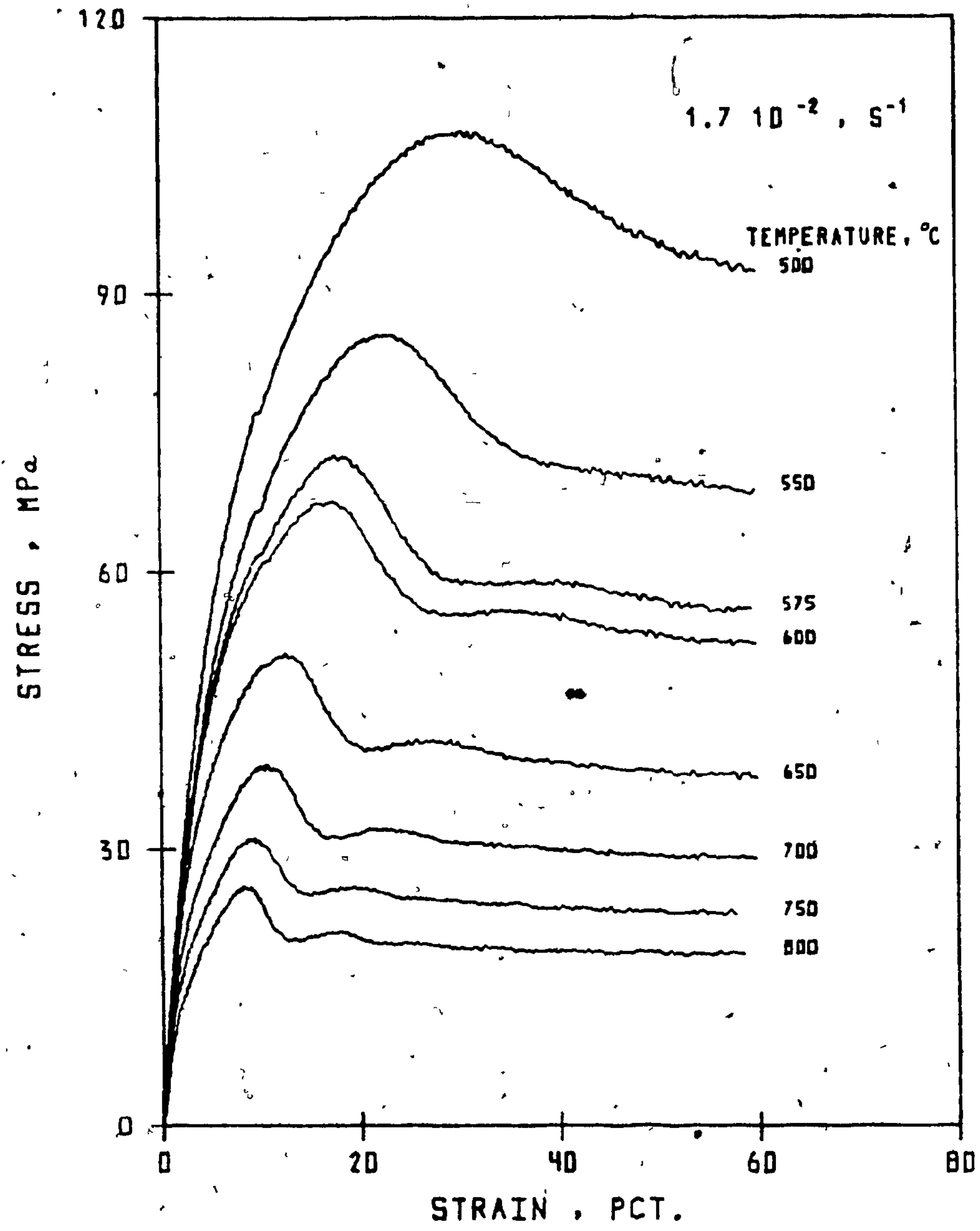

1.7 10⁻², s⁻¹
TEMPERATURE, °C
500
550
575
600
650
700
750
800
STRESS, MPa
120
90
60
30
0
STRAIN, PCT.
0
20
40
60
80

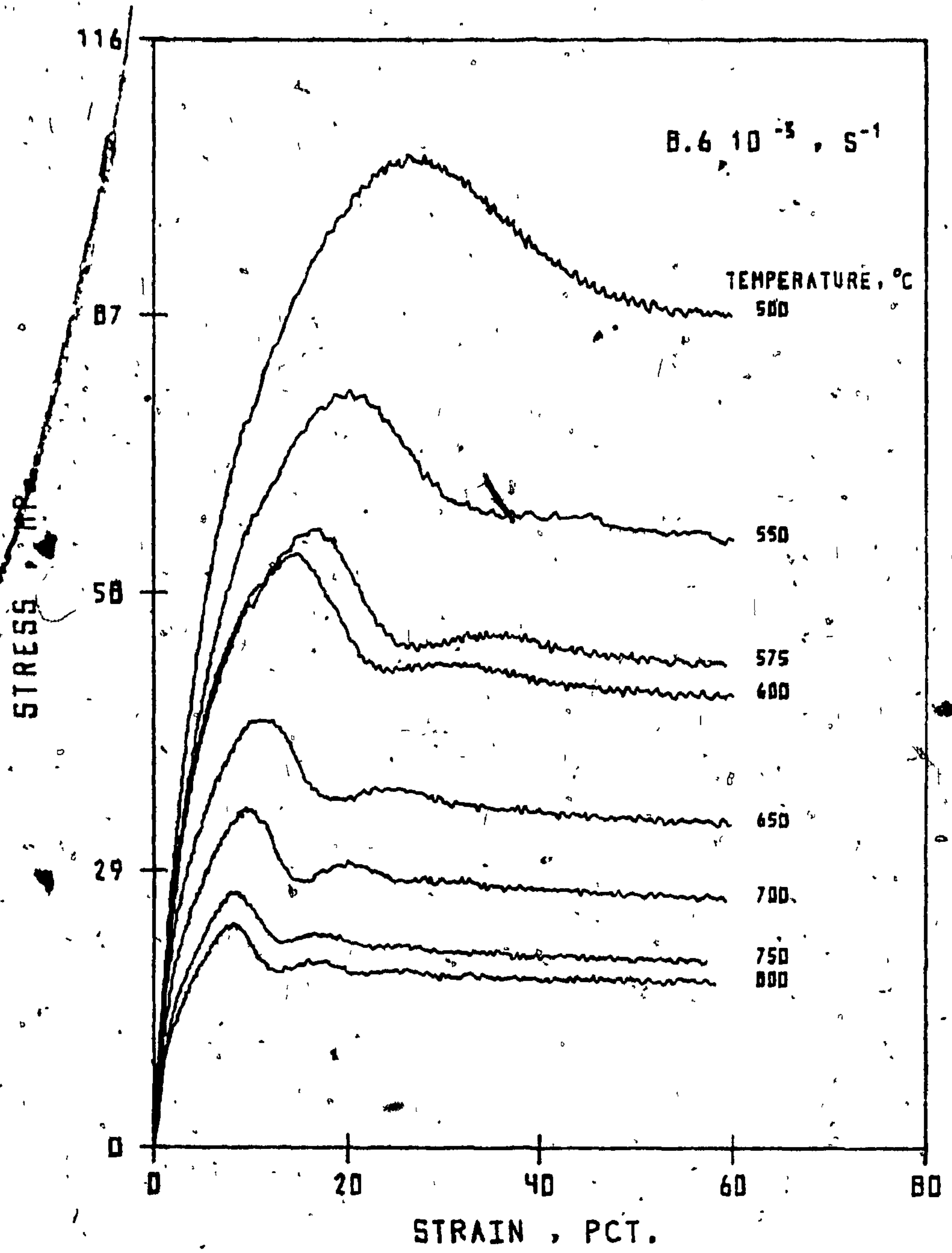
8.6 10 -5 , S-1
TEMPERATURE, °C
500
550
575
600
650
700
750
800
116
87
58
29
0
STRESS , MPa
0
20
40
60
80
STRAIN , PCT.

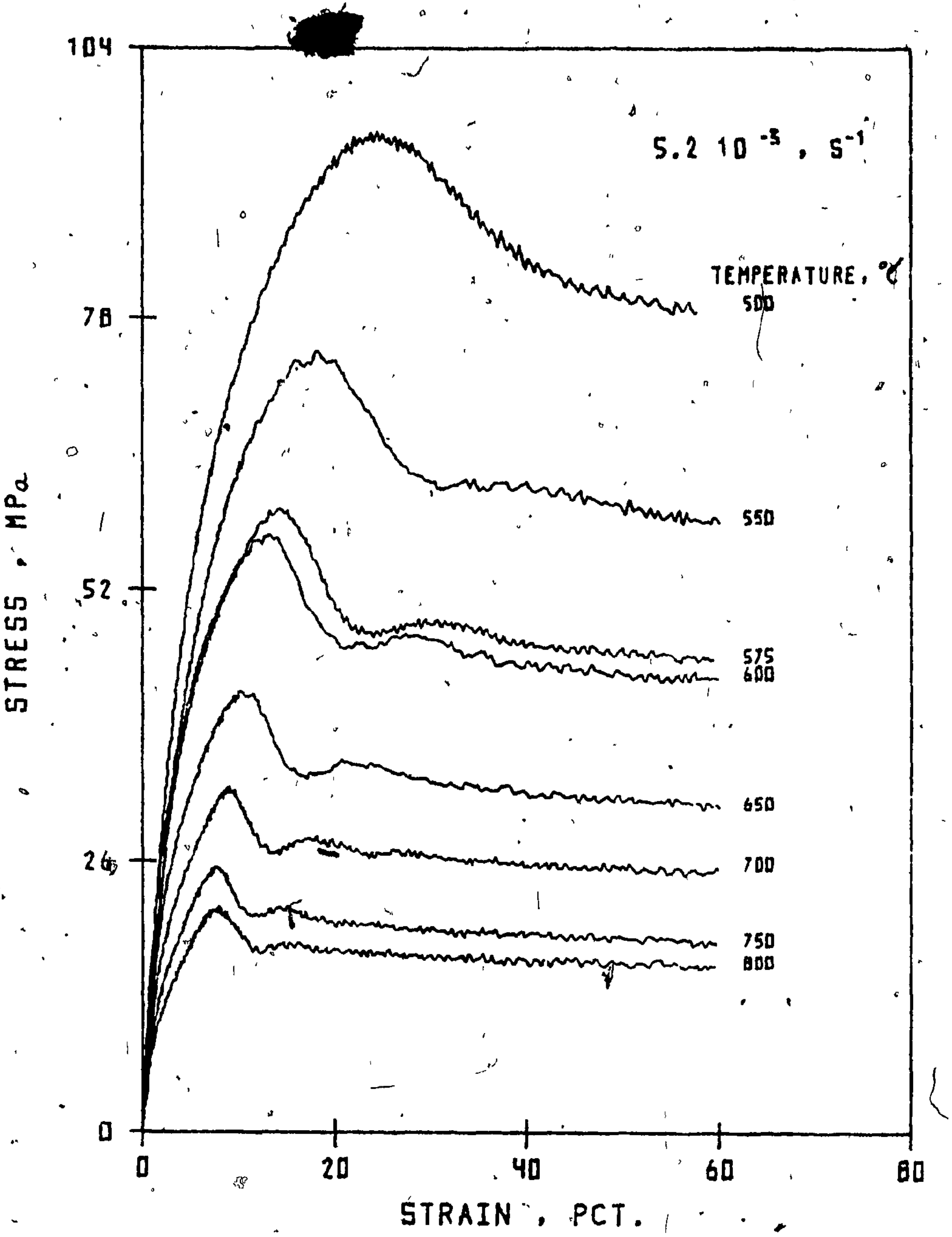
104
78
52
26
0
STRESS , MPa
0
20
40
60
80
STRAIN , PCT.
5.2 10 -5 , S-1
TEMPERATURE, °C
500
550
575
600
650
700
750
800

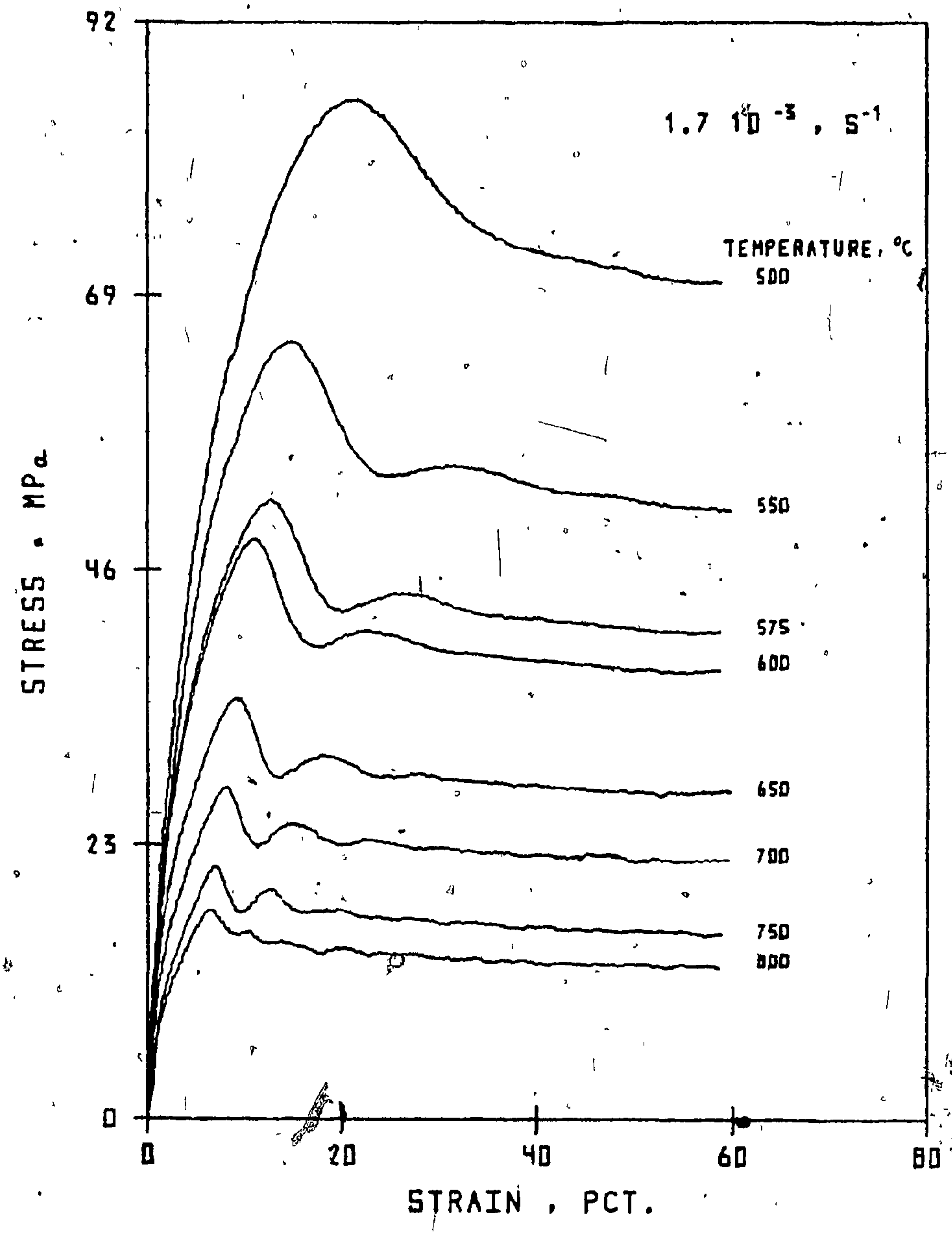
1.7 10^-3 , S^-1
TEMPERATURE, °C
500
550
575
600
650
700
750
800
92
69
46
23
0
0
20
40
60
80
STRESS , MPa
STRAIN , PCT.

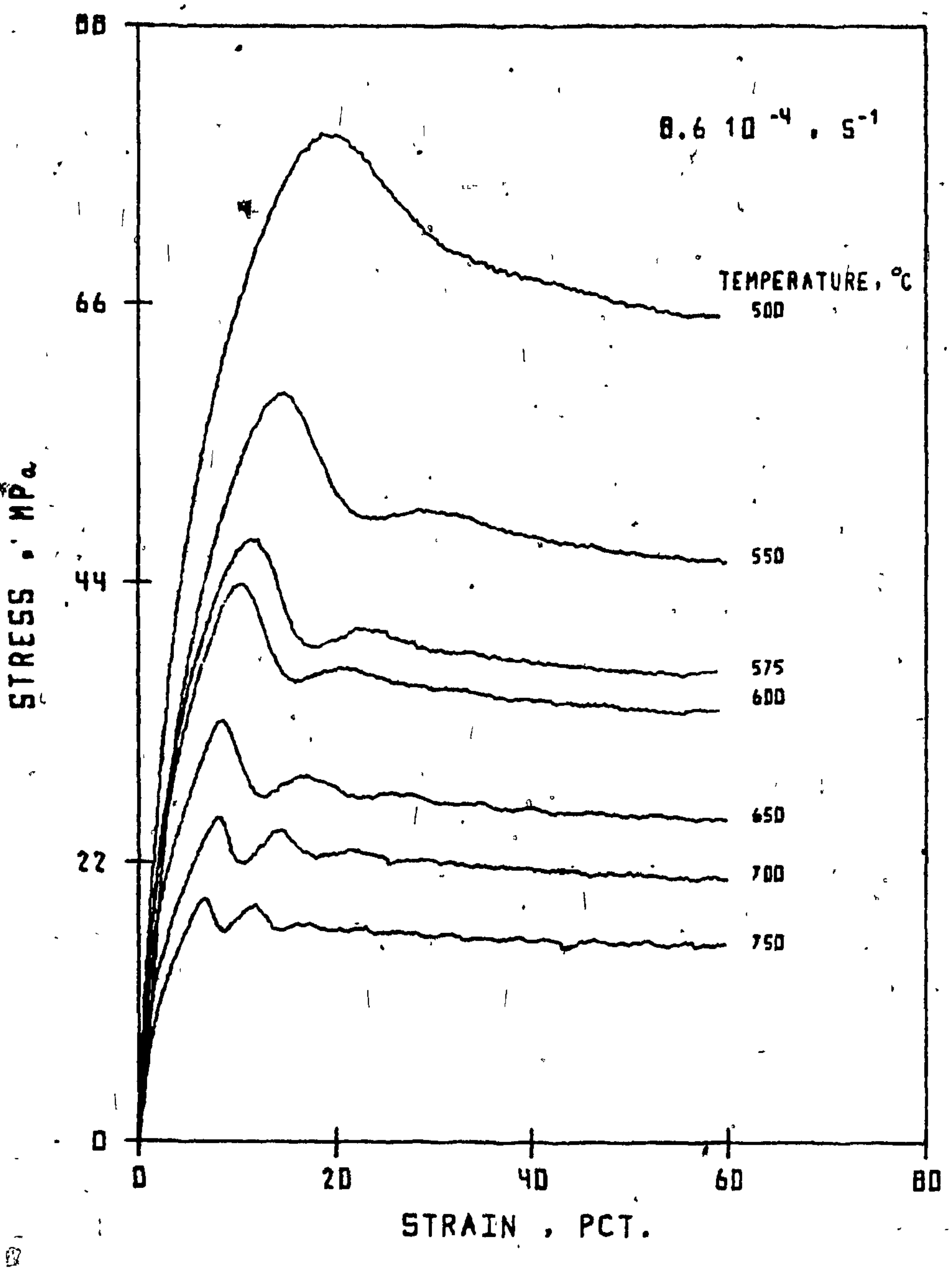

8.6 10 -4 , S-1
TEMPERATURE, °C
500
550
575
600
650
700
750
STRESS , MPa
0
22
44
66
88
STRAIN , PCT.
0
20
40
60
80

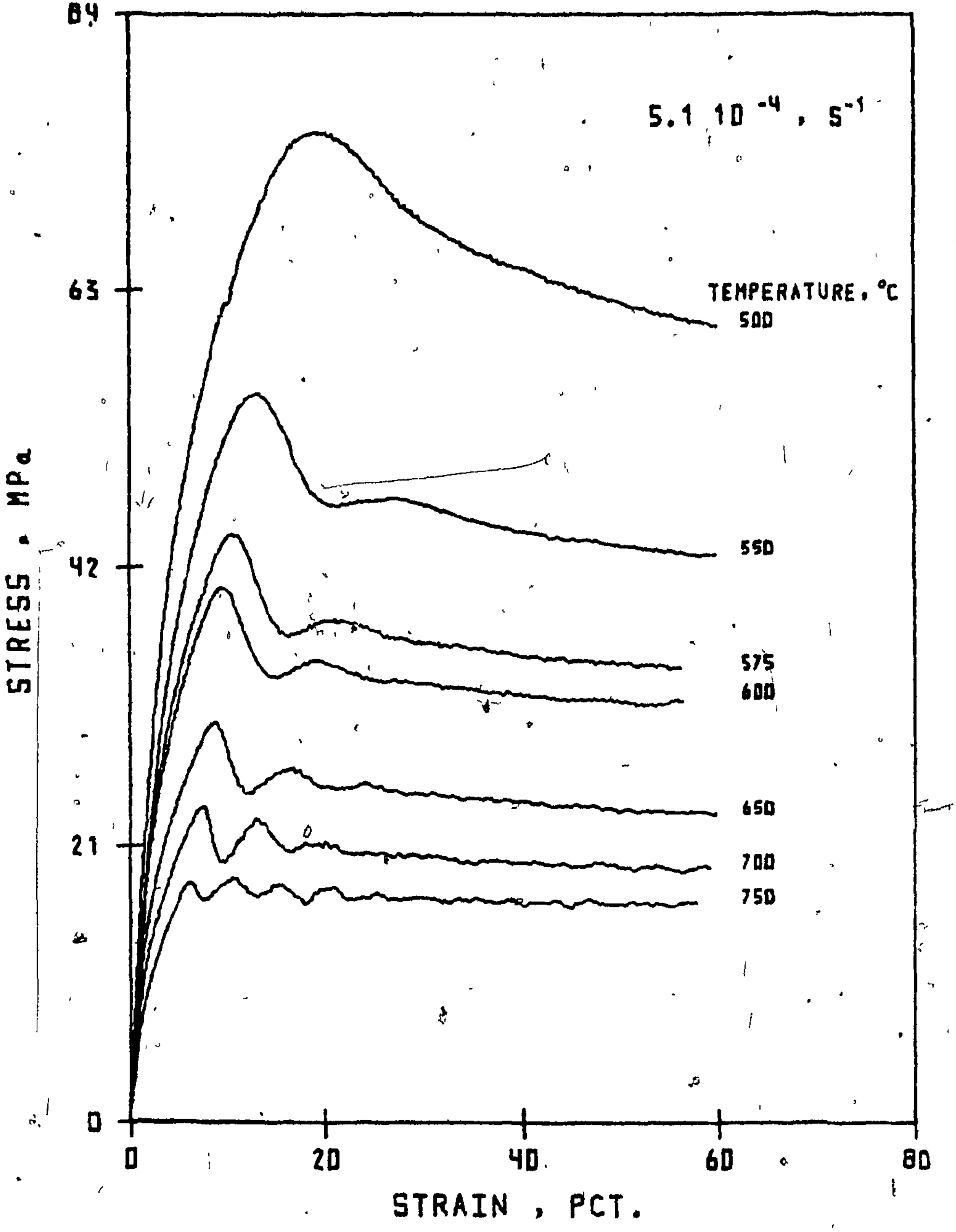
84
63
42
21
0
STRESS , MPa
0
20
40
60
80
STRAIN , PCT.
5.1 10 -4 , S-1
TEMPERATURE, °C
500
550
575
600
650
700
750

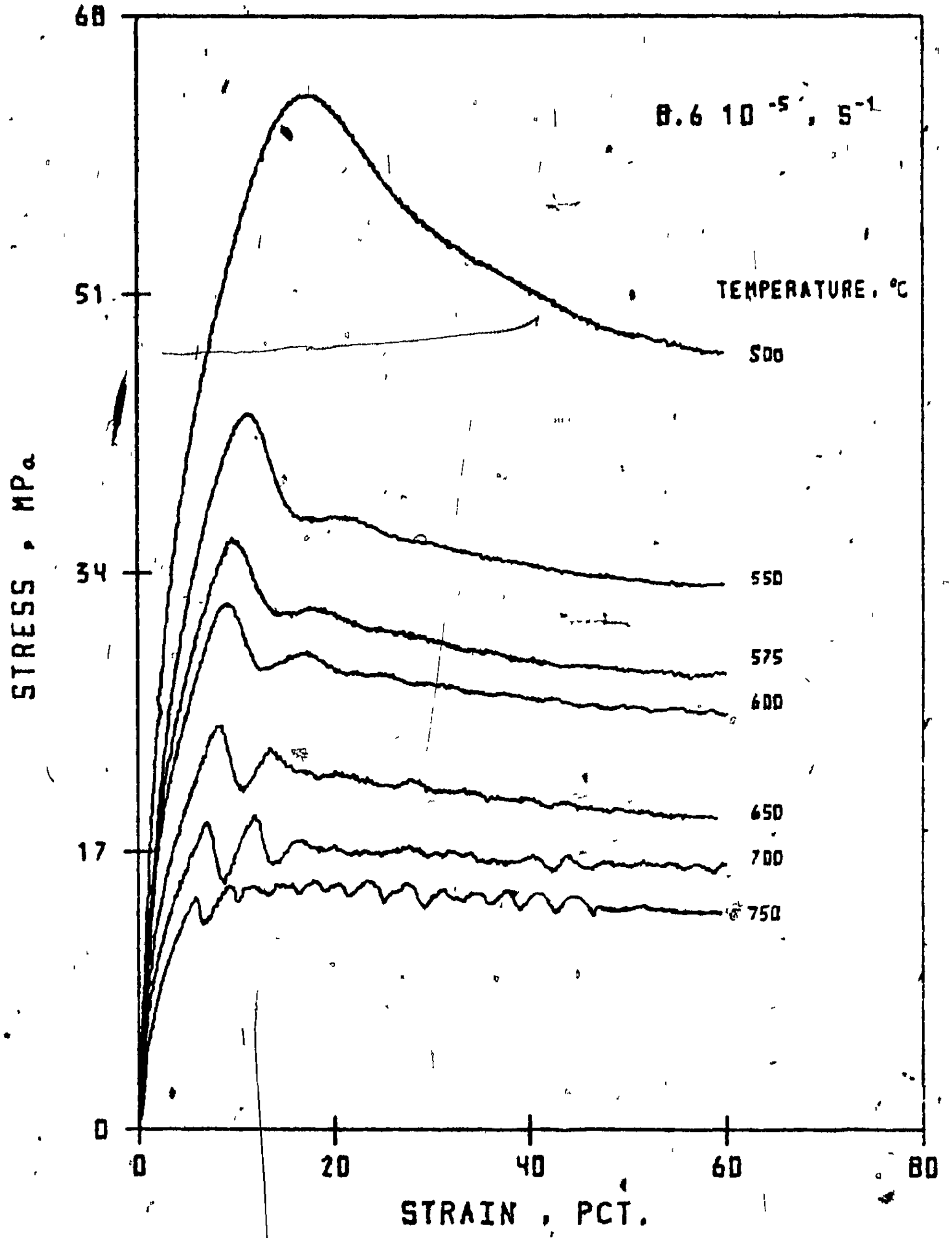
68
51
34
17
0
STRESS , MPa
0
20
40
60
80
STRAIN , PCT.
8.6 10^-5 , S^-1
TEMPERATURE, °C
500
550
575
600
650
700
750

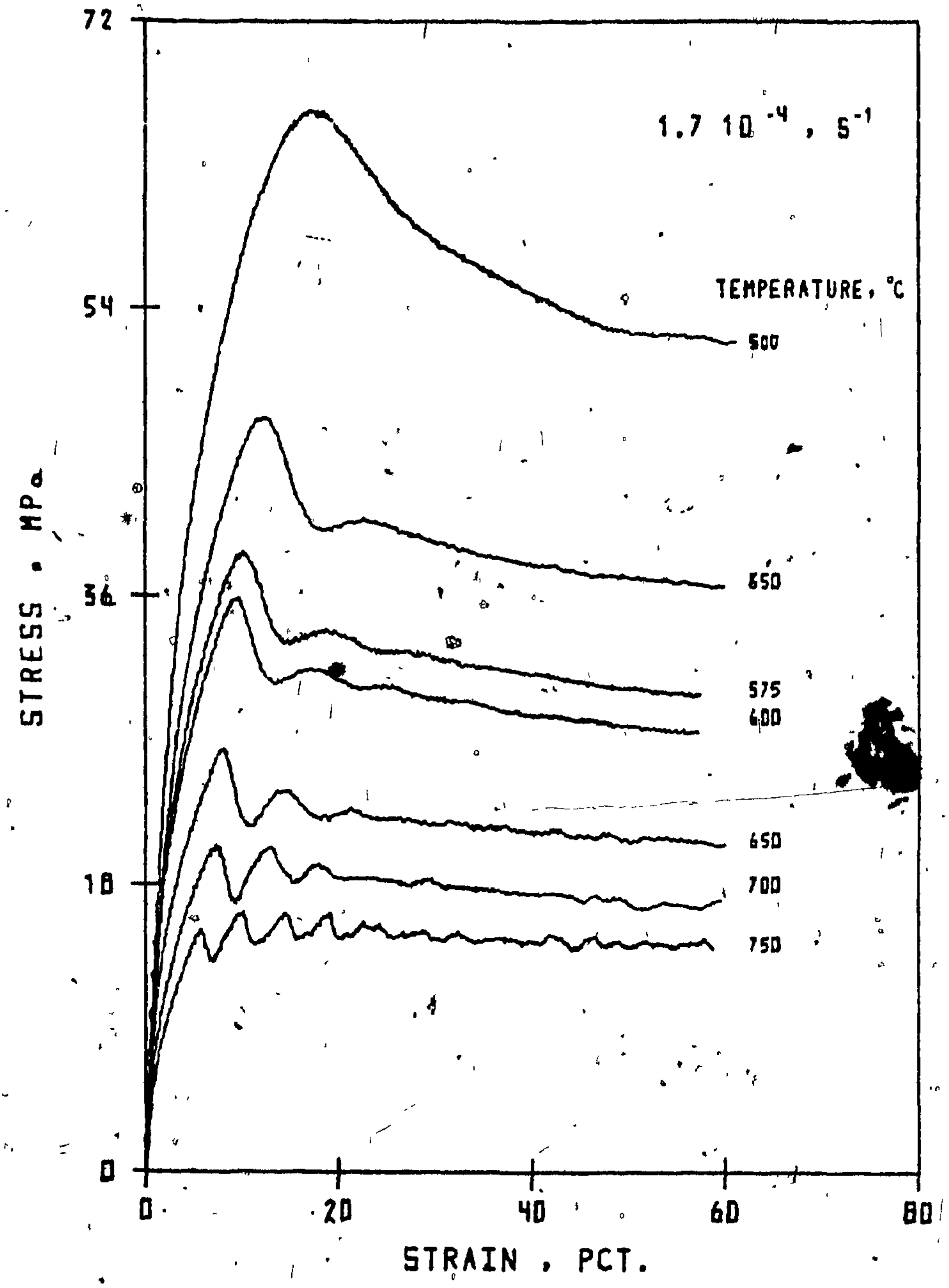

72
54
36
18
0
STRESS , MPa
0
20
40
60
80
STRAIN , PCT.
1.7 10^-4 , S^-1
TEMPERATURE, °C
500
550
575
600
650
700
750

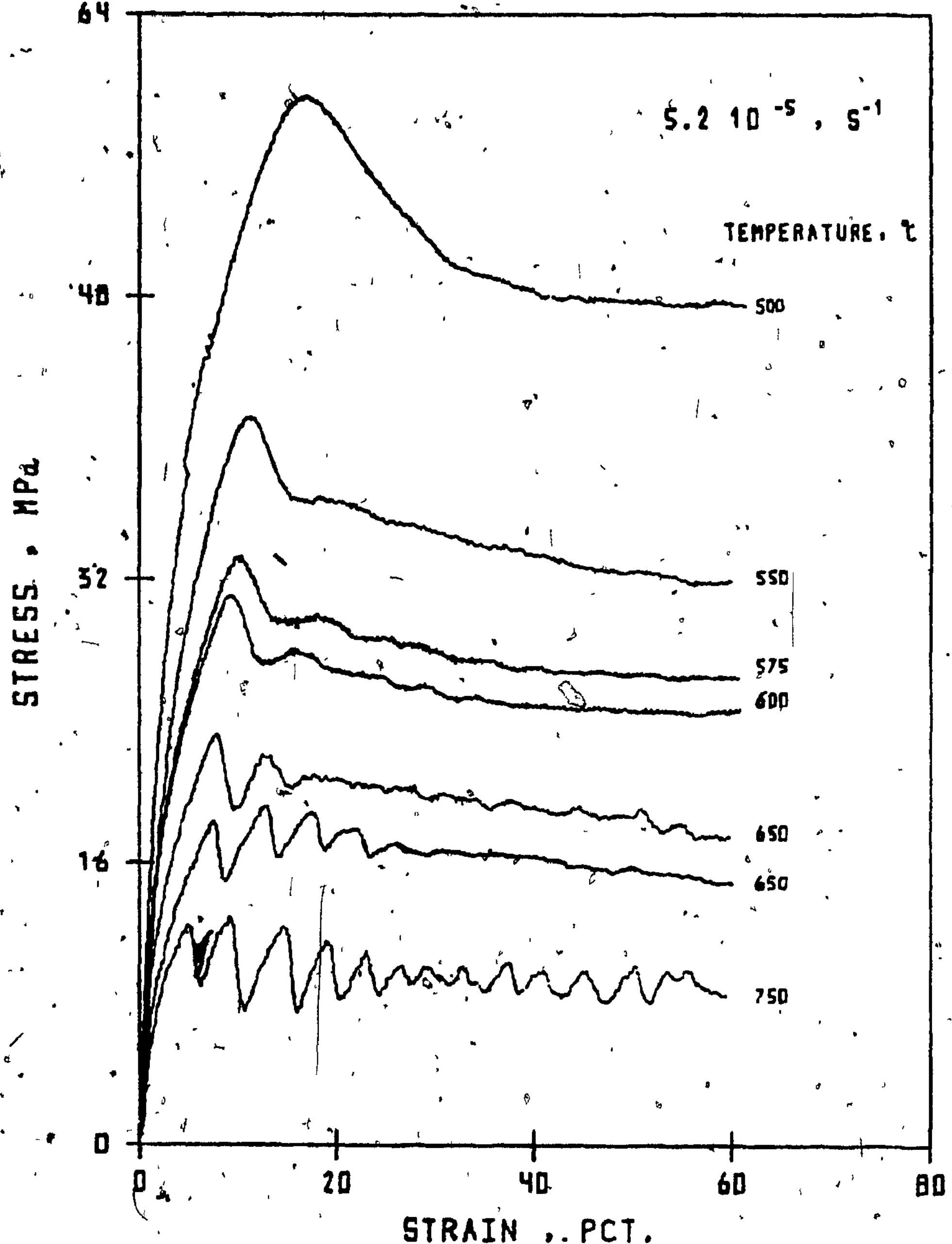
64
48
32
16
0
STRESS , MPa
5.2 10 -5 , s -1
TEMPERATURE, °C
500
550
575
600
650
650
750
0
20
40
60
80
STRAIN ,. PCT.

APPENDIX III

High Temperature Compression Data for OFHC Copper

Temperature ^{o}C	Measured Strain Rate s^{-1}	Yield Stress MN/m^2
500	$5.14x10^{-2}$	45.00
500	$1.73x10^{-2}$	38.74
500	$8.54x10^{-3}$	35.20
500	$5.17x10^{-3}$	32.98
500	$1.72x10^{-3}$	28.91
500	$8.45x10^{-4}$	26.74
500	$5.06x10^{-4}$	25.54
500	$1.68x10^{-4}$	23.56
500	$8.66x10^{-5}$	22.43
500	$5.05x10^{-5}$	21.89
550	$5.37x10^{-2}$	37.56
550	$1.79x10^{-2}$	30.96
550	$8.62x10^{-3}$	28.15
550	$5.26x10^{-3}$	26.97
550	$1.68x10^{-3}$	23.92
550	$8.66x10^{-4}$	22.20
550	$5.09x10^{-4}$	21.40
550	$1.78x10^{-4}$	19.15
550	$8.64x10^{-5}$	17.78
550	$5.25x10^{-5}$	16.77
575	$5.15x10^{-2}$	33.37
575	$1.73x10^{-2}$	28.52
575	$8.66x10^{-3}$	25.85
575	$5.19x10^{-3}$	24.61
575	$1.69x10^{-3}$	21.78
575	$8.49x10^{-4}$	20.48
575	$5.01x10^{-4}$	18.92
575	$1.71x10^{-4}$	16.40
575	$8.45x10^{-5}$	15.19
575	$5.09x10^{-5}$	13.99
600	$5.20x10^{-2}$	29.08
600	$1.75x10^{-2}$	24.90
600	$8.63x10^{-3}$	22.95
600	$5.17x10^{-3}$	22.00
600	$1.67x10^{-3}$	19.42
600	$8.42x10^{-4}$	17.61
600	$5.05x10^{-4}$	16.80
600	$1.69x10^{-4}$	14.62
600	$8.61x10^{-5}$	13.24
600	$5.16x10^{-5}$	11.93

......(cont'd.)

Temperature ^{o}C	Measured Strain Rate s^{-1}	Yield Stress MN/m^{2}
650	5.30×10^{-2}	24.42
650	1.72×10^{-2}	21.35
650	8.67×10^{-3}	19.57
650	5.19×10^{-3}	18.46
650	1.68×10^{-3}	15.84
650	8.59×10^{-4}	14.14
650	5.16×10^{-4}	13.09
650	1.72×10^{-4}	10.63
650	8.65×10^{-5}	9.87
650	5.19×10^{-5}	9.30
700	5.37×10^{-2}	20.25
700	1.74×10^{-2}	17.29
700	8.55×10^{-3}	14.96
700	5.30×10^{-3}	13.99
700	1.69×10^{-3}	11.58
700	8.69×10^{-4}	10.56
700	5.12×10^{-4}	9.84
700	1.69×10^{-4}	8.25
700	8.81×10^{-5}	7.44
700	5.14×10^{-5}	6.96
750	5.17×10^{-2}	16.78
750	1.71×10^{-2}	13.66
750	8.66×10^{-3}	12.06
750	5.27×10^{-3}	11.15
750	1.69×10^{-3}	8.78
750	8.54×10^{-4}	8.10
750	5.08×10^{-4}	7.42
750	1.72×10^{-4}	6.53
750	8.50×10^{-5}	6.00
750	5.19×10^{-5}	5.88
800	5.15×10^{-2}	13.31
800	1.71×10^{-2}	10.53
800	8.50×10^{-3}	9.10
800	5.18×10^{-3}	8.38
800	1.73×10^{-3}	6.99

APPENDIX IV

The Inverse Temperature Dependence of the Logarithm of the Strain Rate at Constant Values of τ/μ

	Temperature °C							
τ/μ, 10^{-5}	500	550	575	600	650	700	750	800
7.0	-	-	-	-	-	-9.167	-7.667	-6.067
8.5	-	-	-	-	-9.633	-7.950	-6.367	-4.950
10.0	-	-	-	-	-8.567	-6.950	-5.500	-4.200
11.5	-	-	-	-9.367	-7.600	-6.100	-4.700	-3.533
13.0	-	-	-9.400	-8.467	-6.800	-5.333	-4.000	-
14.5	-	-9.533	-8.533	-7.575	-6.000	-4.600	-3.433	-
16.0	-	-8.775	-7.733	-6.800	-5.250	-3.967	-	-
17.5	-9.600	-7.933	-7.000	-6.000	-4.600	-3.400	-	-
19.0	-8.733	-7.150	-6.250	-5.267	-3.967	-	-	-
20.5	-7.916	-6.400	-5.550	-4.600	-3.367	-	-	-
22.0	-7.200	-5.667	-4.900	-4.000	-	-	-	-
23.5	-6.600	-5.000	-4.383	-3.500	-	-	-	-
25.0	-6.000	-4.500	-3.900	-3.050	-	-	-	-
26.5	-5.533	-4.050	-3.500	-	-	-	-	-
28.0	-5.100	-3.700	-3.133	-	-	-	-	-

APPENDIX V.

Listing of the Analytical Computer Program ACTANL

```
$WATFIV ,PAGES=55
C                                     ********
C                                     * ACTANL *
C                                     ********
C
C
C
C
C       THIS PROGRAM WAS WRITTEN BY KEN CADIEN, JUNE 15, 1976
C       IT IS THE AIM OF THIS PROGRAM TO CALCULATE THE ACTIVATION
C       PARAMETERS FOR THE HIGH TEMPERATURE FLOW OF O.F.H.C. COPPER,
C       FROM A THERMODYNAMICAL ANALYSIS OF COMPRESSIVE YIELD STESSS DATA.
C
C
C
C       SEGMENT TO INPUT THE DATA.
C
C
C       ***  RAW DATA MATRIX  ***
C
C
C       SIGMA(J,I)=COMPRESSIVE YIELD STRESS, MN/M**2
C       TAUDMU(J,I)=MODULUS-REDUCED YIELD STESS
C       LNEDOT(J,I)=LOGARITHM OF THE IMPOSED TRUE STRAIN RATE
C       T(I)=TEMPERATURE , DEGREES KELVIN
C
C       ***  CROSSPLOT RAW DATA MATRIX  ***
C
C       LET(J,I)=LN STRAIN RATE READ FROM THE X-PLOT
C       TINV(I)=1.0/TEMP READ FROM THE X-PLOT
C       TOU(I)=AT CONSTANT MODULUS-REDUCED YIELD STRESS
C
C       *** CONSTANTS ***
C
C       BK=BOLTZMANN'S CONSTANT=8.3143 J/MOLE K
C       TFAC=TAYLOR FACTOR
C       BV= BURGERS VECTOR FOR COPPER
C
C       MU=SHEAR MODULUS
C       MUZERO= INTERCEPT OF MU VS TEMP AT T=0 K
C       MUSLOP=SLOPE OF MU VS TEMP
C
C
C
        IMPLICIT REAL 8(A-H,L,M,O-Z)
        REAL*8 MUNAME/8H  HILL  /
        DIMENSION T(8),SIGMA(10,8),LNEDOT(10,8),TAUDMU(10,8),TOU(15),
       &TINV(8),LET(15,8),A(3,15),B(3,15),DH(15),X(10),Y(10),W(8),
       &AB(4,5), DCOMU(15),PREXP(15,8),DG( 15,8),SX(7),DS(15,8),SW(4),
       &AA(4,4),BB(4),Z(15),VSTAR(10,8),LNV(16),DST(16),DHT(8)
        TAYFAC=3.100
        BV=2.55
        BK=8.3143D0
        MUZERO=5.3097D04
        MUSLOP=-1.8429D01
C
C       ***  PRINT THE INPUT CONSTANTS  ***
C
        PRINT999,MUNAME,MUZERO,MUSLOP,BK,TAYFAC,BV
  999   FORMAT('1',////'0',3X,'SHEAR MODULUS :',A8,/'0',3X,'MUZERO=',D11.5
```

[redacted]

```
     &,' MN/M**2',/'0',3X,'MUSLOP=',D12.5,' MN/K M**2',/'0',3X,
     &'BOLTZMANN'S CONSTANT=',F6.4,' J/MOLE K',/'0',3X,'TAYLOR FACTOR='
     &,F4.2,/'0',3X,'BURGERS VECTOR=',F4.2,' ANGSTROMS')
C
C     ***  INPUT RAW DATA MATRIX  ***
C
        DO 9 I=1,8
      READ,T(I)
      MU=MUZERO+MUSLOP*T(I)
      DO 9 J=1,10
      READ,SIGMA(J,I),LNEDOT(J,I)
      TAUDMU(J,I)=SIGMA(J,I)/(MU*TAYFAC)
 9    CONTINUE
C
C     *** INPUT CROSS-PLOT DATA MATRIX  ***
C
      DO 12 I=1,8
      TINV(I)=1.0D0/T(I)
      IF(I.GT.1)GO TO 13
      READ,TDU
 13   DO 12 J=1,15
      READ,LET(J,I)
 12   CONTINUE
C
C     ***  PRINT OUT THE INPUTTED DATA  ***
C
      PRINT 14
 14   FORMAT('1',/'+',50X,'RAW DATA MATRIX',//'+',54X,'TEMPERATURE K')
      PRINT 15,T(1),T(2),T(3),T(4),T(5),T(6),T(7),T(8)
 15   FORMAT(' ',9X,8F14.1)
      DO 16 J=1,10
      PRINT 17,(SIGMA(J,I),I=1,8),(LNEDOT(J,I),I=1,8),(TAUDMU(J,I),I=1,8
     &)
 17   FORMAT('0',1X,'SIGMA',3X,8F14.2//'+',1X,'LNEDOT',2X,8F14.3//'+',1X
     &,'TAUDMU',2X,8E14.3)
 16   CONTINUE
      PRINT 18
 18   FORMAT('1',/'0',50X,'CROSS-PLOT DATA',//'0',54X,'TEMPERATURE K')
      PRINT 19,T(1),T(2),T(3),T(4),T(5),T(6),T(7),T(8)
 19   FORMAT(' ',3X,'TAUDMU',8F12.1)
      DO 21 J=1,15
      PRINT20,TDU(J),(LET(J,I),I=1,8)
 20   FORMAT('0',2X,D9.3,F10.3,7F12.3)
 21   CONTINUE
C
C
C     SEGMENT TO CALCULATE THE ACTIVATION ENTHALPY,FREE ENERGY, ENTROPY,
C     VOLUME , AND THE PRE-EXPONENTIAL FACTOR
C
C
C
      DO 1 J=1,15
      DO 2 I=1,8
      X(I)=TINV(I)
      Y(I)=LET(J,I)
      W(I)=1.0D0
 2    CONTINUE
 5    SUMX=0.0D0
      SUMY=0.0D0
      SUMXY=0.0D0
```

[redacted]

```
      SUMX2=0.0D0
      SUMY2=0.0D0
      SUMW=0.0D0
      NCNT=0
      DO 6 I=1.8
      IF(Y(I).GT.-1.0D0)GO TO 6
      NCNT=NCNT+1
      SUMX=SUMX+W(I)*X(I)
      SUMY=SUMY+W(I)*Y(I)
      SUMXY=SUMXY+X(I)*Y(I)*W(I)
      SUMX2=SUMX2+X(I)*X(I)*W(I)
      SUMY2=SUMY2+Y(I)*Y(I)*W(I)
      SUMW=SUMW+W(I)
 6    CONTINUE
      D=NCNT
      SUMW=SUMW/D
      SUMY=SUMY/D
      SUMX=SUMX/D
      SUMXY=SUMXY/D
      SUMX2=SUMX2/D
      SUMY2=SUMY2/D
      A(1.J)=(SUMXY*SUMW-SUMX*SUMY)/(SUMX2*SUMW-SUMX*SUMX)
      B(1.J)=(SUMX2*SUMY-SUMX*SUMXY)/(SUMX2*SUMW-SUMX*SUMX)
      A(2.J)=(SUMXY*SUMW-SUMX*SUMY)/(SUMY2*SUMW-SUMY*SUMY)
      B(2.J)=(SUMY2*SUMX-SUMY*SUMXY)/(SUMY2*SUMW-SUMY*SUMY)
      B(2.J)=-B(2.J)/A(2.J)
      A(2.J)=1.0D0/A(2.J)
      E=SUMXY*(SUMY*SUMY-SUMX*SUMX)+SUMX*SUMY*(SUMX2-SUMY2)
      F=SUMW*SUMX*(SUMY2-SUMX2)+SUMX*(SUMY*SUMY+SUMX*SUMX)-2.0D0*SUMW*SU
     +MY*SUMXY
      G=SUMW*(SUMXY*SUMW-SUMX*SUMY)
      FUNC=DSQRT(F**2-4.0D0*E*G)
      B1=(-F+FUNC)/(2.0D0*E)
      B2=(-F-FUNC)/(2.0D0*E)
      A1=(SUMW-B1*SUMY)/SUMX
      A2=(SUMW-B2*SUMY)/SUMX
      N=8
      YA=(1.0D0-A1*X(N))/B1
      YB=(1.0D0-A2*X(N))/B2
      IF(DABS(Y(N)-YA).GT.DABS(Y(N)-YB))GO TO 7
      A(3.J)=A1
      B(3.J)=B1
      GO TO 8
 7    A(3.J)=A2
      B(3.J)=B2
 8    A(3.J)=-A(3.J)/B(3.J)
      B(3.J)=1.0D0/B(3.J)
 1    CONTINUE
      PRINT 32
 32   FORMAT('1',//'0',10X,'TAUDMU',16X,'DH.K.J./MOLE',6X,'DG/MU.B**3/AT
     &OM')
      DO 30 I=1.15
      DH(I)=-BK*A(3.I)
      DGDMU(I)=DH(I)/(MUZERO*10.0568D0)
      DHKJ=DH(I)/1.0D3
      PRINT 31.TOU(I).DHKJ.DGDMU(I)
 31   FORMAT('0',10X.D9.3.15X.F6.2.15X.F5.3)
 30   CONTINUE
      PRINT 39.T(1).T(2).T(3).T(4).T(5).T(6).T(7).T(8)
 39   FORMAT('1',//'+',50X,'PRE-EXP - DG  MATRIX ...UNITS OF DG ARE K.J.
```

[redacted]

```
      &/MOLE',//'+',54X,'TEMPERATURE K',//'+',3X,'TAUDMU',8F12.1)
       DO 35 J=1,15
       DO 33 I=1,8
       IF(LET(J,I).GT.-1.0DC)GO TO 34
       MU=MUZERC+MUSLCP*T(I)
       DG(J,I)=DH(J)*MU/MUZERO
       PREXP(J,I)=(DG(J,I)/(BK*T(I)))+LET(J,I)
       DS(J,I)=-(MUSLCP/MU)*DG(J,I)
       GO TO 38
 34    DG(J,I)=0.0D0
       PREXP(J,I)=0.0D0
       DS(J,I)=0.0D0
 38    DG(J,I)=DG(J,I)/1.0D3
 33    CONTINUE
       PRINT 36,TDU(J),(DG(J,I),I=1,8),(PREXP(J,I),I=1,8)
 36    FORMAT('0',2X,D9.3,F10.2,7F12.2//'+',9X,8F12.3)
 35    CONTINUE
       PRINT 80,T(1),T(2),T(3),T(4),T(5),T(6),T(7),T(8)
 80    FORMAT('1',//'0',40X,'ACTIVATION ENTROPY MATRIX (J./MOLE K)',
      &/'0',54X,'TEMPERATURE K'//'+',3X,'TAUDMU',8F12.1)
       DO 81 J=1,15
       PRINT 83,TDU(J),(DS(J,I),I=1,8)
 83    FORMAT('0',2X,D9.3,D10.3,7D12.3)
 81    CONTINUE
C
C
C      PROGRAM SEGMENT THAT CALCULATES THE EXPERIMENTAL ACTIVATION VOLUME
C      FROM THE RAW DATA, THEN THIS DATA IS FITTED TO THE EQUATION:
C      V = A*EXP(B*TDU+C*TDU**2+D*TDU**3)
C
C      MODIFIED TO :
C
C      LN(V)= A'+B*TDU+C*TDU**2+D*TDU**3
C
C
       K=1
       SX(1)=0.0D0
       SX(2)=0.0D0
       SX(3)=0.0D0
       SX(4)=0.0D0
       SX(5)=0.0D0
       SX(6)=0.0D0
       SX(7)=0.0D0
       SW(1)=0.0D0
       SW(2)=0.0D0
       SW(3)=0.0D0
       SW(4)=0.0D0
C
       PRINT 47,T(1),T(2),T(3),T(4),T(5),T(6),T(7),T(8)
 47    FORMAT('1',/'0',30X,'EXP. ACT. VOL. =(K*T/MU) ((D LNEDOT)/(D TAUDM
      &U)) AT CONST. T  ...  UNITS OF VSTAR : 100 B**3/ATOM'
      &                //'+',54X,'TEMPERATURE K'//'+',15X,8F12.1)
 49    NDIM=0
       DO 40 J=1,10
       X(J)=TAUDMU(J,K)
       Y(J)=LNEDOT(J,K)
       IF(Y(J).GT.-1.0D0)GO TO 40
       NDIM=NDIM+1
 40    CONTINUF
       SX(1)=SX(1)+DFLOAT(NDIM)
```

[redacted]

```
C
C         DIFFERENTIATION SEGMENT ( SSP SUBROUTINE DDGT3)
C
          CALL DDGT3(X,Y,Z,NDIM,IER)
          MU=MUZERO+MUSLOP*T(K)
          FAC=BK*T(K)/MU
          XFAC=FAC*9.89686D0
          DO 44 I=1,NDIM
          VSTAR(I,K)=Z(I)*(XFAC/1.0D04)
   44     CONTINUE
          IF(NDIM.LT.10)GO TO 61
          GO TO 62
   61     ND=NDIM+1
          DO 63 I=ND,10
          VSTAR(I,K)=0.0D0
   63     CONTINUE
   62     DO 43 I=1,NDIM
          WX=DLOG(VSTAR(I,K))
          X(I)=X(I) 1.0D03
          SX(2)=SX(2)+X(I)
          SX(3)=SX(3)+X(I)**2
          SX(4)=SX(4)+X(I)**3
          SX(5)=SX(5)+X(I)**4
          SX(6)=SX(6)+X(I)**5
          SX(7)=SX(7)+X(I)**6
          SW(1)=SW(1)+WX
          SW(2)=SW(2)+WX*X(I)
          SW(3)=SW(3)+WX*X(I)**2
          SW(4)=SW(4)+WX*X(I)**3
   43     CONTINUE
          K=K+1
          IF(K.LE.8)GO TC 49
          DO 60 J=1,10
          PRINT 45,(TAUDMU(J,I),I=1,8),(VSTAR(J,I),I=1,8)
   45     FORMAT('0',3X,'TAUDMU',6X,8D12.3//'+',4X,'VSTAR',6X,8F12.2)
   60     CONTINUE
          DO 50 I=1,4
          DO 51 J=1,4
          N=J+I-1
          AA(I,J)=SX(N)
          IF(J.GT.1)AA(I,J)=-AA(I,J)
   51     CONTINUE
          BB(I)=SW(I)
   50     CONTINUE
C
C         SET UP MATRIX AB FOR SUBROUTINE SOLMTX
C
          DO 90 I=1,4
          DO 91 J=1,4
          AB(I,J)=AA(I,J)
   91     CONTINUE
          AB(I,5)=BB(I)
   90     CONTINUE
          N=4
C
C         SUBROUTINE SOLMTX SOLVES A SET OF LINEAR EQUATIONS
C
          CALL SCLMTX(AB,N,BB)
          PRINT 70
   70     FORMAT('1',////'0',30X,'COEFFICIENTS OF THE EQUATION FITTED TO THE
```

[redacted]

```
     & VSTAR-VS-TAUDMU DATA'//'+',35X,'EQN: LN(VSTAR)= A+B*TAUDMU+C*TAUD
     &MU**2+D*TAUDMU**3'
     &                                  //'+',25X,'*** TAUDMU=TAUDMU*1.0D03 *
     &**.')
      PRINT 71,BB(1),BB(2),BB(3),BB(4)
 71   FORMAT('-','A=',D14.7,/'0','B=',D14.7,/'0','C=',D14.7,/'0','D=',D1
     &4.7)
      PRINT 200
 200  FORMAT('1',10X,'TAUDMU',25X,'ACT.VOL. 100 B**3/ATOM.')
      DO 100 I=1,15
      TDX=TDU(I)*1.0D03
      APRIME=DEXP(BB(1))
      LNV(I)=APRIME*(DEXP(-BB(2)*TDX-BB(3)*TDX**2-BB(4)*TDX**3))
      PRINT 101,TDU(I),LNV(I)
 101  FORMAT('0',6X,D12.3,25X,D12.4)
 100  CONTINUE
C
C
C     PROGRAM SEGMENT TO CALCULATE THE VALUES
C     OF  THE ACTIVATION ENTHALPY AND ENTROPY
C     WITH RESPECT TO THE SHEAR STRESS.
C
C
      K=1
      PRINT 400,T(1),T(2),T(3),T(4),T(5),T(6),T(7),T(8)
 400  FORMAT('1',//'+',15X,'DS...DH  MATRIX...UNITS OF DH ARE K.J./MOLE.
     &.UNITS OF DS ARE J./MOLE K  ...W.R.T. TAU'//'+',54X,'TEMPERATURE
     &K'//'+',3X,'TAUDMU',8F12.1)
 301  DO 300 J=1,8
      DHT(J)=(DH(K)/1.0D3)-1.0104D0*LNV(K)*TDU(K)*MUSLOP*T(J)
      DST(J)=(DHT(J)-DG(K,J))*1.0D3/T(J)
      IF(DG(K,J).LT.1.0D-3)DST(J)=0.0D0
 300  CONTINUE
      PRINT 36,TDU(K),(DHT(I),I=1,8),(DST(I),I=1,8)
      K=K+1
      IF(K.LE.15)GO TO 301
      PRINT 777
 777  FORMAT('1')
      STOP
      END

      SUBROUTINE SOLMTX(A,N,X)
      IMPLICIT REAL*8(A-H,O-Z)
      DIMENSION SOL(5   ),X(4),B(4,5),PIV(5),ANEW(4,5),A(4,5)
      INTEGER*4 SIGN,COL,ROW,PERMUT(5),PEROW(5)
      NN=N+1
      WRITE(6,506)
      WRITE(6,499)((A(I,J),J=1,NN),I=1,N)
C
C     *********INITIALIZATION OF THE VARIABLES
      SIGN=1
      DO 100 J=1,N
      PEROW(J)=J
  100 PERMUT(J)=J
      DETA=1.D0
C
C     *********MANIPULATION OF MATRICES (A,B)
C
C
```

[redacted]

```
      DO 8 K=1,N
C
C     ********FIND THE PIVOT
      DO 7 I=K,N
      DO 7 J=K,N
    7 B(I,J)=A(I,J)
      IF(K.EQ.N)GO TO 66
      CALL PIVOT(B,K,N,ROW,COL,AMAX)
      PIV(K)=AMAX
      GO TO 67
   66 AMAX=B(N,N)
      PIV(K)=AMAX
      GO TO 33
 67   CONTINUE
C
C     **********REARRANGE THE MATRICES
      CALL REORD(A,K,N,RCW,CCL,SIGN)
      IF(COL.EQ.K)GC TO 3
      TEMP=PERMUT(COL)
      PERMUT(COL)=PERMUT(K)
      PERMUT(K)=TEMP
 3    IF(ROW.EQ.K)GO TO 33
      TEMP=PEROW(RCW)
      PEROW(ROW)=PEROW(K)
      PEROW(K)=TEMP
 33   DO 6 I=1,N
      DO 6 J=1,NN
      IF(I.EQ.K)GO TO 6
      IF(J.EQ.K)GO TO 6
      ANEW(I,J)=A(I,J)-A(I,K)*A(K,J)/PIV(K)
    6 CONTINUE
      DO 5 J=1,NN
 5    ANEW(K,J)=A(K,J)/PIV(K)
      DO 77 I=1,N
 77   ANEW(I,K)=-A(I,K)/PIV(K)
      ANEW(K,K)=1.0D0/PIV(K)
      DO 13 I=1,N
      DO 13 J=1,NN
 13   A(I,J)=ANEW(I,J)
      DETA=DETA*SIGN*PIV(K)
 8    CONTINUE
      DO 11 I=1,N
   11 SOL(I)=A(I,N+1)
      DO 12 I=1,N
      L=PERMUT(I)
   12 X(L)=SOL(I)
C
C     **DISENTANGLE ROWS
      DO 1 I=1,N
      L=PERMUT(I)
      DO 1 J=1,N
      ANEW(L,J)=A(I,J)
 1    CONTINUE
      DO 99 I=1,N
      DO 99 J=1,N
 99   A(I,J)=ANEW(I,J)
C
C     **DISENTANGLE COLUMNS
      DO 2 J=1,N
      L=PEROW(J)
```

[redacted]

```
      DO 2 I=1,N
      ANEW(I,L)=A(I,J)
    2 CONTINUE
      WRITE(6,507)((ANEW(I,J),J=1,N),I=1,N)
      WRITE(6,900)DETA
      WRITE(6,901)
      WRITE(6,902)(X(L),L=1,4)
      WRITE(6,508)
  499 FORMAT('-','MATRIX AB',//(5D17.8))
  506 FORMAT('1',/////T10,20('*'),'RESULTS',20('*'))
  507 FORMAT('-','INVERSE OF THE MATRIX A'/(4D17.8))
  508 FORMAT('-',100('*'))
  900 FORMAT('-',T10,'DETERMINANT=',D17.8)
  901 FORMAT('-',T5,'SOLUTIONS OF THE SYSTEM')
  902 FORMAT('0',T20,'X =',D17.8/' ',T20,'Y =',D17.8/' ',T20,'Z =',D17.8
     1/' ',T20,'W =',D17.8)
      RETURN
      END

      SUBROUTINE PIVOT(B,K,N,ROW,COL,AMAX)
      IMPLICIT REAL*8(A-H,O-Z)
      DIMENSION B(4,5)
      INTEGER*4 COL,ROW
      ROW=K
      COL=K
      AMAX=B(K,K)
      DO 1 I=K,N
      DO 1 J=K,N
      IF(DABS(B(I,J)).LE.AMAX)GO TO 1
      ROW=I
      COL=J
      AMAX=B(I,J)
    1 CONTINUE
      RETURN
      END

      SUBROUTINE REORD(A,K,N,ROW,COL,SIGN)
      IMPLICIT REAL*8(A-H,O-Z)
      DIMENSION A(4,5)
      INTEGER*4 ROW,COL,SIGN
      IF(ROW.EQ.K)GO TO 2
      SIGN=-SIGN
      NN=N+1
      DO 1 J=1,NN
      TEMPR=A(ROW,J)
      A(ROW,J)=A(K,J)
    1 A(K,J)=TEMPR
    2 IF(COL.EQ.K)GO TO 3
      SIGN=-SIGN
      DO 4 I=1,N
      TEMPC=A(I,COL)
      A(I,COL)=A(I,K)
    4 A(I,K)=TEMPC
    3 RETURN
      END

$DATA
```